Molecular Imaging of Atherosclerosis

Molekulare Bildgebung der Atherosklerose

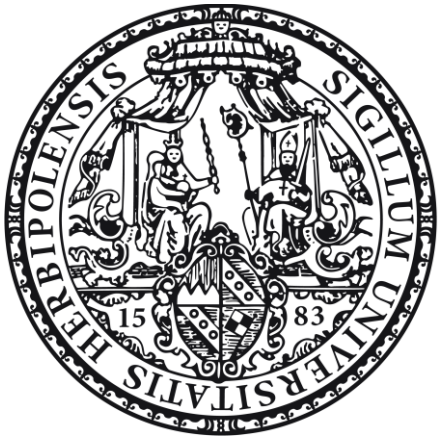

Doctoral thesis

for a doctoral degree

at the Graduate School of Life Sciences,

Julius-Maximilians-Universität Würzburg, Section Biomedicine

submitted by

Marta Michalska

From Wloclawek, Poland

Würzburg 2013

Members of the Thesis Committee:

Chairperson: Prof. Dr. Thomas Dandekar

Primary Supervisor: Prof. Dr. Dr. Wolfgang Rudolf Bauer

Second Supervisor: Prof. Dr. Roland Jahns

Third Supervisor: Prof. Dr. Peter Jakob

Fourth Supervisor: PD Dr. Alma Zernecke

Submitted on:

Date of Public Defence:

Date of Receipt of Certificates:

Considerable parts of this doctoral thesis were disclosed in the published manuscript:

Michalska M., Machtoub L., Manthey H. D., Bauer E., Herold V., Krohne G., Lykowsky G., Hildenbrand M., Kampf T., Jakob P., Zernecke A. and Bauer W. R. (2012). "Visualization of vascular inflammation in the atherosclerotic mouse by ultrasmall superparamagnetic iron oxide vascular cell adhesion molecule-1-specific nanoparticles". Arterioscler Thromb Vasc Biol 32 (10): 2350-2357.

Table of Contents

Summary

Atherosclerosis is an active and progressive condition where the vascular cell adhesion molecules as VCAM-1 play a vital role controlling the recruitment of immune cells within the early and advanced plaques. Therefore targeting of VCAM-1 molecules with specific contrast agent bears the possibility to monitor the VCAM-1 expression, visualize the plaque progression starting at the early alterations, and help to establish early prevention of atherosclerosis before the origin of the thrombus formation, of which late recognition leads to myocardial infarction. Furthermore noninvasive magnetic resonance imaging (MRI) offers the benefit of combining the molecular and anatomic data and would thus enable specific detection of VCAM-1 targeted iron oxide contrast agent within inflammatory process of atherosclerosis.

This thesis exactly presents the VCAM-1 concept as a suitable molecular approach and the potential of specific ultrasmall superparamagnetic iron oxide (USPIO) conjugated to the VCAM-1 binding peptide over unspecific non-targeted USPIO particles for evaluation of atherosclerosis. This work firstly demonstrated that selection of VCAM-1 molecules offers a good and potential strategy for imaging of atherosclerosis, as these vascular cell adhesion molecules are highly expressed in the early phase of inflammation and also continuously up-regulated within the advanced plaques. Secondly, this thesis showed the proof of principle and capability of the newly designed USPIO contrast agent conjugated to the specific cyclic peptide for VCAM-1 recognition. The experimental studies including ultra-high field MRI enabled further *ex vivo* and *in vivo* detection of applied USPIO-VCAM-1 particles within the aortic root region of early and advanced atherosclerotic plaques of 12 and 30 week old apolipoprotein E deficient ($ApoE^{-/-}$) mice. Using a combination of histology and electron microscopy, this study for the first time pointed to distribution of targeted USPIO-VCAM-1 particles within plaque cells expressing VCAM-1 not only in luminal regions but also in deeper medial smooth muscle cell areas. Hence functionalized USPIO particles targeting VCAM-1 molecules allow specific and sensitive detection of early and advanced plaques at the molecular level, giving the new possibilities for early recognition of atherosclerotic plaques before the appearance of advanced and prone to rupture lesions. In contrast to the functionalized USPIO-VCAM-1, utilized non-targeted USPIO particles did not succeed in early plaque

identification limiting visualization of atherosclerosis to advanced forms in atherosclerotic *ApoE*$^{-/-}$ mice.

Zusammenfassung

Atherosklerose ist eine aktive und progressive Erkrankung, bei der vaskuläre Adhäsionsmoleküle wie VCAM-1 eine entscheidende Rolle durch Steuerung der Rekrutierung von Immunzellen in den frühen und fortgeschrittenen Plaques spielen. Ein zielgerichteter Einsatz von VCAM-1-Molekülen mit spezifischen Kontrastmitteln ist daher eine Möglichkeit, die VCAM-1-Expression zu kontrollieren, Plaquewachstum ab einem frühen Zeitpunkt zu visualisieren und eine frühe Prävention von Atherosklerose vor Beginn der Thrombusbildung zu etablieren. Des Weiteren bietet die nichtinvasive Magnetresonanz (MR)-Bildgebung den Vorteil der Kombination molekularer und morphologischer Daten. Sie ermöglicht, mithilfe von entwickelten VCAM-1-markierten Eisenoxidpartikeln, den spezifischen Nachweis entzündlicher Prozesse während der Atherosklerose.

Diese Arbeit belegt, dass mit dem VCAM-1-Konzept eine vielversprechende Herangehensweise gefunden wurde und dass das, mit spezifischen superparamagnetischen Eisenoxid (USPIO) konjugierte VCAM-1-Peptid, gegenüber unspezifischer USPIOs ein erhöhtes Potenzial bei der Untersuchung der Atherosklerose in sich trägt. Im ersten Teil der Arbeit konnte im Mausmodell gezeigt werden, dass gerade das VCAM-1-Molekül ein sinnvoller Ansatzpunkt zur Darstellung und Bildgebung von Atherosklerose ist, da in der frühen Phase der Entzündung die vaskulären Zelladhäsionsmoleküle überexprimiert und auch kontinuierlich, während der fortschreitenden Plaquebildung, hochreguliert werden. Weiterhin beschreibt diese Arbeit die Funktionstüchtigkeit und das Vermögen des neu gestalteten USPIO Kontrastmittels mit dem zyklischen Peptid, in seiner Spezialisierung auf die VCAM-1 Erkennung. Experimentelle Studien mit ultra-Hochfeld-MRT ermöglichten weitere *ex vivo* und *in vivo* Nachweise der eingesetzten USPIO-VCAM-1-Partikel innerhalb der Region um die Aortenwurzel in frühen und fortgeschrittenen atherosklerotischen Plaques von 12 und 30 Wochen alten Apolipoprotein E-defizienten ($ApoE^{-/-}$) Mäusen. Mit ihrer Kombination aus Histologie und Elektronenmikroskopie zeigt diese Studie zum ersten Mal die Verteilung von VCAM-1-markierten USPIO Partikeln nicht nur in luminalem Bereich der Plaques, sondern auch in tieferen Bereichen der medialen Muskelzellen. Dieser spezifische und sensitive Nachweis der frühen und fortgeschrittenen Stadien der Plaquebildung bringt auf molekularer Ebene neue Möglichkeiten zur Früherkennung von atherosklerotischen Plaques vor dem Entstehen von

Rupturen. Im Gegensatz zum USPIO-VCAM-1-Kontrastmittel scheiterten unspezifische USPIO Partikel an der Identifikation früher Plaqueformen und begrenzten die Visualisierung von Atherosklerose auf fortgeschrittene Stadien in *ApoE*$^{-/-}$ Mäusen.

1. Introduction

1.1. Pathogenesis of Atherosclerosis

Atherosclerosis is a pathological condition of the arterial wall (*Ait-Oufella, Taleb et al. 2009*) and the most common cardiovascular disease (*Hansson and Hermansson 2011*), terminating in myocardial infarction, stroke and peripheral vascular disease (*Getz and Reardon 2012*). The process of atherosclerosis is progressive and may develop unnoticed over several years with the origin in early adolescence (*Insull 2009*). Among the genetic and environmental pathogenic aspects, the main risk factor promoting the pathological development of atherosclerosis is hypercholesterolemia (*Libby 2002; Hansson, Robertson et al. 2006; Getz and Reardon 2012*). The prolonged period of elevated cholesterol levels initiates the inflammatory process within the arterial wall and together with the immune cells' recruitment, chronic plaque growth continues (*Hansson and Hermansson 2011*). The linkage of hypercholesterolemia and inflammation in the pathogenesis of atherosclerosis is based on the active presence of vascular cells' adhesion (VCAM-1) molecules (*Iiyama, Hajra et al. 1999; Hansson 2001; Huo and Ley 2001; Libby 2002; Hansson and Hermansson 2011*). These molecules play a pivotal function in the early as well as in the advanced phase of atherosclerosis, controlling the onset and continuation of the immune cells' migration into the inflamed vessels. Due to the fact that these molecules appear only under inflammatory stimuli and that their expression is enormous during the inflammatory cascade of atherosclerosis (*Ley and Huo 2001*), they could constitute a prime target for therapeutic treatment and imaging of cell activation *in vivo*. Available detection methods and monitoring of early and advanced inflammatory processes could further benefit researchers and clinicians who search for the best solution to this disease.

In accordance with the World Health Organization, within the next few years cardiovascular diseases are projected to be the major cause of death not only in the developing countries but worldwide (*Hansson, Robertson et al. 2006; Hansson and Hermansson 2011*). Therefore extensive work on the development of molecular and cellular techniques as well as of imaging methods is necessary to understand and visualize the molecular mechanism of atherosclerosis.

1.2. Molecular mechanisms of immune cells' recruitment within the early and advanced atherosclerotic lesions

1.2.1. Fatty streak formation

The origin of the fatty streaks and the inflammatory process starts through the dysfunction of endothelial cells at the atheroma-prone branching points further associated with the sizeable thickening of intima caused by changes in hemodynamics (*Libby, Ridker et al. 2002; Weber, Zernecke et al. 2008; Insull 2009*). Endothelial dysfunction occurs via oxidized proinflammatory lipoproteins which provoke the activation of endothelial cells within intima (*Chi and Melendez 2007; Hansson and Hermansson 2011*), release of cytokines and expression of adhesion molecules (*Choudhury and Fisher 2009; Insull 2009*) such as membrane receptor CD40 (*Schonbeck and Libby 2001; Phipps 2008*), vascular adhesion molecules (VCAM-1), intercellular adhesion molecule-1 (ICAM-1), and E- and P-selectin (*Schonbeck and Libby 2001; Libby, Ridker et al. 2002; Chi and Melendez 2007*). Among the vascular molecules involved in the activation of the vascular and immune cells within the arterial wall, VCAM-1 merits notice. The activation pattern of these molecules is exceptional and works only under proinflammatory atherosclerotic processes (*Ley and Huo 2001*). VCAM-1 molecules trigger rolling and firm adhesion (*Ley and Huo 2001*) of T-lymphocytes and splenic monocytes ($CD14^{high}/Ly6C^{high}/CD43^{low}$) (*O'Brien, Allen et al. 1993; Libby 2006; Strauss-Ayali, Conrad et al. 2007; Settles, Etzrodt et al. 2011; Quillard and Libby 2012; Robbins, Chudnovskiy et al. 2012*) via α4β1 integrin binding (*Nakashima, Raines et al. 1998; Braun, Pietsch et al. 1999; May, Neumann et al. 2000; Chi and Melendez 2007; Ley, Miller et al. 2011*). Following the firm adhesion, leukocytes enter the arterial wall with help of diverse chemokines. One of the crucial chemokines involved in leukocytes migration is macrophage chemoattractant protein (MCP-1) (*Li and Glass 2002; Libby, Ridker et al. 2002; Soufi, Sattler et al. 2002; Chi and Melendez 2007*). Recruited plaque leukocytes via MCP-1 subsequently secrete platelet-derived growth factor (PDGF) (*Singh, Mengi et al. 2002; Soufi, Sattler et al. 2002*), which further induces the inflammatory process and encourages the smooth muscle cells (SMCs) to participate (*Libby 2002; Doran, Meller et al. 2008; Getz and Reardon 2012*). In response, medial smooth muscle cells mobilize their move towards the intimal region, proliferate, produce extracellular matrix, and secrete cytokines which further stimulate monocytes, mast cells and lymphocytes towards the arterial wall (*Doran, Meller et al.*

2008; Insull 2009; Quillard and Libby 2012). Like activated endothelial cells, smooth muscle cells also express VCAM-1 adhesion molecules (*Li, Cybulsky et al. 1993; Braun, Pietsch et al. 1999; Doran, Meller et al. 2008*). Through the VCAM-1 pathway, these cells can interact with endothelial cells and support leukocyte migration within the atherosclerotic lesions (*Li, Cybulsky et al. 1993; Braun, Pietsch et al. 1999; May, Neumann et al. 2000; Doran, Meller et al. 2008*).

Among recruited immune cells via activated endothelium, monocytes constitute the largest immune cell population of the lesions and give rise to macrophages and dendritic cells (*Weber, Zernecke et al. 2008; Robbins and Swirski 2010; Getz and Reardon 2012; Gui, Shimokado et al. 2012; Robbins, Chudnovskiy et al. 2012*). Assembled plaque macrophages are capable of expressing scavenger receptors such as CD36, CD68, type AI and AII, and LOX-1 (*Choudhury and Fisher 2009*), through which oxidized lipoproteins (oxLDLs) are phagocytized (*Li and Glass 2002; Ley, Miller et al. 2011; Gui, Shimokado et al. 2012*). Within macrophages, oxidized LDLs are modified to cholesterol which is further deposited in lysosomes and maintained in foamy form (fatty streaks) (*Li and Glass 2002; Schrijvers, De Meyer et al. 2007; Choudhury and Fisher 2009; Gui, Shimokado et al. 2012*). Besides the macrophage phagocytosis of oxidized lipoproteins, smooth muscle cells (SMCs) possess a similar function. SMCs express scavenger receptors, which recognize oxLDLs and contribute to foam cells' creation (fatty streaks) (*Schrijvers, De Meyer et al. 2007; Doran, Meller et al. 2008*). Hypercholesterolemia and high lipid deposition within activated endothelium and intimal regions as well as the increased expression of vascular adhesion molecules are crucial in early recognition of atherosclerosis.

1.2.2. Fibroatheroma formation

During atheroma formation there is progressive chronic accumulation of macrophages and other immune cells which expand the plaque size (*Gui, Shimokado et al. 2012*). Despite the role of macrophage foam cells in the control of lipid phagocytosis through scavenger receptors in the plaque growth, high content of cholesterol may lead to apoptosis and necrosis (*Yin, Chaufour et al. 2000; Feng, Yao et al. 2003; Devries-Seimon, Li et al. 2005; Schrijvers, De Meyer et al. 2007; Choudhury and Fisher 2009; Gui, Shimokado et al. 2012*). Such a situation appears when huge macrophage deposits of cholesterol accumulate

outside in extracellular matrix space (*Choudhury and Fisher 2009; Gui, Shimokado et al. 2012*) and this process stimulates macrophage and smooth muscle cells death (*Insull 2009*). Cell necrosis with increasing quantities of extracellular matrix and cholesterol prompts further inflammation (*Tabas 2005; Insull 2009*), which completely changes the morphology of the intima (*Insull 2009*). Lipid rich necrotic cores prevail in the center of the intimal lesions. A fibrous cap surrounds the lipid rich necrotic cores, stabilizes the plaques and protects them from rupture (*Insull 2009*). In addition, during the chronic phase of inflammation, plaque macrophages are releasing matrix metalloproteinases (MMP) and prothrombotic factors which contribute to the destabilization of the plaques' fibrous cap (*Libby, Ridker et al. 2002; Singh, Mengi et al. 2002; Gui, Shimokado et al. 2012*). Smooth muscle cells face the release of MMP and produce instead stabilizing collagen fibrils, which protect the fibrous cap from rupture (*Singh, Mengi et al. 2002*). However there are many other factors interfering in the stability of the plaques and thus provoking the thrombosis. One such factor is interferon gamma, secreted by activated T cells, which accumulates in the vulnerable regions (*van der Wal, Becker et al. 1994; Libby, Ridker et al. 2002; Singh, Mengi et al. 2002*). Interferon gamma hampers the synthesis of collagen in smooth muscle cells and seems to participate in the reversal of stable to vulnerable plaques (*Libby, Ridker et al. 2002; Singh, Mengi et al. 2002*). Growth of advanced fibroatheroma plaques associated with formation of small microvessels (neovascularization) may promote rupture as well (*Moreno, Purushothaman et al. 2006; Slevin, Krupinski et al. 2009*). All of those chronic and complex processes, which involve a variety of different immune cells, cytokines, and pro- versus antithrombotic factors in stabilizing and rupturing of the plaques are detrimental, and present at each phase of atherosclerotic lesion formation. Understanding the whole process of immune cells' recruitment and early and advanced lesion formation is therefore important in order to discover specific molecular targets and effective strategies for detection and treatment of this disease.

1.3. Role of VCAM-1 in early and advanced stages of plaque formation

Human as well as murine vascular cells' adhesion molecule (VCAM-1) is transmembrane glycoprotein (CD106) (*Cybulsky, Fries et al. 1991; Carlos and Harlan 1994; Huo and Ley 2001*). It has been shown that mouse VCAM-1 represents 75% homology to human VCAM-1 molecules (*Hession, Moy et al. 1992*). VCAM-1 is expressed within activated

endothelium (*Cybulsky and Gimbrone 1991; Ley and Huo 2001; Libby 2006*), smooth muscle cells (*O'Brien, Allen et al. 1993; Braun, Pietsch et al. 1999*), and macrophages (*Libby and Li 1993; O'Brien, Allen et al. 1993*) over the inflammatory atherosclerotic period but also within Kupffer cells (*van Oosten, van de Bilt et al. 1995*), dendritic cells (*Libby and Li 1993; Balogh, Aydar et al. 2002*), activated neurons (*Birdsall, Lane et al. 1992*), and fibroblasts (*Chen, Chen et al. 2005*). VCAM-1, briefly mentioned in chapter: 1.2.1. Fatty streak formation), appears to be important and compelling in the early phase of leukocytes' adhesion to endothelium at atheroma-prone sites. In contrast to E- and P-Selectins which capture and mediate rolling of leukocytes at the sites of activated endothelium (*Huo and Ley 2001; Blankenberg, Barbaux et al. 2003*), VCAM-1 is responsible for the adhesion and arrest of white blood cells (*Nakashima, Raines et al. 1998; Ley and Huo 2001)*, especially monocytes and T lymphocytes (*Libby 2006*), via interaction with α4β1 complex promoting the occurrence of these immune cells in the evolving young plaques (*Nakashima, Raines et al. 1998; Braun, Pietsch et al. 1999; May, Neumann et al. 2000; Huo and Ley 2001; Chi and Melendez 2007; Ley, Miller et al. 2011*) (**Figure 1.1**). The endothelial VCAM-1 activation initiates the inflammation. The process of VCAM-1 activation occurs via nuclear factor-kB (NF-kB) (*Blankenberg, Barbaux et al. 2003; Libby 2006*), in response to endothelial cytokine release, and might be influenced by an atherogenic diet and oxidized lipoproteins which accumulate within the intima of the arterial wall (*Iiyama, Hajra et al. 1999; Huo and Ley 2001; Libby 2002; Libby 2006; Chi and Melendez 2007*). It has been previously published (*Nakashima, Raines et al. 1998; Cybulsky, Iiyama et al. 2001*) that VCAM-1 expression begins prior to leukocytes adhesion in cholesterol-fed animal models, giving evidence that cholesterol might induce VCAM-1 expression pattern (*Iiyama, Hajra et al. 1999; Huo and Ley 2001; Libby 2002*). It has been further reported that besides endothelial cells, VCAM-1 molecules appear on intimal smooth muscle cells within the atherosclerotic lesions of human (*O'Brien, Allen et al. 1993; O'Brien, McDonald et al. 1996*) and of apolipoprotein E deficient (*ApoE$^{-/-}$)* mice (*Braun, Pietsch et al. 1999*), leading to the premise that VCAM-1 expression within smooth muscle cells may support leukocytes' transmigration within early and advanced lesions (*Libby and Li 1993; May, Neumann et al. 2000; Huo and Ley 2001; Doran, Meller et al. 2008*). It has also been observed that during leukocytes' adhesion associated with VCAM-1 mechanism, medial smooth muscle cells also express VCAM-1 molecules (*Braun, Pietsch et al. 1999*). Besides the crucial role of these molecules in the early lesions, VCAM-1 also plays an important role in advanced fibroatheroma plaques,

controlling enhanced recruitment of monocytes to impaired arteries from adventitia, and also participating in the neointimal smooth muscle cell proliferation (*O'Brien, Allen et al. 1993; O'Brien, McDonald et al. 1996; Huo and Ley 2001; Ley and Huo 2001*).

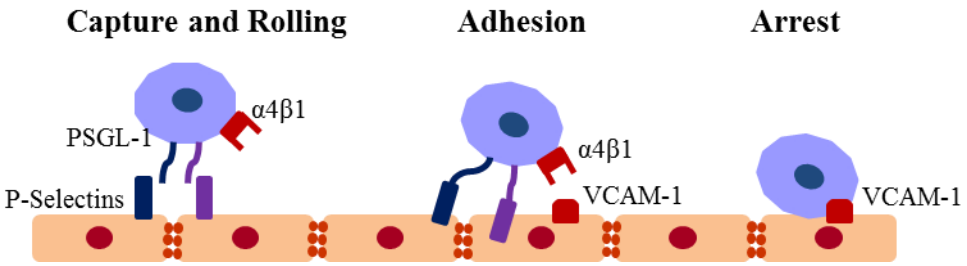

Figure 1.1. VCAM-1 mediated leukocyte adhesion on the activated endothelium at the atheroma-prone sites. P- Selectins capture and induce leukocytes' rolling on endothelium via leukocyte ligand (PSGL-1). In consequence, VCAM-1 molecules cause further adhesion and arrest the leukocytes. Upon arrest, VCAM-1 molecules linked to leukocyte ligands (α4β1) stabilize the adhesion and trigger transmigration. PSGL-1 is the P-selectin glycoprotein ligand-1, α4β1 is an integrin termed very late antigen 4, modified from (*Schnoor and Parkos 2008*).

1.4. Role of α4β1 as a co-receptor of VCAM-1

Ligand α4β1 complex, presented on the surface of leukocytes such as monocytes, T lymphocytes, eosinophils, and basophils (*Cybulsky, Fries et al. 1991; Li, Cybulsky et al. 1993; Carlos and Harlan 1994; May, Neumann et al. 2000; Ley and Huo 2001*), identifies VCAM-1 molecules with the high specificity and due to that plays an important role in leukocytes recruitment. Thus the α4β1 complex and its active binding sites could serve as a therapeutic target for recognition of VCAM-1 molecules (*You, Maxwell et al. 2002*). Knowledge of the mechanism of the α4β1 binding is necessary to design either therapeutic pharmacological inhibitors that would block VCAM-1/α4β1 interaction or small peptides/antibodies that could on the one side enable inhibition and on the other side detect inflammation (*You, Maxwell et al. 2002*). Human and murine α4β1integrin is a transmembrane glycoprotein and consists of α4 (CD49d) chain and β1 (CD29) chain (*Carlos and Harlan 1994; Huo and Ley 2001*). It has been shown that both of the chains participate actively in binding to VCAM-1 (*Hynes 1992; Humphries, Sheridan et al. 1995*). Thus design of specific drugs or peptides having the α4β1active binding sites for VCAM-1 recognition would have unprecedented perspective for targeting and monitoring

VCAM-1 expression in the inflammatory process of atherosclerosis and further would help to inhibit this chronic condition.

1.5. Mouse model of atherosclerosis

Clinical and experimental surveillances of atherosclerosis simultaneously with molecular and cellular investigation of the plaque formation require animal models. Examinations of human atherosclerotic lesions are interfered with due to the limitations in noninvasive identifications of molecular processes (*Virmani, Kolodgie et al. 2000; Corti and Fuster 2011*). There is confined knowledge of human atherosclerotic plaque formation and this knowledge is mainly based on carotid arteries studies or luminal stenosis (*Insull 2009; Libby, DiCarli et al. 2010*). Experimental studies in animal models, especially in genetically modified mice, have elucidated the enormous role of innate and adaptive immune system and lipid metabolism in the regulation of lesion development (*Insull 2009*). Therefore studies utilizing animal models help to understand the biological and pathophysiological mechanism of plaque formation (*Getz and Reardon 2012*). Moreover experimental animals provide excellent *in vivo* possibilities to support and prove *ex vivo* cell culture studies and lead to the next step of cardiovascular imaging and treatment of atherosclerosis (*Daugherty 2002; Meir and Leitersdorf 2004; Vilahur, Padro et al. 2011*). One of the most widely available and widely used models suitable for human translation referring to plaque composition is the transgenic mouse model (*Meir and Leitersdorf 2004; Pendse, Arbones-Mainar et al. 2009; Getz and Reardon 2012*). These genetically backcrossed mice with changed expression profile of specific atheroma-prone genes vastly increased knowledge of the molecular mechanism involved in atherosclerosis (*Daugherty 2002; Zaragoza, Gomez-Guerrero et al. 2011*). The advantage of using a transgenic mouse model is easy handling and breeding, and relatively low maintenance costs (*Getz and Reardon 2012*). Among common experimental models, Apoliporotein E deficient mice (*ApoE*$^{-/-}$) are generally an excellent model for studying atherosclerosis due to prompt and spontaneous development of plaques (*Nakashima, Plump et al. 1994; Reddick, Zhang et al. 1994; Meir and Leitersdorf 2004; Hansson, Robertson et al. 2006; Pendse, Arbones-Mainar et al. 2009; Zaragoza, Gomez-Guerrero et al. 2011*). For instance studies affecting *ApoE* $^{-/-}$ mice enabled the discovery of the mechanism of vascular adhesion mediated leukocyte transmigration (*Dong, Brown et al. 2000*) and the important role of matrix

metalloproteinase-1 (MMP-1) in advanced plaques (*Lemaitre, O'Byrne et al. 2001*). Apolipoprotein E deficient mice (*ApoE* $^{-/-}$) fed a high fat diet are characterized by the elevated cholesterol plasma level (*Plump, Smith et al. 1992; Reddick, Zhang et al. 1994; Meir and Leitersdorf 2004; Getz and Reardon 2012*). Triggered by the high fat diet, monocyte adhesion occurs early in *ApoE*$^{-/-}$ mice and progresses to accelerated fatty streak formation. The fatty streaks initially emerge within the ascending aorta including the aortic root, aortic arch, and the right carotid artery (*Nakashima, Plump et al. 1994*) and progress to fibrous (advanced) plaques due to the increased recruitment of immune cells. These mice also develop small plaques in the descending abdominal aorta (*Nakashima, Plump et al. 1994*). The advanced plaques of older *ApoE*$^{-/-}$ mice are complex and composed of the fibrous cap and the necrotic core. The fibrous cap which stabilizes the plaques is occupied by foamy macrophages and smooth muscle cells. The necrotic core together with the apoptotic cells dominates the center of the plaque and is surrounded by the fibrous cap (*Nakashima, Plump et al. 1994; Nakashima, Raines et al. 1998*).

Besides the studies of molecular mechanism of atherosclerosis using *ApoE*$^{-/-}$ mice, this model is commonly utilized to examine noninvasive changes of the plaque size (*Meir and Leitersdorf 2004; Herold, Wellen et al. 2009*), to characterize and target the various cells participating in the initiation and chronic progression of atherosclerosis (*Jaffer and Weissleder 2004; Libby, Nahrendorf et al. 2010; Quillard and Libby 2012*).

1.6. Visualization of atherosclerosis

Discovery of molecular biological processes involved in pathogenesis of chronic inflammatory condition such as atherosclerosis allows a thorough recognition and estimation of this disease (*Choudhury and Fisher 2009*). The growth of this experimental molecular field, its comprehensive knowledge of genes and proteins associated with atherosclerosis and the need for preclinical and clinical translation in order to visualize this inflammatory process *in vivo*, has resulted in the development of the atherosclerotic molecular imaging techniques (*Chen and Wu 2011; Grenier and Brader 2011*). This expanding field (*Jaffer and Weissleder 2004*) entails further the development of diverse noninvasive imaging modalities (1.6.1. Molecular magnetic resonance imaging modality) and highly refined contrast agents (1.6.3. Contrast agents) (*Choudhury and Fisher 2009;*

McAteer, Akhtar et al. 2010; Chen and Wu 2011). Besides present clinical trials approaching imaging of plaque size (*Toussaint, LaMuraglia et al. 1996; Yuan, Beach et al. 1998; Corti, Fuster et al. 2001; Shaw 2009; Libby, DiCarli et al. 2010; Corti and Fuster 2011*), advances in the preclinical molecular imaging field intensify understanding and monitoring of biological processes involved in plaque formation through the early fatty streaks, advanced to ruptured plaques (*Jaffer, Libby et al. 2006; Shaw 2009; Libby, DiCarli et al. 2010*). This discipline may further contribute to early detection of high risk lesions prior to symptoms arising, giving new possibilities for better designed diagnoses and treatment focused on molecular atherosclerotic therapies (*Jaffer, Libby et al. 2006; Thorek, Chen et al. 2006; Saraste, Nekolla et al. 2009; Shaw 2009*).

Because the aim of molecular imaging approaches is to visualize the atherosclerotic process at the cellular and molecular level (*Weissleder and Mahmood 2001*), properly designed cellular and molecular targets associated with the highly refined contrast agents are needed (*Choudhury and Fisher 2009; McAteer, Akhtar et al. 2010; Chen and Wu 2011; Corti and Fuster 2011; Grenier and Brader 2011*). Possible contrast agents might approach the cells or biomolecules involved in atherosclerosis through cellular (non-targeted) or molecular (targeted) mechanism (*Grenier and Brader 2011*). The existing non-targeted contrast agents focus on detection of advanced atherosclerotic plaques and enable delivery of these imaging agents to cells owing to phagocytic properties. Targeted contrast agents allow to address for instance proteins within the intracellular and extracellular cells' compartments at molecular level (*Jaffer, Libby et al. 2006; Thorek, Chen et al. 2006; Chen and Wu 2011*). The targeted contrast agents may further help to illuminate the very early changes before the onset of the plaque growth as well as to help to distinguish the molecular pattern at the stable to ruptured plaques (*Jaffer, Libby et al. 2006; Thorek, Chen et al. 2006; Chen and Wu 2011; Quillard and Libby 2012*). The concept and examples of cellular (non-targeted) and molecular (targeted) approaches will be presented in the chapter: (1.6.5. Molecular targets for MR Imaging).

1.6.1. Molecular magnetic resonance imaging modality

At present, imaging technologies lean on diverse modalities including x-ray computed tomography (CT), positron emission tomography (PET), single-photon emission computed

tomography (SPECT), intravascular ultrasound (IVUS) and magnetic resonance imaging (MRI) which visualize human atherosclerotic plaques (*Corti, Fuster et al. 2001; Choudhury and Fisher 2009; McAteer, Akhtar et al. 2010; Chen and Wu 2011; Tardif, Lesage et al. 2011*). Besides the highlighted imaging modalities, which enable assessment of the narrowing of the lumen (stenosis) and the plaque composition, the preclinical animal studies utilizing bioluminescence imaging (BLI), fluorescence imaging (FI), ultrasound, small animal MRI, micro-positron emission tomography (micro-PET), or micro–single photon emission computed tomography (microSPECT) help to image the atherosclerotic processes at molecular and cellular level (*Chen and Wu 2011*). Among these diverse approaches magnetic resonance imaging (MRI) has established itself as an outstanding modality for noninvasive cardiovascular disease detection (*Corti, Fuster et al. 2001; Corti and Fuster 2011*). In contrast to other techniques, MRI is capable of combining high spatial resolution (*Quillard and Libby 2012*) and excellent soft tissue contrast with high signal to noise ratio (*Corti, Fuster et al. 2001; Choudhury and Fisher 2009; McAteer, Akhtar et al. 2010*). Further it provides functional data including information about density, distribution, and biochemical contrast variation within the imaged tissue (*Pintaske, Muller-Bierl et al. 2006; Sanz and Fayad 2008; Choudhury and Fisher 2009; Chen, Cormode et al. 2010; McAteer, Akhtar et al. 2010; Chen and Wu 2011; Corti and Fuster 2011; Tardif, Lesage et al. 2011*). This noninvasive and nonionizing technique safely allows three dimensional data acquisition without radiation exposure which makes it suitable for monitoring of patients over time (*Corti, Fuster et al. 2001; Sanz and Fayad 2008; McAteer, Akhtar et al. 2010; Hahn, Singh et al. 2011; Tardif, Lesage et al. 2011*). Beyond magnificent spatial resolution, one disadvantage of MRI is its low sensitivity (*Choudhury and Fisher 2009; Chen, Cormode et al. 2010; McAteer, Akhtar et al. 2010*). This difficulty can however be overcome by the use of cellular and molecular contrast agents (*Choudhury and Fisher 2009; McAteer, Akhtar et al. 2010; Tardif, Lesage et al. 2011*). Thus molecular MR imaging offers the benefit of combining molecular and anatomic information within an MR image (*Jaffer and Weissleder 2004; Chen and Wu 2011; Tardif, Lesage et al. 2011*).

In the field of magnetic resonance (MR) imaging hydrogen nuclei are preferably used (*Chen and Wu 2011*) due to their high magnetic sensitivity and the high abundance in the form of water molecules within the mammalian tissues. The contrast within the imaged mammalian tissues is characterized by two relaxation processes: longitudinal T1 relaxation and transverse T2/T2* relaxation time (*Klug, Kampf et al. 2010*).

1.6.2. Contrast mechanism of Spin Echo and Gradient Echo Development

Acquisition of MR images does involve so called sequences, which enable the measurement of either T1 or T2 relaxation time and thus vary the image contrast within the measured objects. By suitable selection of parameters such as echo time (TE), repetition time (TR) and flip angle of the radiofrequency (RF) pulses, high resolution images can be obtained within a short imaging time, and changes of the relaxation times before and after application of contrast agents can be detected. Two main types of sequences are commonly used in MR imaging: spin echo and gradient echo sequences.

1.6.2.1. Spin Echo sequence

Spin echo sequences are based on the application of one 90^{o} and several subsequent 180^{o} degrees radiofrequency (RF) pulses. Amongst applied 180^{o} degree pulses the spin echos are measured. Application of the first 90^{o} degree pulse brings the magnetization into the transverse plane and generates the signal which then decays due to dephasing of the spins. This signal loss is considered as T2* decay. The application of a 180^{o} degree pulse brings the magnetization in phase and the signal, now defined as T2, is obtained in the form of echos (**Figure 1.2**). Spin echo contrast is based on a combination of T1 and T2 relaxation time which can be defined by changing the parameters such as TE and TR. For instance, a long TE results in T2-weighted images, whereas short TR increases T1 contrast. By these mechanisms, the effects of contrast agent application like gadolinium agents or iron oxide contrast agents can be visualized in *ex vivo* or *in vivo* conditions (*Blackwell, Cranney et al. 1992; Weishaupt, Kochli et al. 2006; Schroder and Faber 2011*).

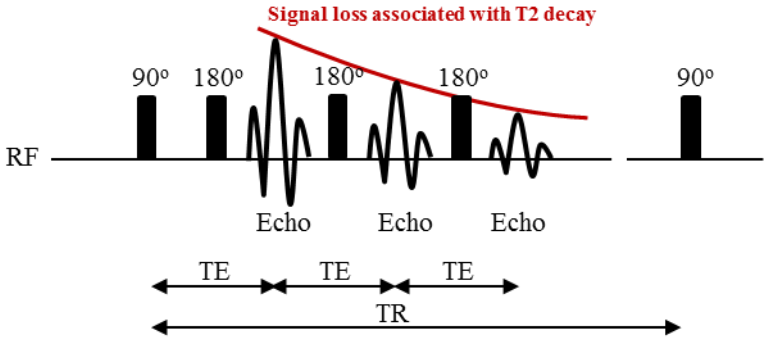

Figure 1.2. Generation of spin echo decay. The 90° degree pulse brings the magnetization into the transverse plane and generates the signal which decays exponentially due to dephasing of the spins. 180° degree pulse brings the magnetization in phase and the signal, obtained in the form of echo, decays after application of subsequent 180° pulses. This signal loss is considered as T2 effect.

1.6.2.2. Gradient Echo sequence

Gradient echo sequences consist of a radiofrequency (RF) pulse of a small flip angle. Application of the RF pulse brings the magnetization intentionally only partly towards the transverse plane and generates the signal which decays due to dephasing of the spins. This signal loss is due to T2*, a combination of the T2 relaxation time and magnetic field inhomogeneity (**Figure 1.3**). To measure T2*, one or more gradient echos are usually applied. Contrast T2*-weighted images require only single echo imaging, whilst T2* mapping entails more. Moreover with applied T2* contrast agents, it is recommended to use short echo times as the effect is so strong that the contrast is generated nearly immediately. The appropriate adjustment of TE and flip angle can detect the alteration within the sample or tissue associated with the contrast agent application, especially with iron oxide contrast agents (*Blackwell, Cranney et al. 1992; Weishaupt, Kochli et al. 2006; Schroder and Faber 2011*).

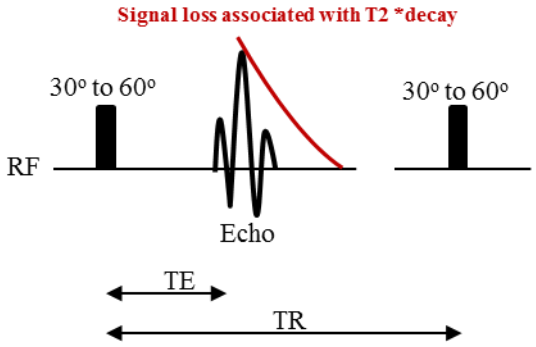

Figure 1.3. **Generation of gradient echo decay.** Application of an RF pulse of small flip angle brings the magnetization partly towards the transverse plane and generate the signal which decays according to the dephasing of the magnetization. This signal loss is considered as T2* effect.

1.6.3. Contrast agents

The T1 and T2 relaxation mechanisms enable displaying of diverse contrasts within the MR image, and owing to that provide morphological information of measured tissues (*Klug, Kampf et al. 2010*). The effect of T1 and T2 can be altered by various contrast agents (*Tang, Muller et al. 2009; Chen, Cormode et al. 2010; Klug, Kampf et al. 2010; Chen and Wu 2011*), which increase the MR sensitivity effect and therefore enhance the image contrast (*Klug, Kampf et al. 2010*). Moreover, use of contrast agents enables the identification of diseased regions at cellular and molecular level (*Weissleder and Mahmood 2001; McAteer, Akhtar et al. 2010*). This information might be important for effective disease recognition, diagnosis and even more for designing new drug therapies (*Jaffer, Libby et al. 2006*). There are two kinds of contrast agents for MR imaging, grouped as positive and negative contrast agents. The positive contrast agents compose of gadolinium chelates (Gd-DTPA), whereas the negative contrast agents consist of superparamagnetic iron oxide particles (*McAteer, Akhtar et al. 2010; Schroder and Faber 2011*). In addition, MR sequence parameters can be chosen in such a way, that iron oxide particles can also be used as positive contrast agents (*Dahnke, Liu et al. 2008; Korosoglou, Weiss et al. 2008*). Gadolinium chelates shorten T1 relaxation time of water protons (spins) and due to that enhance the image contrast by generating positive signal, which appears bright on T1-weighted images (*Choudhury and Fisher 2009; Saraste, Nekolla et al. 2009; McAteer, Akhtar et al. 2010*). Nevertheless, their use in molecular imaging might be not sufficient due to their low MR sensitivity effect (*Bulte and Kraitchman 2004; Debbage*

and Jaschke 2008; McAteer, Akhtar et al. 2010). In contrast to gadolinium agents, superparamagnetic iron oxide agents have gained more attention in the field of molecular imaging, because of their strong effect. These particles shorten T2 and T2* relaxation time of water protons (spins) and due to this phenomenon, they enhance the image contrast by generating a signal loss which appears dark on T2- and T2*-weighted images. This characteristic signal loss pattern is called the blooming effect (*McAteer, Akhtar et al. 2010*). Owing to their strong effect on MR sensitivity, superparamagnetic iron oxide nanoparticles have already been successfully applied in preclinical imaging and have further shown the usefulness in clinical practice (*Weissleder, Elizondo et al. 1990; Kooi, Cappendijk et al. 2003; Bulte and Kraitchman 2004; Corot, Robert et al. 2006; Sosnovik and Caravan 2009*). Researchers have considered iron oxide particles as a suitable tool for cellular and molecular visualization of pathological conditions such as inflammation, atherosclerosis, myocarditis, metastatic lymph nodes, musculoskeletal diseases or degenerative disorders such as multiple sclerosis or Alzheimer's disease (*Hauger, Delalande et al. 2000; Schmitz, Coupland et al. 2000; Litovsky, Madjid et al. 2003; Bulte and Kraitchman 2004; Choi, Moon et al. 2007; Klug, Kampf et al. 2009; Reiner, Lutz et al. 2009; Sigovan, Boussel et al. 2009; Tang, Muller et al. 2009; Sigovan, Bessaad et al. 2010; Weinstein, Varallyay et al. 2010; Grenier and Brader 2011; Leuschner and Nahrendorf 2011; Moon, Park et al. 2012*).

1.6.4. Properties of iron oxide particles

Superparamagnetic iron oxide nanoparticles consist of a maghemite or magnetite (Fe_2O_3, Fe_3O_4) core and a polymer coating such as dextran, carboxydextran, or polyethyleneglycol (PEG) (*Morales, Veintemillas-Verdaguer et al. 1999; Corot, Robert et al. 2006; Thorek, Chen et al. 2006; Laurent, Forge et al. 2008; Amstad, Zurcher et al. 2009; Weinstein, Varallyay et al. 2010*). The coating not only stabilizes the iron oxide particles, but may also strongly influence the phagocytic activity of immune cells (*Corot, Robert et al. 2006; Thorek, Chen et al. 2006; Lipinski, Briley-Saebo et al. 2008; Chen, Cormode et al. 2010; Weinstein, Varallyay et al. 2010*), and may further serve as a link for conjugation of the targeted approaches (*Bulte and Kraitchman 2004; Corot, Robert et al. 2006; Thorek, Chen et al. 2006*). Besides the common dextran and PEG coating, iron particles might also be placed in liposomes or high-density lipoproteins (HDL), as they were previously

demonstrated, to enhance the macrophage phagocytic uptake (*Cormode, Skajaa et al. 2008; Meincke, Schlorf et al. 2008; Chen, Cormode et al. 2010*). The iron oxide particles possess strong superparamagnetic characteristics (*Thorek, Chen et al. 2006*), which are determined by their small size iron core ranging from 4 to 10 nm (*Corot, Robert et al. 2006*) due to that these particles own a strong effect on MR sensitivity. Besides their strong superparamagnetic characteristics, iron oxide particles are biocompatible and biodegradable (*Corot, Robert et al. 2006; Thorek, Chen et al. 2006*). They do not possess any toxicity, and due to this they can be safely used for *in vivo* application (*Corot, Robert et al. 2006; Thorek, Chen et al. 2006; Lipinski, Briley-Saebo et al. 2008; Chen, Cormode et al. 2010*). Referring to the size of the iron particles, there are ultrasmall superparamagnetic particles of iron oxide (USPIO) with the diameter of 20-40 nm, cross linked iron oxide particles (CLIO) with the diameter of 30-60 nm, superparamagnetic particles of iron oxide (SPIO) with the diameter of 60-250 nm, and micrometer sized particles of iron oxide (MPIO) with the diameter of 0.9-8 μm (*McAteer, Akhtar et al. 2010*). In the cardiovascular preclinical imaging field, it has been shown that the large sized iron oxide particles such as SPIO or MPIO (*Schmitz, Coupland et al. 2000; Bulte and Kraitchman 2004; Shapiro, Skrtic et al. 2005; Corot, Robert et al. 2006; McAteer, Akhtar et al. 2010*), when injected into the blood stream of animals, were promptly recognized by immune cells in the spleen, bone marrow, liver, or lymph nodes, resulting in a very fast half-life time of about 2 to 5 minutes (*Oude Engberink, van der Pol et al. 2007; Tang, Muller et al. 2009; McAteer, Akhtar et al. 2010; Weinstein, Varallyay et al. 2010*). In clinical use, the aspect of the rapid clearance of contrast agents is of great consideration, however such a short half-life time of 2 to 5 minutes is not suitable for visualization of the chronic inflammatory process of atherosclerosis. Too short a circulation time hampers the cellular access of large nanoparticles to the regions of interests such as of atherosclerotic plaques. In contrast, small sized iron oxide particles such as USPIOs are a better approach by having a longer half-life time (*Corot, Robert et al. 2006; Weinstein, Varallyay et al. 2010; Chen and Wu 2011; Grenier and Brader 2011*) than SPIOs or MPIOs. That is why, they can circulate in the blood stream for longer, allowing a thriving cells' uptake within the inflamed atherosclerotic tissues (*Kooi, Cappendijk et al. 2003; Modo, Hoehn et al. 2005; Corot, Robert et al. 2006; Tang, Muller et al. 2009; Weinstein, Varallyay et al. 2010*). The cellular transport of USPIOs particles, which is based on phagocytosis is not well known (*Corot, Robert et al. 2006; Grenier and Brader 2011*). There are three theories of how the iron oxide particles reach the atherosclerotic lesions. The first mechanism refers

to USPIO transcytosis through endothelium followed by cellular phagocytosis from resident macrophages via scavenger receptors SR-A (*Bulte and Kraitchman 2004; Corot, Robert et al. 2006; Tang, Muller et al. 2009*). The second mechanism refers to cellular uptake by blood monocytes, which then transfer the iron particles to the inflamed plaques (*Corot, Robert et al. 2006*). The third mechanism, which is less probable, depicts the USPIO uptake and transport to advanced plaques via adventitia (*Corot, Robert et al. 2006*). This issue is still under further investigation in order to find the answer to the question of the iron uptake mechanism (*Corot, Robert et al. 2006*). As USPIOs were mainly designed for cellular non-targeted imaging, and as this approach is nonspecific, it may lead to challenges related to extremely high injection doses for MR detection of inflamed atherosclerotic tissues. Another issue of using non-targeted iron oxide particles is that they allow detection at the very late stage of advanced to ruptured atherosclerotic plaques. Thus targeted iron oxide contrast agents are the better platform for cardiovascular imaging, allowing early and sensitive detection of molecular processes before the appearance of advanced atherosclerotic lesions.

1.6.5. Molecular targets for MR Imaging

There are several molecules and immune cells (described in the chapter 1.2.1. Fatty streak formation and 1.2.2. Fibroatheroma formation), which actively participate in the plaque formation and therefore could become interesting imaging targets. One of the proposed concepts for plaque imaging was phagocytic activity of macrophages (*Ruehm, Corot et al. 2001*), oxidized lipoproteins (oxLDLs) (*Tsimikas and Shaw 2002*), or reactive oxygen species (ROS) production (*Nahrendorf, Sosnovik et al. 2008*). The macrophage phagocytosis or oxLDL molecules, recognized by macrophage scavenger receptors, have potential as molecular imaging targets due to the fact that these processes are accelerated in atherosclerosis and that monocytes and macrophages constitute the largest population of cells within the plaques (*Weber, Zernecke et al. 2008; Saraste, Nekolla et al. 2009; Shaw 2009; Gui, Shimokado et al. 2012*). There have been previously published studies targeting either macrophages and their scavenger receptors or oxidized lipoproteins (oxLDLs) in order to detect advanced plaques by optical, PET, and MR imaging modalities (*Tsimikas, Shortal et al. 2000; Nahrendorf, Zhang et al. 2008; Sigovan, Bessaad et al. 2010; Quillard and Libby 2012*). For instance, agents linked with gadolinium have been introduced to

target the macrophage scavenger receptors and to visualize atherosclerosis in mice (*Amirbekian, Lipinski et al. 2007; Quillard and Libby 2012*). To further visualize murine advanced plaques, macrophage CD68 receptor has also been targeted by use of antibody conjugated to iodine ^{124}I (*Quillard and Libby 2012; Temma and Saji 2012*). ROS production was also approached by targeting myeloperoxidases (MPO) in rabbit atherosclerotic plaques by targeted-gadolinium (*Ronald, Chen et al. 2009; Quillard and Libby 2012*). The successful experimental detection of macrophage phagocytosis with iron oxide nanoparticles or radiolabeled agents in the atherosclerotic animal model was also implemented in clinics (*Kooi, Cappendijk et al. 2003; Pedersen, Graebe et al. 2010*). Another example of molecular targets are matrix metalloproteinases (MMP) which are secreted by active macrophages (*Schafers, Riemann et al. 2004; Lancelot, Amirbekian et al. 2008; Quillard and Libby 2012*). For instance gadolinium and iron oxide contrast agents with MMP-2 and MMP-9 fragments, designed for optical or magnetic resonance imaging, were used as smart probes in order to visualize advanced plaques (*Quillard and Libby 2012*). Imaging of advanced plaques also involves phosphatidylserine, approached by annexin V, presented on death macrophages in the necrotic core of formed plaques (*Kietselaer, Reutelingsperger et al. 2004; Schellenberger, Sosnovik et al. 2004; Jaffer, Libby et al. 2006; Sarai, Hartung et al. 2007; Quillard and Libby 2012*). For example in atherosclerotic mice, linkage of annexin V to gadolinium and SPIO particles enabled MR detection of plaques within abdominal aorta (*Quillard and Libby 2012*). Integrins αvβ3, which are expressed on new plaque microvessels, have also been proposed as a good imaging target (*Quillard and Libby 2012*). It has been published that αvβ3 integrin binding RDG peptide linked to gadolinium nanoparticles enhanced the possibility to visualize advanced plaques in abdominal aorta of atherosclerotic mice and rabbits (*Winter, Morawski et al. 2003; Burtea, Laurent et al. 2008; Quillard and Libby 2012*). Activated platelets, which contribute to thrombus formation at the very last stage of atherosclerosis, have been also approximated. The activity of platelets has been visualized by targeting of glycoprotein IIb/IIIa (LIBS) in atherosclerotic mice (*von zur Muhlen, von Elverfeldt et al. 2008; Quillard and Libby 2012*).

Beyond proposed molecular markers and contrast agents used in animal models, which identify only advanced atherosclerotic plaques, vascular adhesion (VCAM-1) molecules serve as an excellent target due to the fact that they are expressed early within lesions in atherosclerosis. VCAM-1 molecules appear very early on activated endothelial

cells leading to adhesion of leukocytes (*Nakashima, Raines et al. 1998; Braun, Pietsch et al. 1999; Ley and Huo 2001*). The chronic inflammatory process of atherosclerosis with the high level of cytokines and oxidized lipoproteins stimulates not only endothelial cells but also other plaque cells to enhanced expression of VCAM-1 (*O'Brien, Allen et al. 1993; Huo and Ley 2001; Ley and Huo 2001; Libby 2002*). Therefore they represent a valuable marker of early and advanced changes indicating ongoing inflammatory processes within diverse immune cells involved. In order to mark the VCAM-1 within the early and advanced atherosclerotic plaques, there must be a specific ligand which could recognize the adhesion molecules. Previous studies utilized antibodies as ligands to image VCAM-1 molecules by ultrasound (*Kaufmann, Sanders et al. 2007; Ferrante, Pickard et al. 2009*) and by magnetic resonance (MR) imaging (*Kelly, Nahrendorf et al. 2006; Nahrendorf, Jaffer et al. 2006; McAteer, Schneider et al. 2008*). Other studies have focused on optical and nuclear modalities and have shown VCAM-1 expression by functionalized contrast agents linked with perfluorocarbon (*Southworth, Kaneda et al. 2009*), fluorine (*Nahrendorf, Keliher et al. 2009*), and radiolabeled technetium (*Broisat, Hernot et al. 2012*). In the expanding molecular imaging field, use of small peptides offers a promising strategy for VCAM-1 targeting. The advantage of small peptides is their tiny size. As VCAM-1 ligand, they are mostly composed of only several amino acids and due to that the immunogenicity effect is diminished (*Patel, Zaro et al. 2007; Delehanty, Boeneman et al. 2010*). Further they are inexpensive, easy to synthetize, biocompatible, and nontoxic for *in vivo* application. The use of small peptides ensures specific and controlled binding to only targeted cells expressing VCAM-1 (*Patel, Zaro et al. 2007; Delehanty, Boeneman et al. 2010*). To guarantee this specific binding, the amino acid sequence within synthetized peptide needs to resemble the active amino acid binding sites presented in the α4β1 complex expressed on leukocytes (presented in the chapter: 1.4. Role of α4β1as a co-receptor of VCAM-1). Such a ligand binding site enables the interaction with the VCAM-1. Thus small peptides linked with iron oxide nanoparticles can assure on the one site specific and controlled VCAM-1 binding and on the other site represent a compelling approach for MR visualization of the early and advanced atherosclerotic process. Additionally, internalization of targeted USPIO particles within atherosclerotic lesions occurs and might be initiated via receptor mediated endocytosis (*Hillaireau and Couvreur 2009*). However the whole mechanism is still not known (*Nair, Fukuda et al. 2012*).

In summary, USPIO iron oxide nanoparticles conjugated to specific VCAM-1 peptide might offer not only a specific and sensitive MR detection of vascular adhesion molecules in the atherosclerotic plaques, but also permits the internalization of nanoparticles and their capture inside the targeted cells. Thus targeted iron oxide nanoparticles might be suitable for *in vivo* visualization of the cardiovascular system with atherosclerotic inflamed vessels and disturbed blood flow.

1.7. Aims of the thesis

The aim of this thesis was to test the capability of newly developed USPIO particles with gem-bisphosphonate coating and conjugated to specific cyclic VCAM-1 peptide (*Patent WO2004/058275, US 2004/253181, Guerbet Research France*) to visualize early and advanced atherosclerotic plaques in apolipoprotein E deficient (*ApoE*$^{-/-}$) mouse model using the unprecedented combination of ultra-high field MRI, together with the assessment of particle localization by histology and electron microscopy. The thesis involved *ex vivo* and *in vivo* experiments and was divided into four parts.

In the first part of this work atherosclerotic *ApoE*$^{-/-}$ mice were investigated in order to assess the formation of early and advanced plaques and the contribution of vascular cell adhesion (VCAM-1) molecules in the atherosclerotic inflammatory process. These experiments were conducted *ex vivo* and histological staining was performed to visualize the VCAM-1 expression within diverse immune cells involved in the pathophysiological development of atherosclerotic plaques.

The second part of this study examined the feasibility of newly synthesized ultrasmall superparamagnetic iron oxide (USPIO) particles conjugated with (P03011) or without (P3007) VCAM-1 binding peptide. The structure and stability of USPIO-VCAM-1 and USPIO particles were analyzed by electron microscopy. The superparamagnetic characteristics of iron oxide particles in *ex vivo* phantoms were demonstrated by ultra-high magnetic field. Particle pharmacokinetics and biodistribution studies were performed by inductively coupled plasma emission spectroscopy and histology.

Third part involved *in vivo* application and validation of USPIO-VCAM-1 and control USPIO particles in C57Bl/6 control and atherosclerotic *ApoE* $^{-/-}$ mice at different time points in order to monitor VCAM-1 expression and inflammatory process within the 12 and 30 week old atherosclerotic mice. *In vivo* detection of applied USPIO-VCAM-1 and control USPIO particles was conducted at ultra-high magnetic field.

The last part of this study examined cellular distribution of USPIO-VCAM-1 and control USPIO particles by histological assessment and electron microscopy.

2. Materials

2.1. Chemicals

Most of the chemicals used for preparation of histological staining and *ex vivo* MR experiments were supplied from Sigma-Aldrich. The list of chemicals and antibodies supplied from other companies are described in the Magnetic Resonance Imaging and Histology method section.

2.2. Equipment

Analytical Balance (max 120g)	KERN
Analytical Balance (max 2000g) 440-47	KERN
AVANCE 750 MHz Spectrometer	BRUKER BIOSPIN
Channel Selector	BRUKER BIOSPIN
Centrifuge 5415C	EPPENDORF
Cooling Units UWK 45	HAAKE
Cryotom CM1850	LEICA
Fume Adsorber TAZ19	MEDITE
Hood	KOETTERMANN
Emission Spectrometer JY70 Plus	HORIBA JOBIN YVON
Isoflurane Pump	EICKEMEYER
Light microscope Axioskop 2 plus	ZEISS
Fluorescent microscope Axiovision	ZEISS
MS2 Minishaker	IKA
NMR Network Analyzer	AEA TECHNOLOGY

Scantainer	SCANBUR
RCT basic	IKA

2.3. Contrast agents

Non-targeted and targeted ultrasmall superparamagnetic iron oxide nanoparticles were obtained from Guerbet Research Laboratory (France). The synthesis of these particles is explained in patent number WO2004/058 275 (US 2004/253181) Guerbet Research Laboratory (France).

2.3.1. P3007 (USPIO)

Control non-targeted USPIO nanoparticles described in the patent number WO2004/058 275 (US 2004/253181) consist of 5 nm iron oxide core with a layer of more gem-bisphosphonate compounds $(CH(PO_3H_2)_2)_n$. These compounds are equipped with the -L2- linkage via which the amino PEG (polyethyleneglycol 750) group is attached to the compound (*Patent WO2004/058 275, US 2004/253181 Guerbet Research France*), (*Michalska, Machtoub et al. 2012*).

2.3.2. P03011 (USPIO-VCAM-1)

The targeted P03011 contrast agent was synthesized using USPIO iron oxide nanoparticles combined with a VCAM-1 specific peptide. The USPIO particles with 5 nm iron core possess a gem-bisphosphonate $(CH(PO_3H_2)_2)_n$ coating which covers the particles. The particles' covering layer of gem-bisphosphonate compounds is conjugated further to the specific cyclic VCAM-1 peptide via a carboxylate (RCOO-) group. This group enables stable coupling of the VCAM-1 peptide. Beside VCAM-peptide linkage, there are also amino PEG (polyethyleneglycol 750) groups coupled to the layer. The final size of USPIO-VCAM-1 particles is 26 nm. The dissociation constant (K_d) value of the targeted particles is 61 nM. The sequence of the VCAM-1 peptide within the designed contrast agent was

tested within the cloning procedure (4 series of cloning) and the chosen cyclic sequence, composed of amino acids such as Cys-Asn-Asn-Ser-Lys-Ser-His-Thr-Cys (C-NNSKSHT-C), signified the presence of asparagine, serine, lysine, histidine, and threonine within the peptide. The particular amino acids in the peptide demonstrated similarity of α4β1 integrin active sites and further demonstrated high significance for VCAM-1 recognition (K_d=1.03x10^{-5}M) (validation of the cyclic peptide sequence presented in Patent number *WO2004/058 275, US 2004/253181, Guerbet Research France*).

2.3.3. Structure of P3007 and P03011

The iron quantities within the nanoparticles were characterized by atomic absorption spectroscopy (Varian AA10 spectrophotometer). First the sample was mineralized by 40% hydrochloric acid (HCl) and diluted according to a standard series of ferric ions (0, 5, 10, 15 and 20 ppm). The size of contrast agent was determined by Photon Correlation Spectroscopy (Malvern 4700) (*Patent WO2004/058 275, US 2004/253181 Guerbet Research France*) (*Michalska, Machtoub et al. 2012*).

2.4. Experimental fodder

2.4.1. Normal chow diet, SSNIFF Experimental Fodder Rat/Mouse

This fodder is based on highly purified or semisynthetic components required for the animal diet which maintenance the growth and normal metabolism of the animals. The diet composes of 61 % of sugar, 30 % of proteins, 9 % of fat, minerals, and vitamins.

2.4.2. Western diet, SSNIFF Experimental Fodder Rat/Mouse (TD88137)

This diet contains high level of fat and cholesterol (40 %). The cholesterol content (2.071 mg/kg) is adapted to the experimental animal approach to induce specific diseases such as atherosclerosis, obesity, or diabetes type 2. Apart from high content of lipids, this diet is enriched in 40 % of sugar, and 20 % of proteins, minerals, and vitamins.

2.5. Animal model

The animal investigations were affirmed by local authorities (Regierung von Unterfranken, Würzburg, Germany) according to the German protection law of experimental animals. Prior to experiments, the animals were kept in Scantainer (Scanbur, Denmark) with the adjusted temperature of 24^{o} C degree and humidity of 84%.

2.5.1. C57Bl/6 mouse model

C57Bl/6 mice, obtained from Charles River Laboratories Sulzfeld, Germany (strain code 027), were used as a control background experimental animal model. C57Bl/6 is a standard inbred strain utilized for genetic modifications to study the human diseases for example as atherosclerosis (*Knowles and Maeda 2000*). In this study, control C57Bl/6 mice aged 4 weeks were placed on normal diet and examined at 12 and 30 weeks.

2.5.2. Apolipoprotein E deficient (*ApoE*$^{-/-}$) mouse model

ApoE $^{-/-}$ mice, obtained from Charles River Laboratories Sulzfeld, Germany (strain code 002052), served as an atherosclerotic animal model for all experimental measurements. *ApoE*$^{-/-}$ deficient mouse model was developed by genetic modification of C57Bl/6 control mice. These *ApoE*$^{-/-}$ mice possess elevated cholesterol level due to the lack of *ApoE* gene and hence are prone to develop atherosclerotic plaques. The plaque formation in *ApoE*$^{-/-}$ mice resembles human atherosclerotic lesions and due to that phenomenon this animal model is common for studying the pathophysiology of atherosclerosis (*Hartley, Reddy et al. 2000; Meir and Leitersdorf 2004; Pendse, Arbones-Mainar et al. 2009*). In this work, *ApoE*$^{-/-}$ animals aged 4 weeks were kept on a high fat diet for 8 weeks to study the early formation of the plaques and for 26 weeks to study the progression of the advanced plaques.

3. Methods

3.1. Magnetic Resonance Imaging (MRI)

3.1.1. Ultra-high field MR System

All *ex vivo* and *in vivo* studies were conducted on an AVANCE 750 MHz Spectrometer from Bruker Biospin GmbH (Rheinstetten, Germany). The MR system consists of a vertical 17.6 Tesla ultra-high field superconducting magnet. This magnetic field is created by an electric current in the coils composed of superconducting wires. The advantage of these superconducting elements is that they can sustain very high electric currents without losses. The superconductivity is enabled by cooling the coils inside the MR system by liquid helium (*Schroder and Faber 2011*). Furthermore, the system is equipped with integrated shim coils to keep the magnetic field homogeneous. The inside diameter of the system is 89 mm. The MR system further comprises a 57 mm gradient system with a strength of 0.2 T/m and a 40 mm gradient system with a strength of 1 T/m. Both of the gradient units are actively shielded. The system also possesses an external gradient cooling unit (HAAKE) to regulate and adjust the temperature to all designed experiments.

3.1.2. Tuning and matching of the radio-frequency (RF) coils

During the tuning and matching procedure of a coil, the coils resonance frequency is tuned to the Larmor frequency (750 MHz) and its impedance is matched to that of the system (50 Ohm). This procedure is performed by connecting the proton channel of the RF coil to the NMR Network Analyzer (AEA TECHNOLOGY). Good tuning and matching of the RF coils to 750 MHz frequency and to 50 Ohm enables good and high signal to noise ratio (SNR). Afterwards, the coil is connected to the spectrometer.

3.1.3. Shimming

The AVANCE 750 MHz spectrometer possesses an integrated system of coils for shimming in order to maintain a homogenous magnetic field. Shimming is performed by superimposing additional fields to the main field distorted by the sample before the MR

scan to avoid magnetic field inhomogeneities (*Schroder and Faber 2011*). MR imaging begins after completion of the shimming procedure.

3.1.4. Sequences used for MR scans

There are individual sequences developed in the Experimental Physics by Dr. Volker Herold (*Herold, Wellen et al. 2009; Herold 2010*) used for MR imaging and each of the sequences will be described separately in the *ex vivo* and *in vivo* MRI measurements section.

3.2. MR Software

3.2.1. ParaVision 4

MR images were acquired using software ParaVision version 4 from Bruker Biospin GmbH (Rheinstetten, Germany). The software is designed for the routine MR measurements and manages the protocols and the sequences which are used for the experiments. The data acquired during the MR scan was transferred further as a DICOM file or the original data, and reconstructed in Matlab.

3.2.2. Matrix Laboratory (Matlab)

Acquired MR images were reconstructed in Matlab which is a commercial software provided by MathWorks (Natick, MA, USA). This is a program for data imaging. This software performs data reconstruction, programming, and diverse graphical presentations of the MR data.

3.3. *Ex vivo* and *in vivo* measurements at 17.6 T ultra-high field MR System

Ex vivo and *in vivo* MR imaging was conducted on a 17.6 T vertical bore MR system (Bruker Biospin GmbH, Rheinstetten, Germany), using a 40 mm gradient system with a strength of 1 T/m. For *ex vivo* measurements a 5 mm ^{1}H scroll coil and for *in vivo* measurements a 25 mm ^{1}H birdcage coil was used (*Tropp 1989; Lanz, Ruff et al. 2001; Lykowsky 2010*).

3.4. *Ex vivo* MRI measurements

Validation of the contrast agent dose and calculation of relaxivity (r2) values of iron oxide contrast agents was executed via *ex vivo* MRI experiments.

3.4.1. MR measurement of the contrast agent dose

3.4.1.1. Preparation of the agar phantoms

Reagents:

4 % Formaldehyde	Sigma-Aldrich
1.5 % Agarose Agarose Distilled water	AppliChem
P3007 (USPIO)	Guerbet Research Laboratory
P03011 (USPIO-VCAM-1)	Guerbet Research Laboratory

Protocol: Validation of the contrast agent dose was performed in control C57Bl/6 and *ApoE*$^{-/-}$ mice injected with the P03011 (USPIO-VCAM-1) contrast agent ranging from 100 µmol up to 600 µmol iron oxide/kg body weight. Hearts and aortae were isolated after 1 hour, 6 hours and 24 hours. The same procedure was performed with the control P3007 (USPIO) contrast agent. First of all C57Bl/6 and *ApoE*$^{-/-}$ mice were injected with 100, 300

and 600 µmol iron oxide / kg body weight and after 1 hour, 6 hours, and 24 hours hearts and aortae were excised. Hearts and aortae were further placed in 4 % formaldehyde for 1 up to 12 hours. After fixation, the hearts and aortae were placed in 5 mm NMR tube and cast in 1.5 % agarose.

3.4.1.2. 5 mm ^{1}H scroll coil

The 10 mm wide and 44 mm long scroll coil with inner diameter of 5 mm was used for *ex vivo* measurements. The coil is characterized by its excellent homogeneity and good signal to noise (SNR) and consists of a copper strip and a dielectric Teflon medium, which are rolled up together over a polyoxymethylene cylinder. This ensures that the capacity of the scroll coil cannot change by thermal expansion during the measurement (*Grant, Sit et al. 2007*) (*Lykowsky 2010*).

3.4.1.3. Sequence

Fast Low-Angle Shot (FLASH) scout sequence

Coronal, sagittal, and axial FLASH scout scans were utilized to image and orientate the measured object and served as a reference for setting the geometry of the further measurements. The parameters of the FLASH sequence were following: TR/TE= 60/2.9 milliseconds, with an image resolution of 219 µm^2 with a (28 x 28) mm^2 coronal, sagittal, and axial field of view, BW = 79 kHz, NA = 1, number of echo images = 1, slice thickness = 1 millimeter, excitation pulse = hermite. The duration time of the image acquisition is 30 seconds.

T2-weighted 3D Multi Spin Echo (MSME) sequence

An MSME sequence was used to obtain T2 values. The parameters of the 3D Multi Spin Echo (MSME) sequence were as follow: TR/TE = 1500/4.5 milliseconds, with an isotropic image resolution of 78 µm^3 with a (5 x 5 x 20) mm^3 transverse field-of-view, BW = 75 kHz, NA = 2, number of echo images 40, excitation and refocusing pulse = hermite. The

experiment duration is 13 hours. Phantom data were reconstructed in Matlab (The MathWorks Inc, Natick, MA, USA) and zerofilled inplane from a 64 x 64 to a 128 x 128 matrix. The quantification of the signal decay was calculated by fitting the T2 values pre- and post-contrast via a non linear least square fit to the function $s(t) = \exp(-t/T2)$.

3.4.2. MR measurement of relaxation rate (r2)

Protocol: Relaxivity (r2) values of iron oxide contrast agent were measured using a 2D MSME sequence (described above) and calculated in Matlab following the equation:

$$1/T2^{Fe} = (1/T2^{O}) + \lambda[Fe] \times \Delta C^{Fe}$$

$$r2^{Fe} = 1/T2^{Fe}$$

$$r2^{O} = 1/T2^{O}$$

$$\Delta r^{Fe-O} = r2^{Fe} - r2^{O}$$

$$\lambda[Fe] = \Delta r^{Fe-O}/\Delta C^{Fe}$$

where $T2^{Fe}$ is the relaxation time of the sample containing iron oxide particles, $T2^{O}$ is the relaxation time of the pure buffer in which iron oxide is diluted, in this case NaCl. The following dilutions of iron oxide particles were prepared: 0.05 mmol, 0.1 mmol, 0.5 mmol, and 1 mmol. Δr^{Fe-O} is the relaxation rate of the iron oxide particles, and ΔC^{Fe} is the concentration of iron oxide. $\lambda[Fe]$ is the relaxivity of the iron oxide particles measured [$mmol^{-1}$ s^{-1}].

3.5. *In vivo* MRI measurements

In vivo measurements were conducted on 12 and 30 week old C57Bl/6 and *ApoE*$^{-/-}$ mice before and 1 hour, 6, and 24 hours after injection of P03011 (USPIO-VCAM-1) and P3007 (USPIO) contrast agent.

3.5.1. Preparation of the mouse for the measurement

Reagents:

Isoflurane	Abbott
P3007 (USPIO)	Guerbet Research Laboratory
P03011 (USPIO-VCAM-1)	Guerbet Research Laboratory

Protocol: C57Bl/6 and *ApoE*$^{-/-}$ mice were anaesthetized by placing them into the specially designed box filled with 4 % isoflurane and 0.2 L/minute oxygen for 3 to 5 minutes under the hood (Koettermann). The mice were transferred afterwards and prepared for the measurement on the table equipped with 1-1.5 % isoflurane pipe and a fume adsorber (TAZ 19 Medite). The regulation of the isoflurane and oxygen level was controlled via isoflurane pump (Eickemeyer). During this time the linear birdcage 25 mm coil, used for *in vivo* study, was prepared. The coil was firstly placed under the red light and warmed up. The procedure of warming the coil helped to sustain physiological temperature of the mouse body. Further the mice were positioned inside the coil exactly within the center of the coil to guarantee the best signal to noise ratio (SNR) of the heart region. To control the ECG signal, an ECG balloon was placed in the center of the coil, within the chest where the apex of the mouse heart is, to control the triggering of the heart. The ECG balloon was further connected to the ECG trigger Unit HR from Rapid Biomedical. This device enabled exact monitoring of the health state of the mouse, allowing adjustment of the anaesthesia level. Moreover, the ECG signal was used as trigger for the MR measurements to rule out artifacts caused by the motion.

3.5.2. Linear 25 mm ^{1}H birdcage coil

In vivo studies were performed with a custom built linear birdcage coil with 25 mm diameter and 35 mm inner leg length. The increased diameter compared to standard coils facilitated *in vivo* measurements of mice with a body weight of 20 to 30 g in the 40 mm gradient insert. The 25 mm inner diameter tube served as a rail for the animal fixation and provided with the easy access of the desired heart location. The advantage of linear

birdcage coil use for *in vivo* animal studies is the high sensitivity, and homogeneity through the transversal plane (*Hayes 1985; Lykowsky 2010; Schroder and Faber 2011*).

3.5.3. Sequence

All sequences used for *in vivo* MRI were ECG triggered.

Scout longitudinal Fast Low-Angle Shot (FLASH) sequence

Longitudinal FLASH scout movies (CINE FLASH) were acquired and used to image and orientate the mouse heart. During the CINE FLASH scans the ECG signal of the cardiac cycle was triggered to acquire the MR data allowing the phase and readout encoding steps and further data reconstruction (**Figure 3.1**).

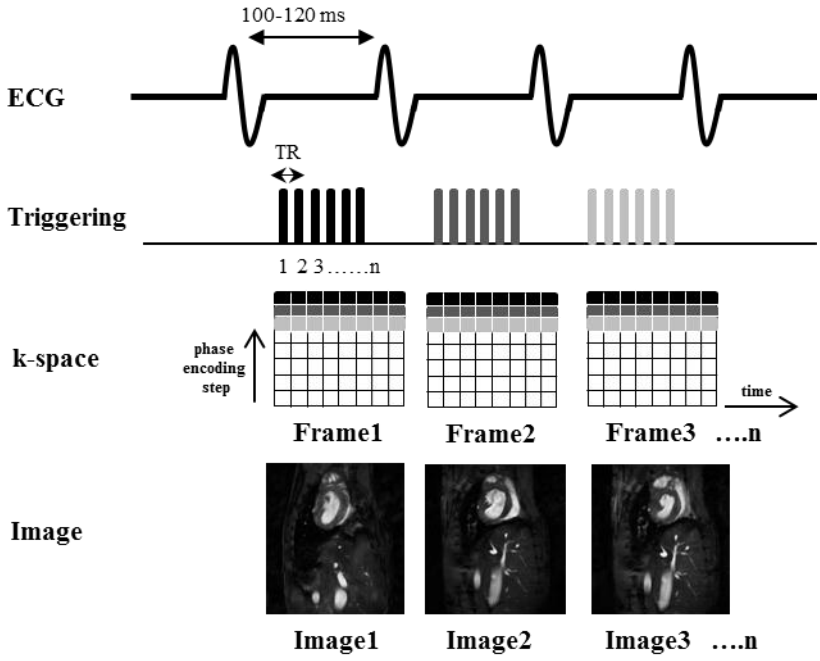

Figure 3.1. CINE FLASH MR images of the mouse heart. ECG signal of the heart rate is triggered and the acquired data is encoded in the k-space allowing further reconstruction of the frame images of the heart cycle.

The parameters of the FLASH scout were as follow: TR/TE = 7/1.5 milliseconds, with an isotropic image resolution of 117 μm^2 with a (30 x 30) mm^2 sagittal field-of-view, BW = 75 kHz, NA = 1, number of echo images 1, excitation pulse = gauss, number of slices = 1,

slice thickness = 0.8 mm, number of movie frames = 8. Duration time of scan is 30 seconds. Within the CINE FLASH image two transverse slices were positioned in order to perform the second scan using the Transversal FLASH sequence (**Figure 3.2**).

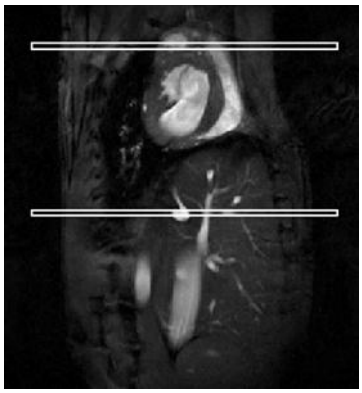

Figure 3.2. Scout longitudinal Fast-Low Angle Shot (FLASH) image of the mouse trunk with two transversal slices positioned within the heart (the upper slice) and within the liver (the lower slice) used for the acquisition of ascending and descending aorta.

Transversal Fast Low-Angle Shot (FLASH) sequence

Transversal FLASH movies were acquired to visualize ascending and descending aorta. This scan used the geometry from the scout longitudinal FLASH image (**Figure 3.2** and **Figure 3.3 A**) with one slice positioned within the ascending aorta in the heart (**Figure 3.3 B**) and one slice positioned within the descending aorta within the lower part of the mouse body (**Figure 3.3 C**). The parameters of the FLASH sequence were: TR/TE = 14/1.8 milliseconds, with a non-isotropic image resolution of 117 x 234 μm^2 with a (30 x 30) mm^2 transversal field-of-view, BW = 75 kHz, NA = 1, number of echo images 1, excitation pulse = gauss, number of slices = 2, slice thickness = 1 mm, number of movie frames = 8. Duration time of the measurement is 30 seconds.

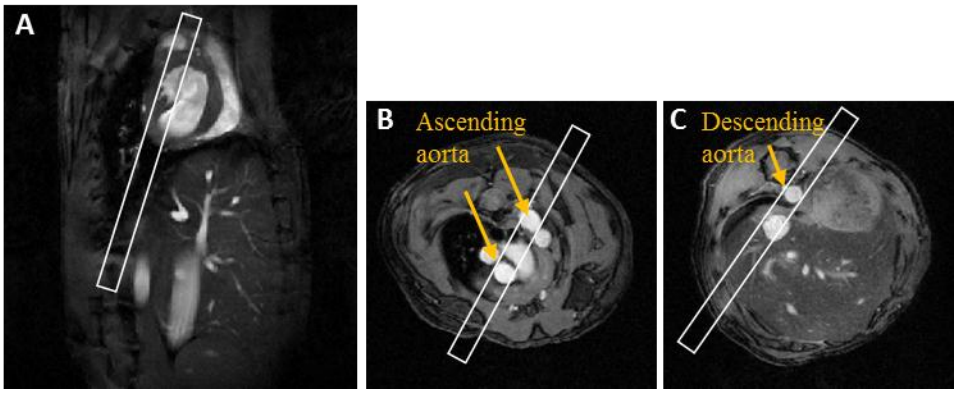

Figure 3.3. Longitudinal Fast Low-Angle Shot (FLASH) image of the mouse trunk with the slice selection (**A**). Transversal image of the ascending (**B**) and descending (**C**) aorta. The selected slices within the longitudinal (**A**) and transversal (**B**, **C**) images assured proper acquisition of the entire mouse aorta.

Longitudinal Fast Low-Angle Shot (FLASH) sequence

The last longitudinal FLASH movie was acquired to image diastolic and systolic moment of the heart (**Figure 3.4**). This scan used the geometry from the previous transversal FLASH image (**Figure 3.3**). The FLASH sequence used the following details: TR/TE = 12/1.8 milliseconds, with an isotropic image resolution of 117 μm^2 with a (30 x 30) mm^2 sagittal field-of-view, BW = 75 kHz, NA = 1, number of echo images 1, excitation pulse = gauss, number of slices = 1, slice thickness = 1.4 mm, number of movie frames = 8. Duration time is 30 seconds.

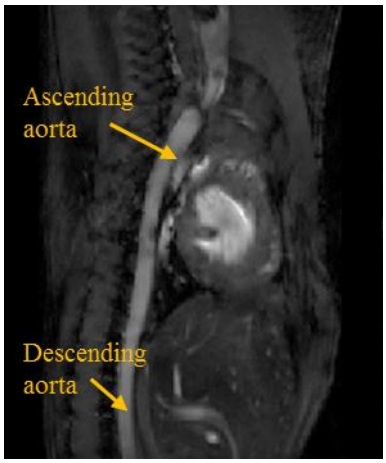

Figure 3.4. Longitudinal Fast Low-Angle Shot (FLASH) image of the ascending and descending aorta.

T2*-weighted Fast Low-Angle Shot (FLASH) sequence

A T2*-weighted FLASH sequence in axial slice-orientation was used to image the aortic root region (**Figure 3.5 B**). The iron oxide contrast agent distribution was visualized using the bright blood method of the FLASH sequence: TR/TE = 3/1 milliseconds, with an isotropic image resolution of 98 μm^2 with a 30 x 30 mm^2 transverse field-of-view and a slice thickness of 0.5 mm, BW = 200 kHz, NA = 8, number of echo images 1, excitation pulse = gauss, number of slices = 1, slice thickness = 0.5 mm, duration time = 8 minutes.

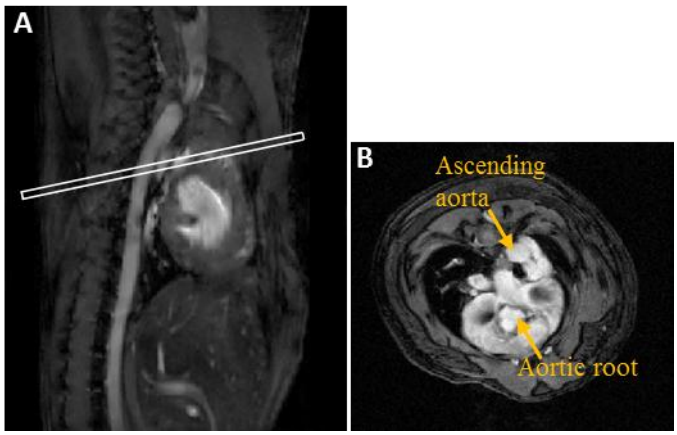

Figure 3.5. Longitudinal FLASH image (A) with the selected slice for the T2*-weighted image acquisition (B).

3.5.4. Data Analysis

The feasibility of P03011 (USPIO-VCAM-1) and P3007 (USPIO) contrast agent was scrutinized by investigating the signal loss within the aortic root from control C57Bl/6 and *ApoE*$^{-/-}$ mice before and after contrast agent administration. T2*-weighted *in vivo* MR images were analyzed for signal to noise ratio (SNR) and contrast to noise ratio (CNR) variations of the signal intensity loss caused by iron oxide nanoparticles. Mean signal intensity (SI) was calculated by drawing a region of interest (ROI) within the aortic lumen to assess the mean blood signal (SI_{blood}) and within the aortic plaque area of the root for the mean plaque signal ($SI_{aortic\ wall}$) estimation (**Figure 3.6**). Due to the time interval between the MR measurements and changing the position of the mouse inside the coil, the parameters such as standard deviation (SD) of the mean background signal and mean blood signal intensity, were measured and utilized as a reference for contrast to noise ratio (CNR) correction (*Michalska, Machtoub et al. 2012*).

SNR values were calculated using the formula (*Kuo and Herlihy 2008; Schroder and Faber 2011*):

$SNR_{pre} = SI_{aortic\ wall\ pre} / SD_{noise\ pre}$

$SNR_{post} = SI_{aortic\ wall\ post} / SD_{noise\ post}$

CNR values were estimated using the following calculations (*Kuo and Herlihy 2008; Klug, Kampf et al. 2009*):

$CNR_{pre} = (SI_{blood\ pre} - SI_{aortic\ wall\ pre}) / SD_{noise\ pre}$

$CNR_{post} = (SI_{blood\ post} - SI_{aortic\ wall\ post}) / SD_{noise\ post}$

The statistical representation of SNR and CNR was demonstrated by 1-way ANOVA test (GraftPad Prism Software). Data were statistically relevant in case of $P<0.05$.

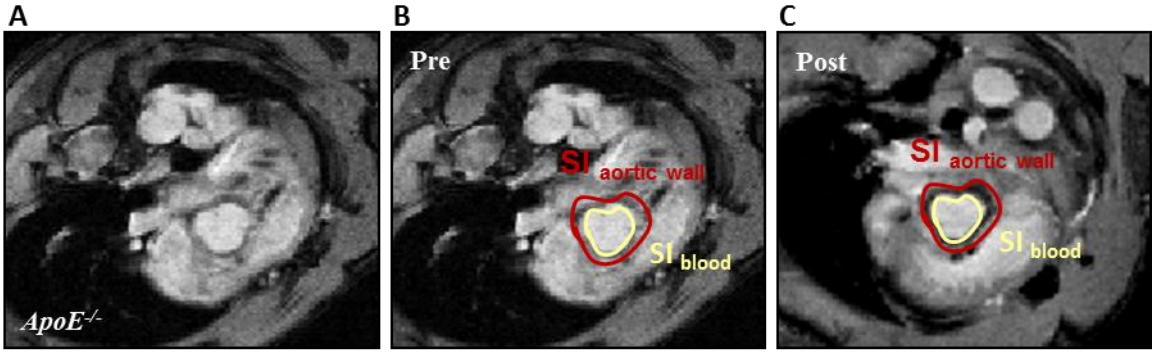

Figure 3.6. T2*-weighted image of aortic root region of atherosclerotic *ApoE*$^{-/-}$ mouse (A, B) prior to and (C) post contrast agent application. (**B**, **C**) Region of interest (ROI), pre and post iron contrast agent injection was drawn within the aortic lumen to assess the mean blood signal (SI_{blood}) and within the aortic plaque area of the root for the mean plaque signal ($SI_{aortic\ wall}$) estimation.

3.6. Histological staining

3.6.1. Tissue preparation

After *in vivo* MRI experiments, the control C57Bl/6 and *ApoE*$^{-/-}$ animals were prepared for further histological examination. After cervical dislocation of the mouse neck, the heart with ascending aorta and other organs including brain, lungs, liver, kidneys, spleen, para-aortic lymph nodes, and skeletal muscle were excised and rinsed with 2 ml of NaCl. All tissue organs were next washed 3 minutes with Phosphate Buffered Saline (PBS), and 5 minutes cooled in isopentane (-20° C) followed by freezing in liquid nitrogen. Organs were then fixed in Tissue-Tek (Sakura, Netherlands) at -24^{o} C degrees in the cryotome and cryosliced at 8 µm for (immune) histology, Haematoxylin & Eosin Staining, Oil Red O Staining, and at 25 µm for Prussian Blue Staining. Prepared tissue sections were kept at room temperature overnight to allow drying of the sliced sections. Dried sections were then transferred into the cooling boxes and kept in -20^{o} C degrees until the beginning of the staining procedure.

3.6.2. Immune-Histological staining

3.6.2.1. CD 68 VCAM-1 double staining

Principle: The distribution of adhesion molecules VCAM-1 (CD106), macrophages (CD68) and their co-localization within the aortic wall of the atherosclerotic mice was demonstrated by immunofluorescent method using specific antibodies linked to the fluorescent dye (immune-double staining).

Reagents:

PBS (Dulbecco, L182-50)	Biochrom
3 % Blocking Goat Serum (S-1000)	Vector Laboratories
10 µg/mL Streptavidin-FITC (SA-5001)	Vector Laboratories
Avidin/Biotin Blocking (SP-2001)	Vector Laboratories
10 µg/mL Streptavidin Alexa Fluor 546 (S11225)	Invitrogen

1μg/mL DAPI Staining (268298) Merck

Vectashield Mounting Medium Vector Laboratories

Antibody targeting Macrophages (CD68):

- 1^{o} primary antibody CD68 (MCA 1957) AbD Serotec

Rat anti mouse (0.25 mg/mL, 1:75 diluted in 3% goat serum)

- secondary biotinylated antibody (BA-9400) Vector Laboratories

Goat anti rat (1:300 diluted in 3% goat serum)

Antibody targeting VCAM-1 (CD106):

- 2^{o} primary VCAM-1 biotinylated Linaris

(0.1 mg/mL, 1:50 diluted in 3% goat serum)

Protocol: After tissue fixation for 5 minutes in ice-cold acetone the prepared 8 μm slides were stained utilizing the following procedure: the dried slides were washed 3 times in PBS, and blocked with 3 % blocking goat serum for 20 minutes. After the blocking step, the slides were incubated with the first primary antibody (CD 68) for 90 minutes, washed 3 times with PBS, and then the secondary biotinylated antibody was added for 30 minutes. Further, the slides were incubated with Streptavidin-FITC mixture for 30 minutes and washed in PBS for 5 minutes. Sections were then blocked by Avidin/Biotin Blocking solution for 15 minutes, and washed in PBS for 5 minutes. Then the second primary VCAM-1 biotinylated antibody was incubated overnight at 4^{o} C. Secondary detection for VCAM-1 was performed using streptavidin-Alexa Fluor 546 solution. Sections were washed in PBS for 5 minutes and counterstained with DAPI for visualization of nuclei, then coverslipped using Vectashield anti-fade mounting medium. Images were taken using a Zeiss Axiovision fluorescent microscope (Carl Zeiss MicroImaging GmbH, Germany).

3.6.2.2. vWF VCAM-1 double staining

Principle: The distribution of adhesion molecules VCAM-1 (CD106) and endothelial cells (vWF) and their co-localization within the aortic wall of the atherosclerotic mice was demonstrated by immune-double staining.

Reagents:

PBS (Dulbecco, L182-50)	Biochrom
3 % Blocking Rabbit Serum (S-5000)	Vector Laboratories
10 µg/mL Streptavidin-FITC (SA-5001)	Vector Laboratories
Avidin/Biotin Blocking Kit (SP-2001)	Vector
10 µg/mL Streptavidin Alexa Fluor 546 (S11225)	Invitrogen
1µg/mL DAPI Staining (268298)	Merck
Vectashield Mounting Medium (H-1000)	Vector Laboratories

Antibody targeting Endothelial cells (vWF):

- 1^{o} primary antibody vWF (ab11713) Abcam

Sheep anti mouse (1:100 diluted in 3 % rabbit serum)

- secondary biotinylated antibody (BA-6000) Vector Laboratories

Rabbit anti sheep (1:300 diluted in 3% rabbit serum)

Antibody targeting VCAM-1 (CD106):

- 2^{o} primary VCAM-1 biotinylated Linaris

(0.1 mg/ml, 1:50 diluted in 3 % rabbit serum)

Protocol: After tissue fixation for 5 minutes in ice-cold acetone the prepared 8 µm slides were stained utilizing the following procedure: the dried slides were washed 3 times in

PBS, and blocked with 3 % blocking rabbit serum for 20 minutes. After the blocking step, the slides were incubated with the first primary antibody (vWF) for 90 minutes, washed 3 times with PBS, and then the secondary biotinylated antibody was added for 30 minutes. Further, the slides were incubated with Streptavidin-FITC mixture for 30 minutes and washed in PBS for 5 minutes. Sections were then blocked by Avidin/Biotin Blocking solution for 15 minutes, and washed in PBS for 5 minutes. Then the second primary VCAM-1 biotinylated antibody was incubated overnight at 4^{o} C. Secondary detection for VCAM-1 was performed using streptavidin-Alexa Fluor 546 solution. Sections were washed in PBS for 5 minutes and counterstained with DAPI for visualization of nuclei, then coverslipped using Vectashield anti-fade mounting medium. Images were taken using a Zeiss Axiovision fluorescent microscope (Carl Zeiss MicroImaging GmbH, Germany).

3.6.2.3. α smooth muscle actin VCAM-1 double staining

Principle: The distribution of adhesion molecules (VCAM-1) and smooth muscle cells (α smooth muscle actin, α SMA) and their co-localization within the aortic wall of the atherosclerotic mice was demonstrated by immune-double staining.

Reagents:

PBS (Dulbecco, L182-50)	Biochrom
3 % Blocking Goat Serum (S-1000)	Vector Laboratories
10 μg/mL Streptavidin-FITC (SA-5001)	Vector Laboratories
Avidin/Biotin Blocking Kit (SP-2001)	Vector Laboratories
10 μg/mL Streptavidin Alexa Fluor 546 (S11225)	Invitrogen
1μg/mL DAPI Staining (268298)	Merck
Vectashield Mounting Medium (H-1000)	Vector Laboratories

Antibody targeting smooth muscle cells (α smooth muscle actin, α SMA):

- 1^{o} primary antibody α SMA (ab7817) Abcam

Rabbit anti mouse (1:100 diluted in 3 % goat serum)

- secondary biotinylated antibody (BA-1000) Vector Laboratories

Goat anti rabbit (1:300 diluted in 3 % goat serum)

Antibody targeting VCAM-1 (CD106):

- 2^{o} primary VCAM-1 biotinylated Linaris

(0.1 mg/ml, 1:50 diluted in 3 % goat serum)

Protocol: After tissue fixation for 5 minutes in ice-cold acetone the prepared 8 μm slides were stained utilizing the following procedure: the dried slides were washed 3 times in PBS, and blocked with 3 % blocking goat serum for 20 minutes. After the blocking step, the slides were incubated with the first primary antibody (α SMA) for 90 minutes, washed 3 times with PBS, and then the secondary biotinylated antibody was added for 30 minutes. Further, the slides were incubated with Streptavidin-FITC mixture for 30 minutes and washed in PBS for 5 minutes. Sections were then blocked by Avidin/Biotin Blocking solution for 15 minutes, and washed in PBS for 5 minutes. Then the second primary VCAM-1 biotinylated antibody was incubated overnight at 4^{o}C. Secondary detection for VCAM-1 was performed using streptavidin-Alexa Fluor 546 solution. Sections were washed in PBS for 5 minutes and counterstained with DAPI for visualization of nuclei, then coverslipped using Vectashield anti-fade mounting medium. Images were taken using a Zeiss Axiovision fluorescent microscope (Carl Zeiss MicroImaging GmbH, Germany).

3.6.3. Staining of the tissue / cell structure

3.6.3.1. Haematoxylin Eosin (H&E) Staining

Principle: Morphology, structure, and the composition of the diverse cells within the aortic wall of the control and atherosclerotic mice were shown by Haematoxylin Eosin (H&E) Staining according to the Lillie Mayer's method (*Fischer, Jacobson et al. 2008*).

Reagents:

Haematoxylin

3g Haematoxylin (3816.2)	Roth
0.5g Natriumjodat (6525)	Merck
125g Aluminiumkaliumsulfate (1.01042)	Merck
125g Chloralhydrate (1.02425)	Merck
2.5g Citric Acid	
add 2.5 ml distilled water	

Bluing Agent

Eosin

1g Eosin (1.5935)	Merck
add 100 ml distilled water	

96% Ethanol	Sigma Aldrich
Xylene (16446)	Sigma Aldrich
Rotihistol (6640.2)	Roth
Entellan, Mounting Medium (1.07960)	Merck

Protocol: After 5 minutes washing in distilled water, all 8 µm slides were incubated with haematoxylin for 10 minutes, rinsed with distilled water for 10 minutes. The sections were then washed in distilled water and incubated with eosin for 5 minutes, dehydrated in 100 % ethanol, followed by Xylene and Rotihistol for 5 minutes each and cover slipped. The H&E stained images were acquired with the magnification of x 10 and x 20 and analyzed with SPOT Basic software (SPOT Imaging Solutions-Diagnostic Instruments, Inc, USA).

3.6.3.2. Oil Red O Staining

Principle: Lipids within the aortic wall of the atherosclerotic mice were detected by Oil Red O Staining.

Reagents:

0.5 g Oil Red O stock solution (00625) Sigma-Aldrich

100 ml Isopropanol (1.09634) Merck

30 ml Oil Red working solution

20 ml Distilled water

Glycerol-Gelatine

10 g Gelatin

60 ml Distilled Water

70 ml Glycerol

0.25 g Phenol

Protocol: 8 µm sections of mouse aortas were fixed in 4 % formaldehyde and washed in distilled water for 10 minutes. After this step the slides were in 60% isopropanol and stained with fresh Oil Red O solution for 15 minutes. Again submerged in 60 % isopropanol for 5 minutes slides were counterstained in haematoxylin for 3 minutes for the nuclear stain. The slides were then rinsed with distilled water and imbedded in glycerol gelatine. The Oil Red O stained images were acquired with the magnification of x 20 and x 40 and analyzed with SPOT Basic software (SPOT Imaging Solutions-Diagnostic Instruments, Inc, USA) (*Kinkel, Fernyhough et al. 2004*).

3.6.3.3. Prussian Blue (PB) Staining

Principle: Iron oxide particles within the aortic wall of the atherosclerotic mice were detected using the method described by Mallory.

Reagents:

-20°C Aceton (32201)	Sigma-Aldrich
-20°C Methanol (32213)	Sigma-Aldrich
Potassium hexacyano-ferrate (1.04984)	Merck
37% Hydrochloric Acid (1.00317)	Merck
0.1% Nuclear-fast Red (1.15939)	Merck

Working solution

5% Potassium Ferrocyanide

5% Hydrochloric Acid

Entellan, Mounting Medium (1.07960)	Merck

Protocol: The 25 µm sections of the mouse aortic wall were fixed in cold acetone and methanol (1:1) for 10 minutes. After drying slides were incubated in working solution for 30 minutes, rinsed with distilled water, counterstained with nuclear fast red solution for 5 minutes, washed, dehydrated in Ethanol and cover slipped. The images were taken with Zeiss light microscope (Axioskop 2 plus). The iron stained images were acquired with the magnification of x 20 and x 40 and analyzed with SPOT Basic software (SPOT Imaging Solutions-Diagnostic Instruments, Inc, USA) (*Schroeter, Saleh et al. 2004*).

3.6.3.4. Picrosirius Red Staining

Principle: The collagen within the aortic wall of the atherosclerotic mice was detected by picrosirius red staining (*Junqueira, Bignolas et al. 1979*).

Reagents:

Picric Acid (80450)	Fluka

Sirius Red

0.1 % in picric acid

1L distilled water

96 %, 75 %, 50 % Ethanol

Xylene-Rotihistol

Protocol: The sections were stained in picrosirius red for 20 minutes, washed in distilled water for 2 times, dehydrated in 96 %, 75 %, and 50 % ethanol, followed by Xylene-Rotihistol incubation and cover slipped. The images of each section were recorded under bright field with the magnification of x 20 and x 40 and analyzed with SPOT Basic software (SPOT Imaging Solutions-Diagnostic Instruments, Inc, USA).

3.7. Pharmacokinetics (PK)

3.7.1. Blood sample preparation

Control C57Bl/6 and *ApoE*$^{-/-}$ mice were prepared for pharmacokinetics assessment of P03011 (USPIO-VCAM-1) and P3007 (USPIO) particles. The control and atherosclerotic mice were firstly anaesthetized with 2.5 % isoflurane 0.2 L/min oxygen and placed under the fume adsorber. 600 µmol/ kg body weight of P03011 (USPIO-VCAM-1) and P3007 (USPIO) contrast agent was injected intravenously and the blood samples were taken from the eye via retro-orbital bleed after 30 minutes, 2 hours, 5 hours, and 24 hours and further collected into microtainer SST tubes (BD Becton, Dickinson Company, NJ, USA). The control blood samples from the mice without application of contrast agent were also collected. The samples were further centrifuged 2 minutes at 13000 g and serum was taken for ICP-ES analysis to estimate the iron content within the plasma at different time after the blood collection (*Michalska, Machtoub et al. 2012)*.

3.7.2. Inductively coupled plasma emission spectroscopy (ICP-ES) measurement

200 µl of the serum samples taken from the animals before and after 30 minutes, 2, 5, and 24 hours after contrast agent application, were transferred into the special glass tubes made from quartz. The quartz tubes containing serum were then filled with 1 ml of 65 % HNO_3 and incubated for 10 hours at 160-170^{o} C degree. Prior to the measurements the quartz

samples were diluted with ultrapure water. The iron content within the samples was determined as mg/L via ICP-ES (Horiba Jobin Yvon GmbH, France).

3.7.3. Data Analysis

The circulation time of nanoparticles was calculated by the following equation: $N(t)=N_0e^{-bt}$ and fitted via the nonlinear least square fit: $T_{1/2}=\log(2)/b$, $dT_{1/2}=(\log(2)db)/b^2$. N_0 means the original amount of iron particles that declines within time, N(t) is the iron content that rests and has not yet disappeared after a time t, and $T_{1/2}$ is the half-life time of the declining contrast agent, fitted value b is linked to half-life time ($T_{1/2}$), the db is the error of the fitted value b, and $dT_{1/2}$ is the error of the half-life time (*Michalska, Machtoub et al. 2012*).

3.8. Electron Microscopy (EM)

Principle: Beside histological examination of iron oxide nanoparticles within the aortic wall of the atherosclerotic mice, these particles were further examined and visualized utilizing electron microscopy device from Zeiss EM10. Electron microscopy method enables, more than histology, investigation of iron nanoparticles localization in the extra- and intracellular compartments.

Reagents:

2.5 % Glutaraldehyde	Sigma-Aldrich
50 mM cacodylate pH 7.2 50 mM KCl, 2.5 mM $MgCl_2$	
Cacodylate	Sigma-Aldrich
Osmium tetroxide (OsO_4)	Sigma-Aldrich
0.5 % uranyl acetate	Sigma-Aldrich
100 % Ethanol	Sigma-Aldrich

Protocol: Hearts containing the aortic root were fixed with 2.5 % glutaraldehyde for 12 hours at 4° C. Embedded hearts were washed three times for 5 minutes with 50 mM cacodylate (pH 7.2) and then fixed 2 hours at 4°C with 2 % osmium tetroxide mixed with 50 mM cacodylate (pH 7.2). Hearts were then washed with H_2O and stored overnight at 4°C with 0.5 % uranyl acetate (in H_2O). After incubation, the tissue of the embedded hearts was dehydrated in ethanol, fixed in Epon812 and ultrathin sectioned. Ultrathin sections were either analyzed directly or stained with 2 % uranyl acetate (in ethanol) followed by lead citrate. Nanoparticles were best visible on ultrathin sections that were not post stained. Sections were analyzed with a Zeiss EM10 and EM900 (Zeiss, Oberkochen, Germany). Negatives were digitalized by scanning and processed by Adobe Photoshop (*Prufert, Vogel et al. 2004; Michalska, Machtoub et al. 2012*).

4. Results

4.1. Characterization of atherosclerotic plaques

The experiments within the first part of this thesis were designed in order to investigate the involvement of diverse immune cells and the contribution of vascular cell adhesion (VCAM-1) molecules in the early lesions and advanced plaque progression. Aortic wall morphology of control C57Bl/6 and atherosclerotic *ApoE*$^{-/-}$ mice aged 12 and 30 weeks was presented by histological staining utilizing haematoxylin and eosin (H&E) stain method and Prussian Blue staining. Analysis of immune cell distribution and their co-localization with VCAM-1 molecules within early and advanced atherosclerotic plaques was presented by double immunofluorescent staining.

4.1.1. Early atherosclerotic plaques

The observation of the aortic wall of young 12 week old *ApoE*$^{-/-}$ mice fed a high cholesterol diet for 8 weeks showed that these mice developed mild lesions which appeared within ascending aorta (**data not shown**, and **Figure 4.1**). The aortic root regions of these 12 week old *ApoE*$^{-/-}$ mice revealed explicit changes (**Figure 4.1**) characterized by recruited leukocytes into subendothelium. The thickening process at the early stage was modest and occurred only to a lower extent at the atheroma-prone sites retaining the media region unaltered. In contrast to visible changes within ascending aorta from young 12 week old atherosclerotic *ApoE*$^{-/-}$ mice, control C57Bl/6 mice kept on a normal chow diet did not develop any lesions (**Figure 4.1**). The morphology of the control C57Bl/6 root region represented the normal intimal and medial areas of aortic wall.

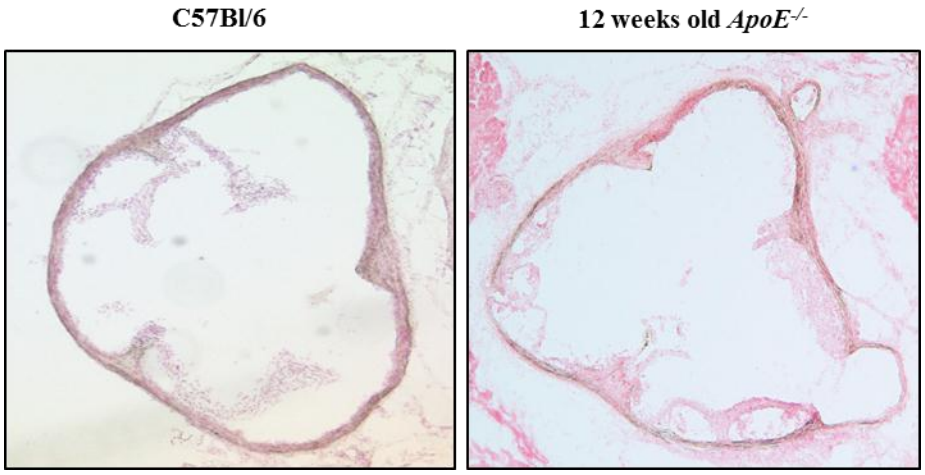

Figure 4.1. Morphology of the aortic wall from control C57Bl/6 and 12 week old atherosclerotic *ApoE*$^{-/-}$ mice (representative image of histological examinations from n=3 mice, magnification x5).

The cellular distribution of endothelial cells, macrophages, and smooth muscle cells within aortic root region from young *ApoE*$^{-/-}$ mice was further analyzed by immunofluoresent method. The distribution of fat droplets (detected by Oil Red O Staining) and collagen deposition (detected by Picrosirus Staining) was also performed (**Figure 4.2** and **Figure 4.3**). The young 12 week old *ApoE*$^{-/-}$ mice exposed to high fat diet developed mild lesions which composed of newly recruited leukocytes mostly monocytes. The phagocytosis process of oxidized lipoproteins was also presented in the young atherosclerotic plaques within aortic root region (**Figure 4.2 B**).

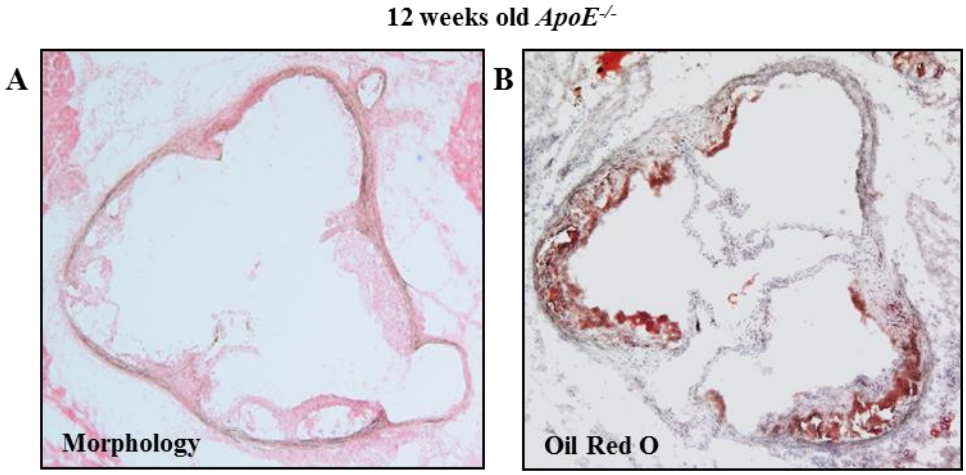

Figure 4.2. Distribution of the fat droplets demonstrated by red stained region on Oil Red O staining image (B) within the early plaques of aortic root region from 12 week old *ApoE*$^{-/-}$ mice (A) (representative image from n=3 *ApoE*$^{-/-}$ mice, magnification x5).

The fat droplets presented by Oil Red O staining were distributed within the intimal endothelial and smooth muscle cells as well as within the deeper region of the formed plaques where the recruited macrophages as foam cells were detected (**Figure 4.2 B** and **Figure 4.3 C-E**). The endothelial cells presented by von Willenbrand factor (vWF) immunofluorescent staining were localized throughout the intimal region of atherosclerotic wall (**Figure 4.3 C**). The content of newly recruited macrophages of young 12 week old *ApoE*$^{-/-}$ mice was demonstrated by CD68 immunofluorescent staining (**Figure 4.3 D**). The monocytes/macrophages appeared within the atheroma-prone sites and further localized as foam cells abundantly within the subendothelial region of formed early plaques. The smooth muscle cells migration into intimal region of the aortic root from 12 week old *ApoE*$^{-/-}$ mice was also observed (**Figure 4.3 E**). These immune staining pointed already the manifestation of inflammatory process within young plaques. Besides the large macrophage colony within the early lesions, these plaques were also characterized by the substantial collagen deposits within the regions where the intimal smooth muscle cells resided (**Figure 4.3 F**). The immunofluorescent staining of vascular cell adhesion molecules (**Figure 4.3 B**) showed that the VCAM-1 expression appeared in the intimal line where endothelial, smooth muscle cells resided and demonstrated their co-localization with VCAM-1 (**Figure 4.3 B**, **C**, **E**). Further in the deeper region of the plaque where the macrophages were present, the strong VCAM-1 expression emerged (**Figure 4.3 B**, **D**). The VCAM-1 upregulation was also highly detected within the medial smooth muscle cells in the elastic lamina regions (**Figure 4.3 B**, **E**).

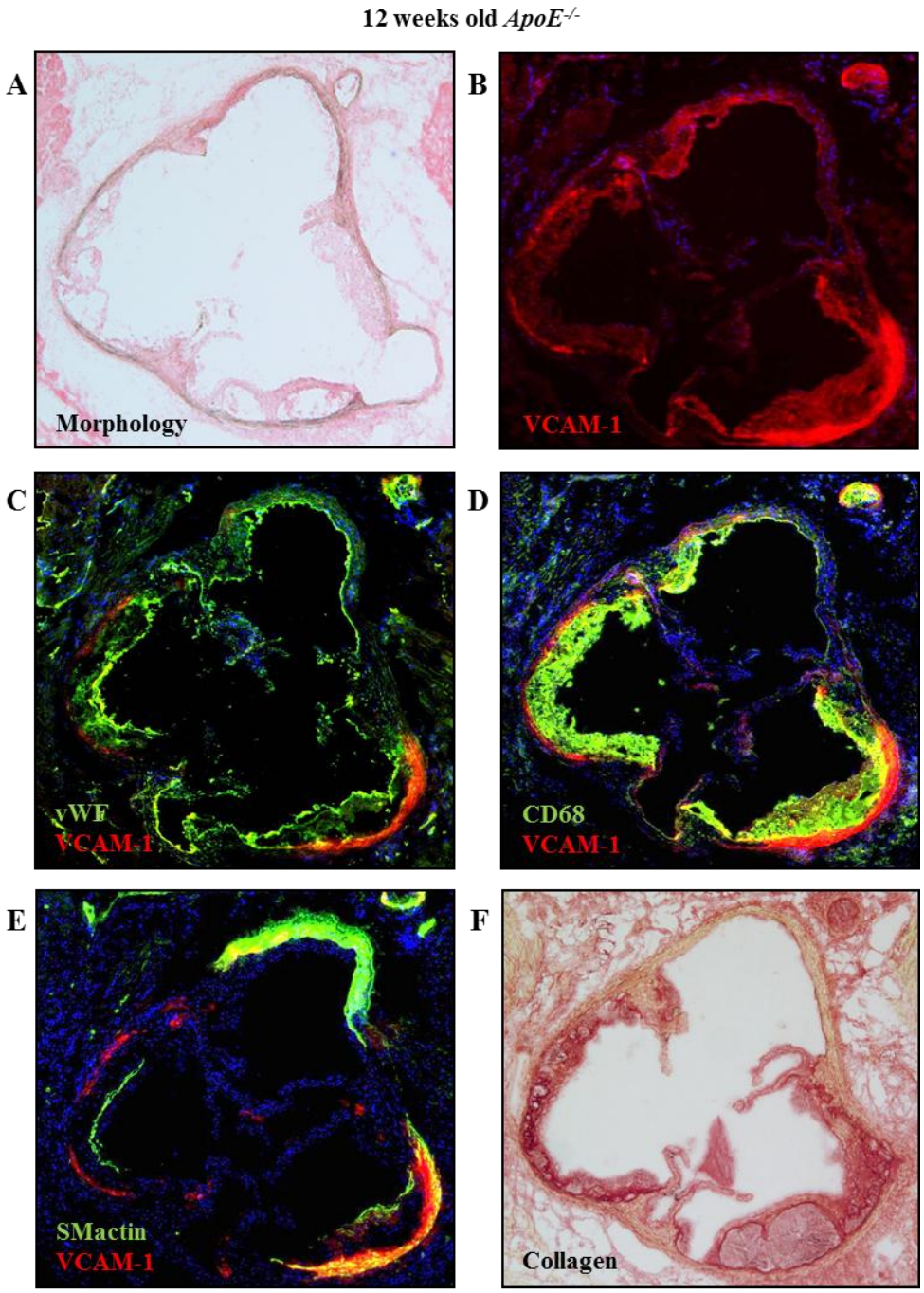

Figure 4.3. Cellular distribution and VCAM-1 molecules (CD106) expression pattern within the aortic root region from 12 week old atherosclerotic *ApoE*$^{-/-}$ mice. (**A**) Morphology of the aortic root from young 12 week old *ApoE*$^{-/-}$ mice, (**B**) Immunofluorescent staining of VCAM-1 (CD106) within the intima and media, (**C-E**) Double immunofluorescent staining of VCAM-1 (red stain) within endothelium (vWF) (green stain), macrophages (CD68) (green stain), and smooth muscle cells (SM actin) (green stain). Yellow merge represents co-localization of VCAM-1 molecules with endothelium (vWF), macrophages (CD68), and smooth muscle cells (SMactin). (**F**) Collagen deposition within the intimal and medial region. Representative images of histological examinations from n=3 mice, magnification x5.

4.1.2. Advanced atherosclerotic plaques

The experiments within this work revealed that *ApoE*$^{-/-}$ mice fed a high fat diet for 26 weeks possessed mature plaques within ascending aorta affecting aortic root, aortic arch, and the bifurcation region. Besides the marked changes within ascending aorta, the enhanced and sophisticated inflammatory process affected also the descending aorta leading to lesions' development within abdominal region (**data not shown**). The composition of the advanced plaques within ascending and descending aorta was similar and composed of foam cells which created the fibrous cap. These plaques were characterized further by the presence of necrotic cores beneath the fibrous cap. The morphology of the aortic wall within the aortic root of intimal and medial region was significantly altered. In contrast to the young *ApoE*$^{-/-}$ mice, the thickening process of aortic root region was homogenous and occurred throughout the whole aortic wall. Driven by the enhanced chronic inflammation, the advanced thickening process caused the narrowing of lumen and provoked further changes within the medial elastic lamina regions (**Figure 4.4**).

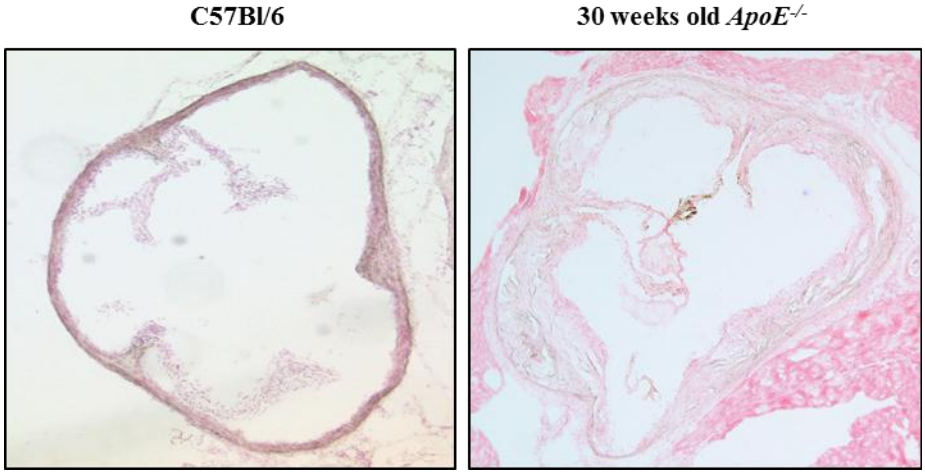

Figure 4.4. Morphology of the aortic wall from control C57Bl/6 and 30 week old atherosclerotic *ApoE*$^{-/-}$ mice (representative image of histological examinations from n=3 mice, magnification x5).

The cellular distribution of diverse immune cells involved in the advanced plaque formation was demonstrated by double immunofluorescent staining. The fat and collagen deposition was indicated by Oil Red O and Picrosirus Staining (**Figure 4.5** and **Figure 4.6**). 30 week old *ApoE*$^{-/-}$ mice demonstrated fat droplets within the intimal region where endothelial and smooth muscle cells occurred and also deeper in the subendothelial fibrous cap region and necrotic core where foamy and apoptotic macrophages were localized (**Figure 4.5 B** and **Figure 4.6 C-E**).

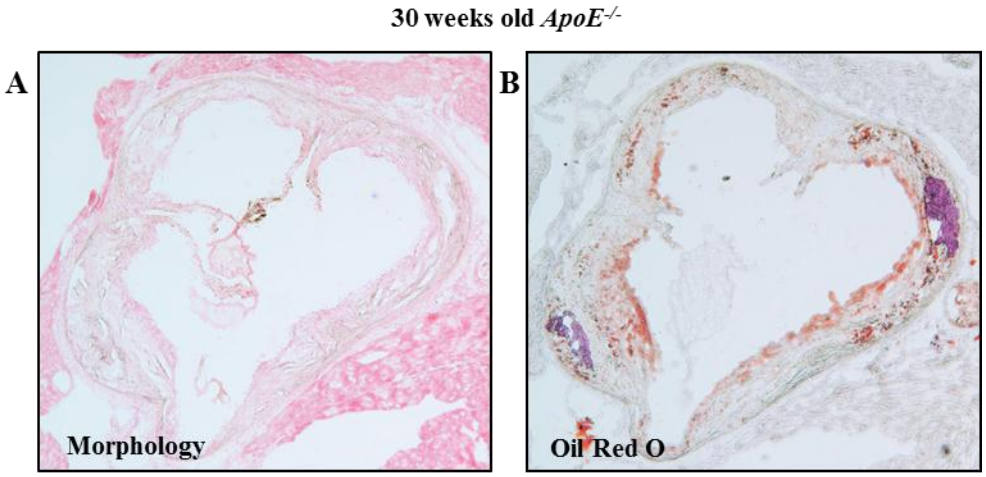

Figure 4.5. Distribution of the fat droplets demonstrated by red stained region on Oil Red O staining image (B) within the advanced plaques of aortic root region from 30 week old *ApoE*$^{-/-}$ mice (A) (representative image from n=3, magnification x5).

Within advanced plaques immune cells were broadly distributed and altered the plaque composition (**Figure 4.6**). These plaques were characterized by presence of foamy and fibrous lesions and differed from the early plaques (**Figure 4.1** and **Figure 4.4**). Macrophages, presented by CD68 immunofluorescent staining, appeared as foamy cells within the fibrous region and to a lower extent within the region of necrotic core of 30 week old *ApoE*$^{-/-}$ mice (**Figure 4.6 D**). The necrotic core of advanced plaques contained besides foamy macrophages also smooth muscle cells and was characterized by the presence of apoptotic cells. The smooth muscle cells, demonstrated by immunofluorescent staining of α-smooth muscle actin (SM actin), were found within intimal and deeper regions of the advanced lesions (**Figure 4.6 E**). Collagen deposits were abundantly detected within intima where smooth muscle cells were present and also deeper within the necrotic core region where medial smooth muscles emerged (**Figure 4.6 F**). The staining of vascular cell adhesion molecules (**Figure 4.6 B**) revealed enhanced VCAM-1 expression within the endothelial as well as intimal smooth muscle cells (**Figure 4.6 B, C,** and **E**). Further VCAM-1 was detected in the deeper region of the fibrous plaque localized to foamy macrophages (**Figure 4.6 D**) and also within the medial smooth muscle cells (**Figure 4.6 E**).

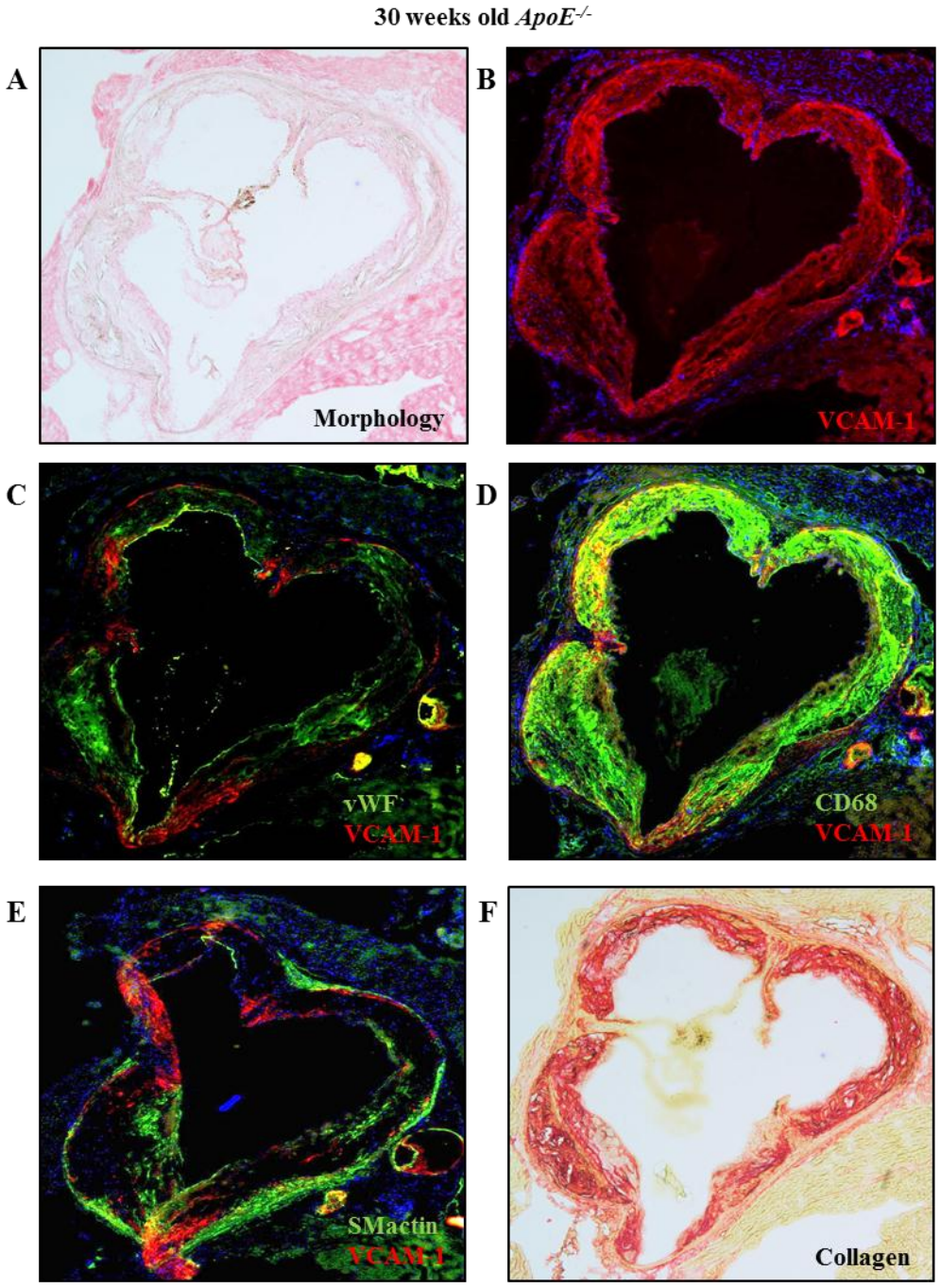

Figure 4.6. Cellular distribution and VCAM-1 molecules (CD106) expression pattern within the aortic root region from 30 week old atherosclerotic *ApoE*$^{-/-}$ mice. (**A**) Morphology of the aortic root from 30 week old *ApoE*$^{-/-}$ mice, (**B**) Immunofluorescent staining of VCAM-1 (CD106) within the intima and media region, (**C-E**) Double immunofluorescent staining of VCAM-1 (red stain) within endothelium (vWF) (green stain), macrophages (CD68) (green stain), and smooth muscle cells (SM actin) (geen stain). Yellow merge represents co-localization of VCAM-1 molecules with endothelium (vWF), macrophages (CD68), and smooth muscle cells (SMactin). (**F**) Collagen deposition within the intimal and medial region. Representative images of histological examinations from n=3 mice, magnification x5.

4.2. *Ex vivo* validation studies of newly developed USPIO particles conjugated to the specific VCAM-1 binding peptide

The second part of this thesis focused on determination of newly developed ultrasmall superparamagnetic iron oxide (USPIO) particles conjugated to VCAM-1 peptide (P03011) as a potential agent for visualization and monitoring the VCAM-1 expression within the immune cells involved in the pathogenesis of atherosclerosis. Non-conjugated USPIOs were also utilized as control particles for evaluation of particle unspecific binding. The structure of the non- and targeted iron oxide nanoparticles was demonstrated by electron microscopy, their superparamagnetic characteristics by magnetic resonance measurement at 17.6T MR system. The optimal injection dose of USPIO-VCAM-1 and USPIO was determined in MR experiments of *ex vivo* agar phantoms of atherosclerotic root region. The assessment of imaging time and pharmacokinetic analysis as well as biodistribution studies were performed by inductively coupled plasma emission spectroscopy and histology.

4.2.1. Characterization of USPIO conjugated to the VCAM-1 peptide

The synthetized 5 nm iron core of ultrasmall superparamagnetic iron oxide particles possessed a layer which consisted of gem-bisphosphonate compounds $(CH(PO_3H_2)_2)_n$ that covered the particles (*Patent number WO2004/058 275, US 2004/253181, Guerbet Research France*). The particle covering layer of gem-bisphosphonate compounds was either conjugated to the specific cyclic VCAM-1 peptide via a carboxylate (RCOO-) group (USPIO-VCAM-1) or not (USPIO). Both of the particles were stabilized with the polyethylene glycol (PEG) chain (*Patent number WO2004/058 275, US 2004/253181, Guerbet Research France*). The diameter of the ultrasmall superparamagnetic iron oxide particles was 26 nm and the iron particle size, its dispersion property with (USPIO-VCAM-1) or without (USPIO) vascular cell adhesion molecule-1 binding peptide was assessed by electron microscopy. The iron oxide USPIO-VCAM-1 (P03011) as well as USPIO (P3007) particle demonstrated homogenous dispersion and spherical size. Both of nanoparticles maintained and preserved stability in the solution (**Figure 4.7**).

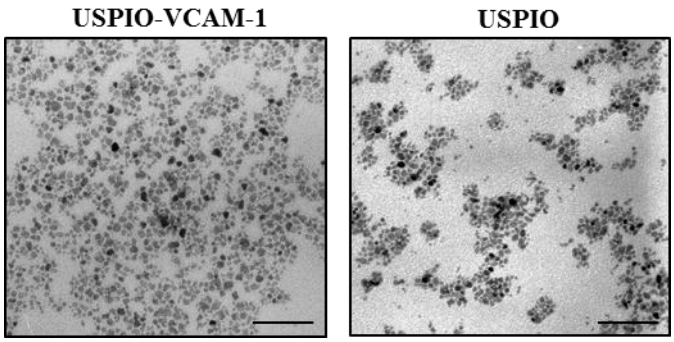

Figure 4.7. The structure of USPIO-VCAM-1 (P03011) and control USPIO (P3007) contrast agent demonstrated by electron microscopy. Representative images n= 2. Scale bar is around 1 µm.

After verification of the iron oxide structure, USPIO-VCAM-1 (P03011) and USPIO (P3007) contrast agents were further measured at 17.6 T MR system in order to test the superparamagnetic characteristics of both nanoparticles. Measurement of iron oxide T2 relaxation time and fitted T2 map at different concentration of iron oxide enabled to establish the relaxivity rate (r2) which constituted at 98 mM^{-1} s^{-1} (**Figure 4.8 A-B**). In the presence of the gradually increasing concentration of iron oxide (Fe) contrast agent the measured relaxivity rate (r2) raised linearly (**Figure 4.8 A-B**).

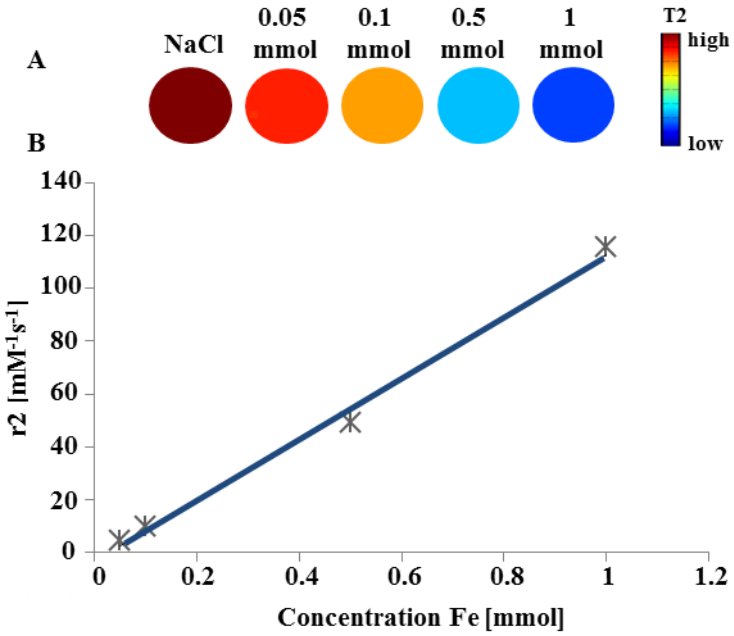

Figure 4.8. (A) T2 map at different concentration of iron oxide particles. (B) The relaxivity rate (r2) of USPIO particles measured at 17.6 T MR System in the presence of increasing amount of iron particles.

4.2.2. Half-life time of USPIO particles conjugated to the VCAM-1 peptide

As USPIO-VCAM-1 as well as USPIO nanoparticles were newly developed for *in vivo* animal application, pharmacokinetic analyses of both components in the control C57Bl/6 and *ApoE*$^{-/-}$ mice were conducted subsequently. Half-life time assessment of USPIO-VCAM-1 (P03011) and control USPIO (P3007) particles was calculated by measuring the blood clearance before and after injection of both nanoparticles by inductively coupled plasma emission spectrometry (ICP-ES). Serum samples, which were collected before the injection of USPIO-VCAM-1 and control USPIO from the healthy control C57Bl/6 and atherosclerotic *ApoE*$^{-/-}$ mice, were measured firstly. The analyzed serum samples prior to the injection of both nanoparticles revealed no detectable iron content. Further the serum samples from the intravenously injected control and atherosclerotic *ApoE*$^{-/-}$ mice treated with either USPIO-VCAM-1 or USPIO alone were examined at 30 minutes, 2 hours, 5 hours, and 24 hours. The concentration of iron particles in the collected serum samples of *ApoE*$^{-/-}$ mice at 30 minutes after 600 µmol/kg dose of USPIO-VCAM-1 (P03011) application was calculated to be around 598.23±124.4 mg iron/L. The iron content in the serum samples of *ApoE*$^{-/-}$ mice analyzed at 24 hours post USPIO-VCAM-1 (600 µmol/kg) injection reverted virtually to the base line with the iron concentration of 10.44±2.88 mg iron/L. The measured clearance of the iron oxide from the blood samples of *ApoE*$^{-/-}$ mice at the different time points enabled the assessment of the half-life time of USPIO-VCAM-1 contrast agent, which was calculated to be about 4±2.4 hours in *ApoE*$^{-/-}$ mice (**Figure 4.9**).

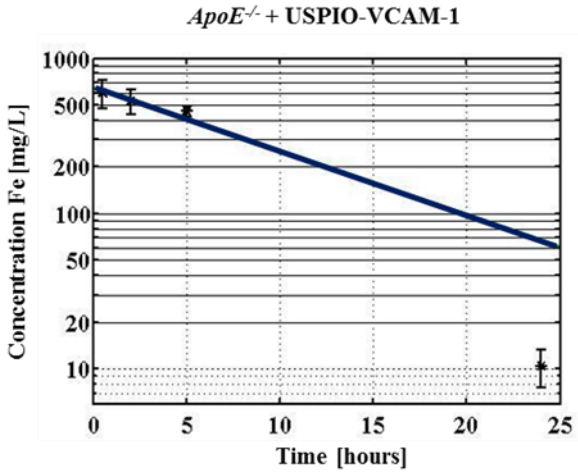

Figure 4.9. Serum concentration of iron oxide particles measured as mg/L prior and 30 minutes, 2 hours, 5 hours, and 24 hours after intravenous injection of USPIO-VCAM-1 (P03011) agent in the *ApoE*$^{-/-}$ mice (n=5). The estimation of iron oxide was performed via ICP-ES measurement.

In contrast, the measured serum sample of USPIO-VCAM-1 injected control C57Bl/6 mice (600 µmol/kg) after 30 minutes post-injection showed the iron content of around 715.54±53.21 mg iron/L. The iron content in the serum sample of control mice was roughly cleared with the calculated value of 75.48±21.1 mg iron/L within 24 hours.

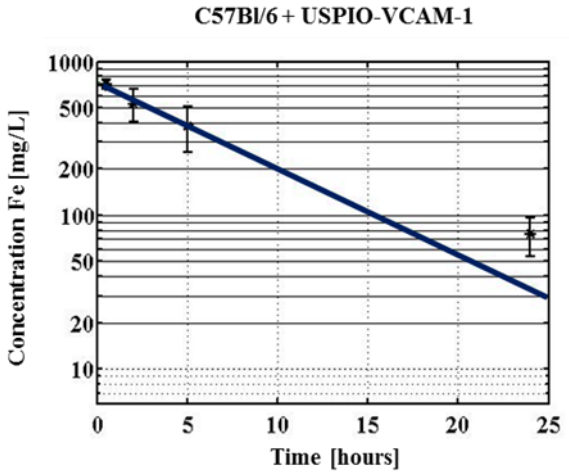

Figure 4.10. Serum concentration of iron oxide (Fe) particles measured as mg/L prior and 30 minutes, 2 hours, 5 hours, and 24 hours after intravenous injection of USPIO-VCAM-1 (P03011) agent in the control C57Bl/6 mice. The estimation of iron oxide was performed via ICP-ES measurement (n=5). This figure was published in a similar format in (*Michalska, Machtoub et al. 2012*).

The estimated half-life time of USPIO-VCAM-1 particles in the control group of C57Bl/6 mice was 7.2±2.5 hours (**Figure 4.10**). The pharmacokinetic analyses of iron clearance from *ApoE*$^{-/-}$ mice injected with 600 µmol/kg of USPIO (P3007) demonstrated the high iron content in the serum samples collected after 30 minutes post-injection and resulted in the concentration of 660.62±8.8 mg iron/L. The high USPIO iron oxide amount was cleared from the blood stream within 24 hours and reverted to the level of 21.94±8.03 mg iron/L. The calculated half-life time of USPIO in *ApoE*$^{-/-}$ mice was 6.0±1.3 hours (**Figure 4.11**).

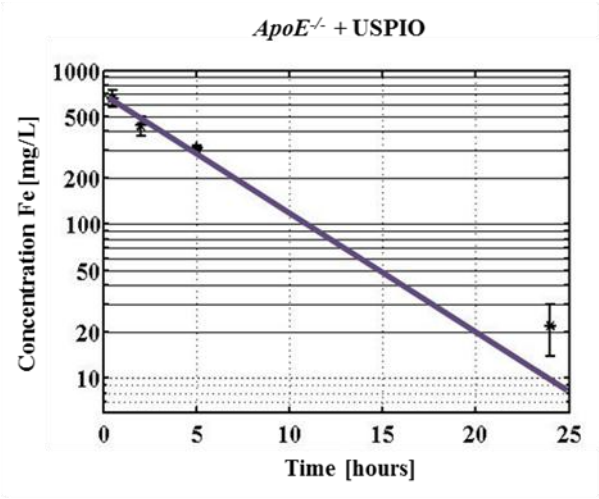

Figure 4.11. Serum concentration of iron oxide (Fe) particles measured as mg/L prior and 30 minutes, 2 hours, 5 hours, and 24 hours after intravenous injection of USPIO (P3007) agent in the atherosclerotic *ApoE*$^{-/-}$ mice. The estimation of iron oxide was performed via ICP-ES measurement (n=5). This figure was published in a similar format in (*Michalska, Machtoub et al. 2012*).

In control C57Bl/6 mice the analyzed iron content in the serum samples after 30 minutes post 600 µmol/kg of USPIO (P3007) injection was about 792.16±196.83 mg iron/L. After 24 hours the iron concentration within the serum samples of control mice decreased to the level of 53.26±21.4 mg iron/L. The half-life time of USPIO in the control C57Bl/6 mice was calculated to be about 5.0±1.7 hours (**Figure 4.12**).

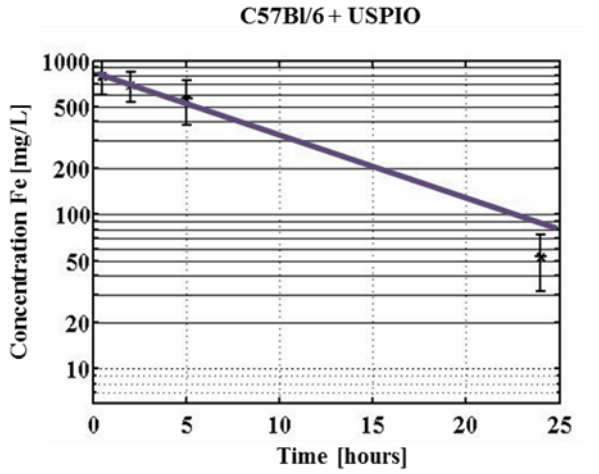

Figure 4.12. Serum concentration of iron oxide (Fe) particles measured as mg/L prior and 30 minutes, 2 hours, 5 hours, and 24 hours after intravenous injection of USPIO (P3007) agent in the control C57Bl/6 mice. The estimation of iron oxide was performed via ICP-ES measurement (n=5). This figure was published in a similar format in (*Michalska, Machtoub et al. 2012*).

The assessment of USPIO-VCAM-1 (P03011) and USPIO (P3007) particles clearance enabled to estimate the optimal *in vivo* imaging time. Due to the fact that USPIO-VCAM-1 and USPIO particles were cleared from the blood stream within 24 hours, the control C57Bl/6 and *ApoE*$^{-/-}$ animals were intended for MR imaging pre and 24 hours post contrast agent application.

4.2.3. Biodistribution of USPIO particles conjugated to the VCAM-1 peptide

Following the completion of pharmacokinetics studies, the biodistribution was performed. The localization of USPIO-VCAM-1 and USPIO particles within the excised organs as liver, lungs, spleen, lymph nodes, kidneys, brain, and muscle from control C57Bl/6 and *ApoE*$^{-/-}$ mice was determined by Prussian Blue staining. Young and old *ApoE*$^{-/-}$ mice were injected with 600 μmol/kg dose of USPIO-VCAM-1 (P03011) particles and excised organs were analyzed pre and 24 hours post particle application. The *ApoE*$^{-/-}$ mice injected with USPIO-VCAM-1 demonstrated massive amount of iron oxide nanoparticles within the liver and the spleen (**Figure 4.13 A-C**). The positions where these particles were distributed were mostly associated to macrophages within the whole liver and the splenic red pulp (**Figure 4.13 A**). P03011 particles were also identified histologically in the lymph node especially within subcapsular sinus and in the cortex and medulla region of the kidneys (**Figure 4.13 B**). Additionally to that, lungs, brain, and skeletal muscles were free from iron particles (**Figure 4.13 C**). The same results were observed within the group of control C57Bl/6 mice injected with 600 μmol/kg dose of USPIO-VCAM-1 particles (**data not shown**).

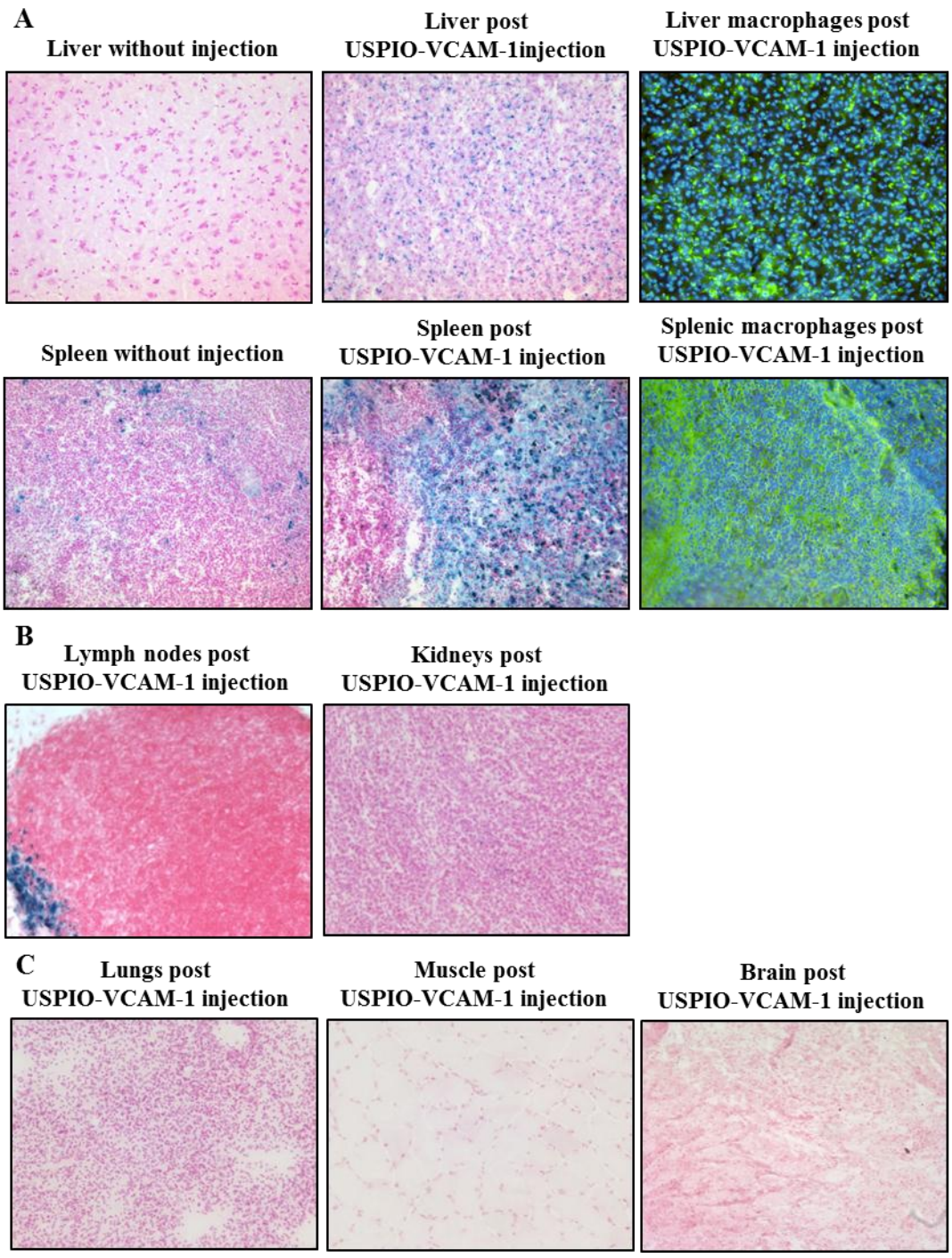

Figure 4.13. Distribution of USPIO-VCAM-1 particles within dissected organs from *ApoE*$^{-/-}$ mice. (**A**, **B**) While not found before injection, iron oxide particles were localized to macrophages within the liver, and spleen, as well as within the lymph nodes and the kidneys. (**C**) There was no iron deposition in the lung, skeletal muscle or brain. Representative images from n= 6. This figure was published in a similar format in (*Michalska, Machtoub et al. 2012*).

In contrast, injection of 600 µmol/kg dose of USPIO particles resulted in iron accumulation mostly within the liver and the spleen of young and old *ApoE*$^{-/-}$ mice analyzed 24 hours post contrast agent application (**Figure 4.14 A**). There was no iron particles observed within the lymph nodes, kidneys, skeletal muscles, lungs, or brain (**Figure 4.14 B**). Control USPIO injected C57Bl/6 mice (600 µmol/kg dose) emerged the same findings as USPIO injected *ApoE*$^{-/-}$ mice (**data not shown**).

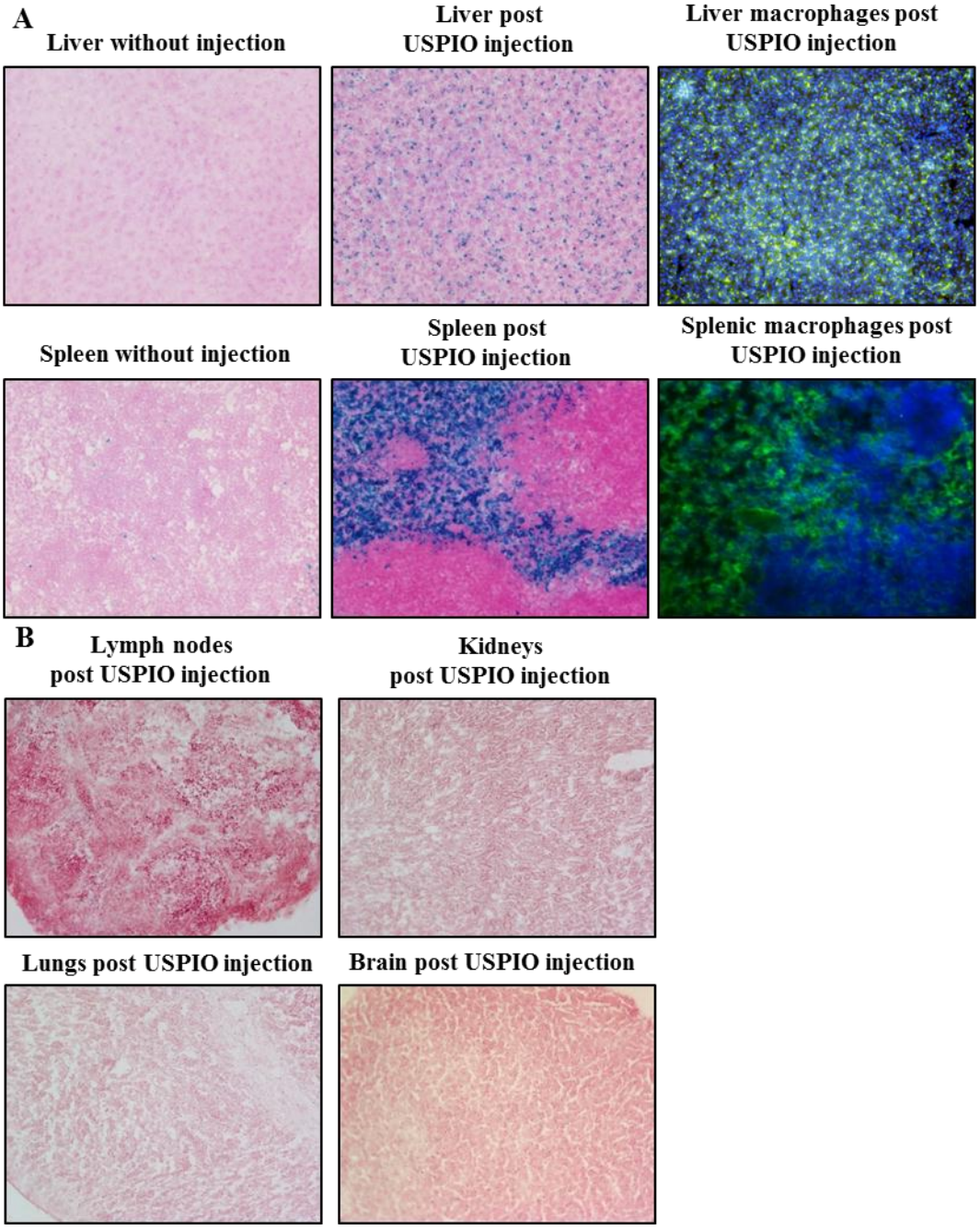

Figure 4.14. (A) Localization of USPIO particles within the liver and spleen of *ApoE*$^{-/-}$ mice. (**B**) There was no iron deposition in the kidneys, lung, skeletal muscle or brain. Representative images from n= 6.

4.2.4. *Ex vivo* dose-dependent evaluation of USPIO-VCAM-1 for *in vivo* application

Feasibility of USPIO-VCAM-1 contrast agent application together with control USPIO particles was investigated via *ex vivo* MR measurement of the agar phantoms containing aortic root regions from control C57Bl/6 and atherosclerotic *ApoE*$^{-/-}$ mice. Initially agar phantoms of aortic root region from non-injected control and atherosclerotic mice were measured. The non-injected agar phantoms of aortic roots from control C57Bl/6 as well as *ApoE*$^{-/-}$ mice demonstrated no darkening within aortic wall (**Figure 4.15**).

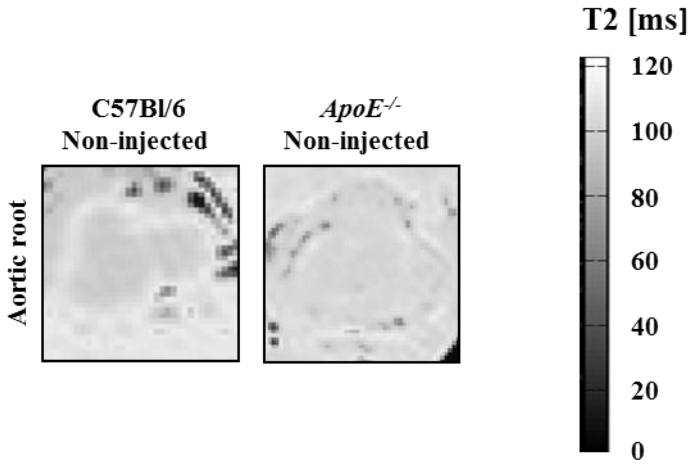

Figure 4.15. T2-weighted images of *ex vivo* agar phantoms of aortic root regions from control C57Bl/6 and *ApoE*$^{-/-}$ mice (n=3). T2 map of control and atherosclerotic root region signified the T2 time of 120 milliseconds.

Further there was dose-dependent study of USPIO-VCAM-1 and USPIO performed. These experiments were planned in order to determine optimal injection dose that could assure the best MR contrast visible *in vivo*. The dose of 100, 300, and 600 μmol/kg dose of USPIO-VCAM-1 and USPIO was *in vivo* applied into *ApoE*$^{-/-}$ mice and the aortic root regions were further excised after 24 hours and MR measured. *Ex vivo* MR measurements of aortic root regions from *ApoE*$^{-/-}$ mice injected with either 100 or 300 μmol/kg dose emerged no significant alterations. The calculated T2 maps from these phantoms confirmed and pointed the similar T2 time of 100 milliseconds as in the case of non-injected control and *ApoE*$^{-/-}$ mice. However the injection of 600 μmol/kg dose of USPIO-VCAM-1 particles demonstrated significant signal loss within the atherosclerotic lesions of aortic wall pointing also the decline in T2 relaxation time from 100 to 10 milliseconds (**Figure 4.16**).

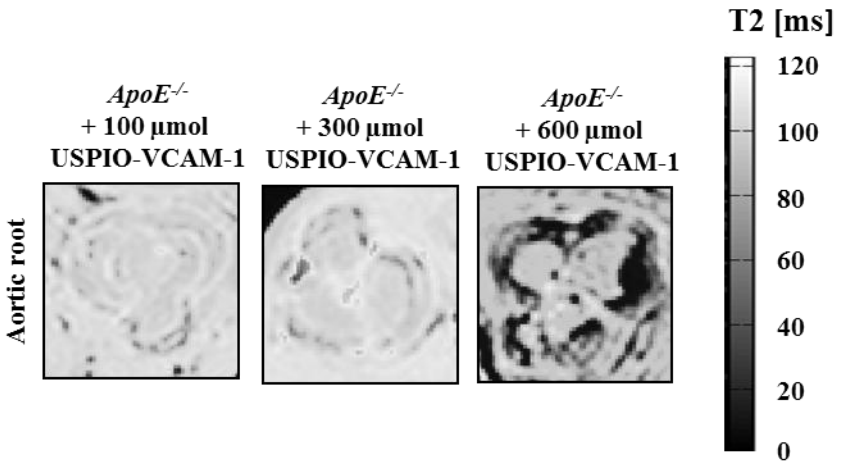

Figure 4.16. T2-weighted images of aortic root from USPIO-VCAM-1 injected *ApoE*$^{-/-}$ mice (n=3). The *ex vivo* measurements were conducted 24 hours after contrast agent application and have indicated significant darkening within the aortic wall after injection of 600 µmol/kg dose.

As the dose of 600 µmol/kg USPIO-VCAM-1 particles, examined after 24 hours, demonstrated significant signal loss within the aortic roots of *ApoE*$^{-/-}$ mice measured in agar phantoms, this dose was selected for all subsequent *ex vivo* and *in vivo* MR experiments.

4.2.5. *Ex vivo* determination of early and advanced lesions by newly developed USPIO particles conjugated to the VCAM-1 peptide

To test the USPIO-VCAM-1 specific binding to vascular cell adhesion (VCAM-1) molecules expressed within early and advanced inflamed lesions, aortae from 12 and 30 week old healthy control C57Bl/6 and *ApoE*$^{-/-}$ mice were excised and investigated as next. *Ex vivo* MR measured agar phantoms of aortic root region from 12 and 30 week old C57Bl/6 mice, excised 24 hours after intravenous injection of 600 µmol/kg dose of USPIO-VCAM-1, indicated no signal loss within the aortic wall (**data not shown**). Whereas *ex vivo* agar phantoms of atherosclerotic root regions from young and old *ApoE*$^{-/-}$ mice, injected with USPIO-VCAM-1 and analyzed after 24 hours, revealed significant alterations. The group of 12 week old *ApoE*$^{-/-}$ mice injected with 600 µmol/kg dose of USPIO-VCAM-1 particles were examined first and the *ex vivo* MR measurements of the young atherosclerotic roots demonstrated significant partial darkening associated with the contrast agent injection (**Figure 4.17 A**). The *ex vivo* T2-weighted MR images of agar

phantoms from 30 weeks old *ApoE*$^{-/-}$ mice injected with 600 µmol/kg dose of USPIO-VCAM-1 particles revealed very strong signal loss within the whole aortic root region of advanced plaques (**Figure 4.17 B**).

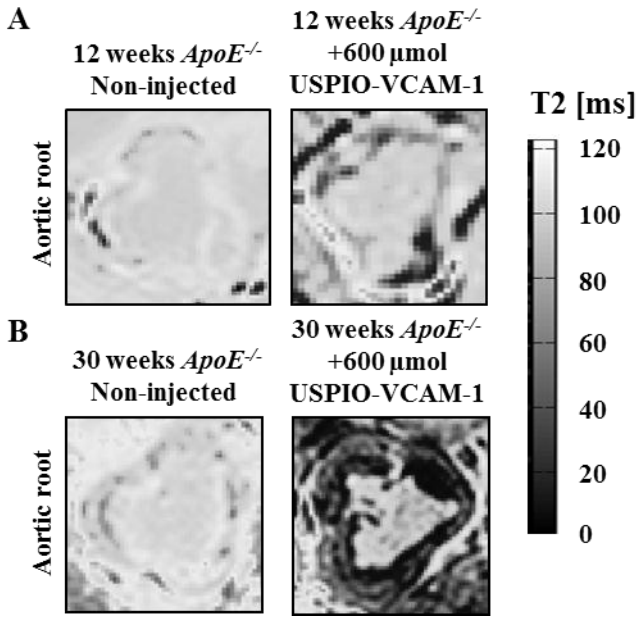

Figure 4.17. T2-weighted images of aortic root from USPIO-VCAM-1 injected 12 and 30 week old *ApoE*$^{-/-}$ mice (n=3). Significant signal loss within aortic root of (**A**) 12 week old and (**B**) 30 week old *ApoE*$^{-/-}$ mice injected with 600 µmol/kg USPIO-VCAM-1 particles.

While not observed in the healthy control group of C57Bl/6 mice, 600 µmol/kg dose of newly developed USPIO-VCAM-1 contrast agent enabled firstly *ex vivo* detection of the early and advanced inflammatory process within the aortic root from 12 and 30 week old *ApoE*$^{-/-}$ mice by MR imaging. Further *ex vivo* T2-weighted images of USPIO-VCAM-1 injected *ApoE*$^{-/-}$ mice allowed observing the thickening process of the arterial wall. The MR measurements were compared with the histological observations from the 12 and 30 week old *ApoE*$^{-/-}$ mice and confirmed these findings (**Figure 4.18 A-D**).

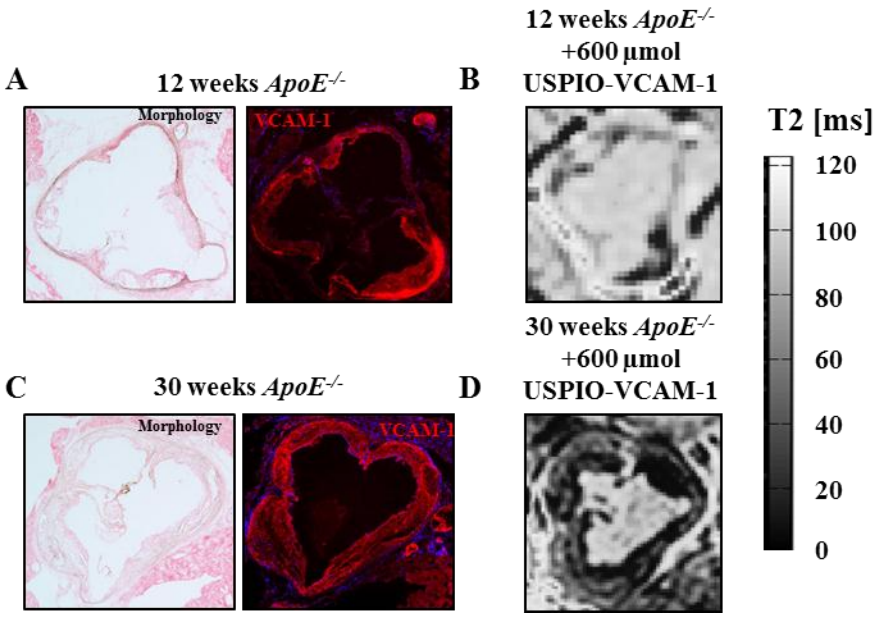

Figure 4.18. Histological and MR assessment of the inflammation within early and advanced lesions from atherosclerotic *ApoE*$^{-/-}$ mice (n=3). (**A**) Morphology and VCAM-1 expression (red stain) within the aortic root of the young plaques from 12 week old *ApoE*$^{-/-}$ mice, (**B**) T2-weighted image of aortic root from 12 week old *ApoE*$^{-/-}$ mice measured after USPIO-VCAM-1 application, (**C**) Morphology and VCAM-1 expression within the aortic root of the advanced plaques from 30 week old *ApoE*$^{-/-}$ mice, (**D**) T2-weighted image of aortic root from 30 week old *ApoE*$^{-/-}$ mice measured after USPIO-VCAM-1 injection.

Application of USPIO-VCAM-1 particles into 12 week old *ApoE*$^{-/-}$ mice revealed a significant partial signal loss within the aortic wall observed on T2-weighted images, in areas where strong VCAM-1 expression was detected via histology (**Figure 4.18 A-B**). In the group of 30 week old *ApoE*$^{-/-}$ mice, application of USPIO-VCAM-1 particles demonstrated strong and significant darkening within the arterial wall. The signal loss observed on T2-weighted *ex vivo* MR images of advanced lesions was correlated with the strong and expanded VCAM-1 expression within intima and media of atherosclerotic aortic wall presented by histological staining. With the help of *ex vivo* MR images and histology it was feasible to localize the USPIO-VCAM-1 particles within the early and advanced lesions where the VCAM-1 expression was detected and further estimate the thickness of the aortic wall within the 12 and 30 week old *ApoE*$^{-/-}$ mice (**Figure 4.18 B, D**).

As next USPIO contrast agent was examined *ex vivo* and compared to USPIO-VCAM-1 particles within the group of healthy control C57Bl/6 as well as 12 and 30 week old *ApoE*$^{-/-}$ mice. *Ex vivo* MR measurements of agar phantoms containing aortic roots of 12 and 30 week old healthy control C57Bl/6 mice showed no signal loss after application of

600 µmol/kg dose of USPIO particles (**data not shown**). The agar phantoms containing aortic root regions of 12 week old *ApoE*$^{-/-}$ mice, measured 24 hours post 600 µmol/kg dose of USPIO injection, indicated no alterations within the aortic wall (**Figure 4.19 A**). Only application of USPIO particles into 30 week old *ApoE*$^{-/-}$ mice demonstrated mild signal alterations within aortic root detected on T2-weighted *ex vivo* images (**Figure 4.19 B**).

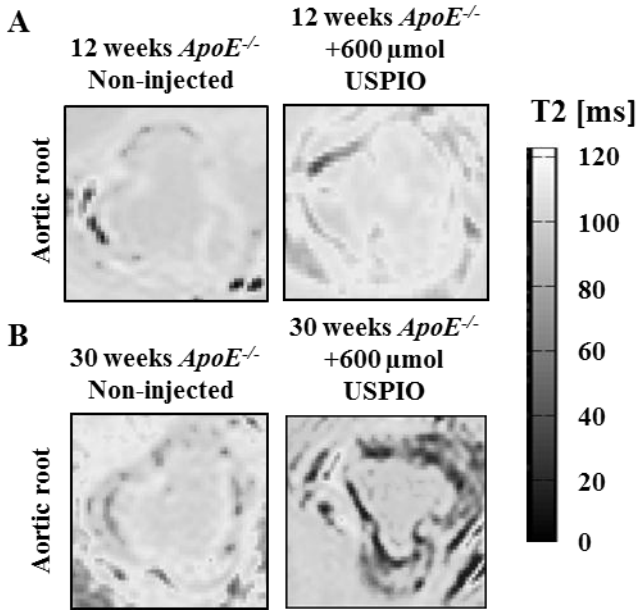

Figure 4.19. T2-weighted images of aortic root from USPIO injected 12 and 30 week old *ApoE*$^{-/-}$ mice (n=3). (**A**) No alteration observed within aortic root of 12 week old and (**B**) mild signal loss within aortic root of 30 week old *ApoE*$^{-/-}$ mice injected with 600 µmol/kg dose of USPIO particles.

Comparing non- and targeted approach, USPIO-VCAM-1 particles visualized significantly early and advanced lesions of 12 and 30 week old *ApoE*$^{-/-}$ mice *ex vivo*. In contrast, USPIO particles did not provide with notable results. Application of USPIO particles did not allow to assess early lesions of 12 week old *ApoE*$^{-/-}$ mice *ex vivo*. Within advanced plaques USPIOs caused the darkening however the signal loss was not significant when compared to detected USPIO-VCAM-1 particles (**Figure 4.20**).

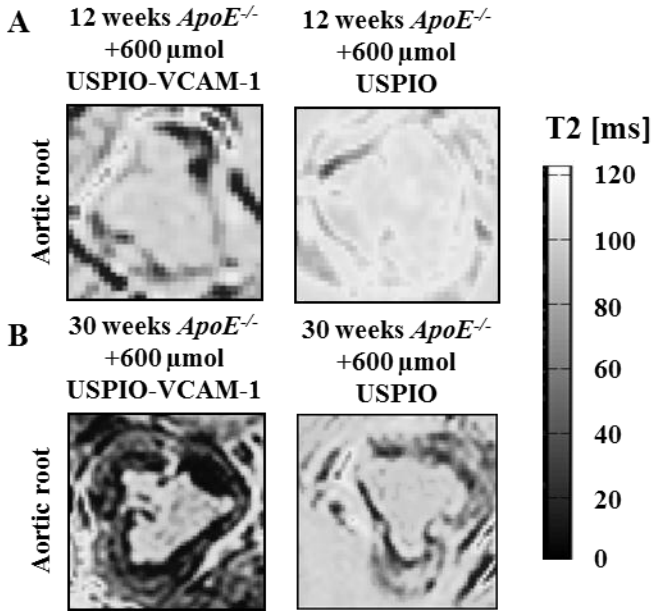

Figure 4.20. Visualization of the early and advanced atherosclerotic plaques from 12 and 30 week old *ApoE*$^{-/-}$ mice (n=3). (**A**) T2-weighted MR images of 12 week old *ApoE*$^{-/-}$ mice injected with either USPIO-VCAM-1 or USPIO particles, (**B**) T2-weighted MR images of 30 week old *ApoE*$^{-/-}$ mice injected with either USPIO-VCAM-1 or USPIO particles.

4.3. *In vivo* application of newly developed iron oxide nanoparticles

After completion of *ex vivo* validation studies on iron oxide nanoparticles conjugated with (USPIO-VCAM-1) or without (USPIO) specific cyclic VCAM-1 peptide, both of nanoparticles were implemented and tested *in vivo*. These experiments were designed in 12 and 30 week old healthy control C57Bl/6 and atherosclerotic *ApoE*$^{-/-}$ mice and performed at 17.6 T ultra-high magnetic field.

4.3.1. *In vivo* determination of early and advanced lesions by newly developed USPIO conjugated to the VCAM-1 peptide

Ex vivo experimental part on USPIO-VCAM-1 and USPIO particles allowed firstly to assess the structure of iron oxide nanoparticles, their superparamagnetic characteristics, and further to establish the half-life time for optimal imaging time, and the most favorable injection dose. As dose of 600 µmol/kg iron oxide USPIO-VCAM-1 particles gave the best appreciable contrast and significant signal loss within the aortic root of 12 and 30 week old

ApoE$^{-/-}$ mice, observed in *ex vivo* MR experiments, this dose was implemented in all *in vivo* MR experiments. Applied 600 μmol/kg dose of control non-targeted USPIO particles revealed non-significant and only light darkening within aortic root of 30 week old *ApoE*$^{-/-}$ mice in *ex vivo* MR measured agar phantoms. In spite of that, USPIO particles were also applied in *in vivo* experiments and compared with the results obtained from targeted USPIO-VCAM-1 particles.

Prior to the final *in vivo* MR examination of control C57Bl/6 and *ApoE*$^{-/-}$ mice, the *in vivo* preliminary MR trial was conducted in order to verify optimal *in vivo* MR imaging time with that proposed by pharmacokinetic data. As first the group of control C57Bl/6 mice was injected with 600 μmol/kg dose of USPIO-VCAM-1 and USPIO contrast agent and analyzed at 1 hour, 6 hours, and 24 hours by ultra-high MRI. Regarding to the pharmacokinetic data (**Figure 4.10** and **4.12**) both of the nanoparticles circulated in the blood stream at 1 hour and 6 hours. It was also difficult to obtain the clear MR image of the whole aorta as well as of the aortic root region at that time. In both cases, USPIO-VCAM-1 and USPIO content declined from the blood within 24 hours and at this time point high signal to noise image of the whole aorta and the aortic root was obtained using FLASH MR sequence (**Figure 4.10** and **4.12**, **data not shown**). Good correlation between *in vivo* MRI and pharmacokinetic analyses (**Figure 4.9** and **4.11**) was also observed within the group of *ApoE*$^{-/-}$ mice. *In vivo* MRI, acquired 1 hour post 600 μmol/kg dose of USPIO-VCAM-1, hindered to image aorta and aortic root region (**Figure 4.21**).

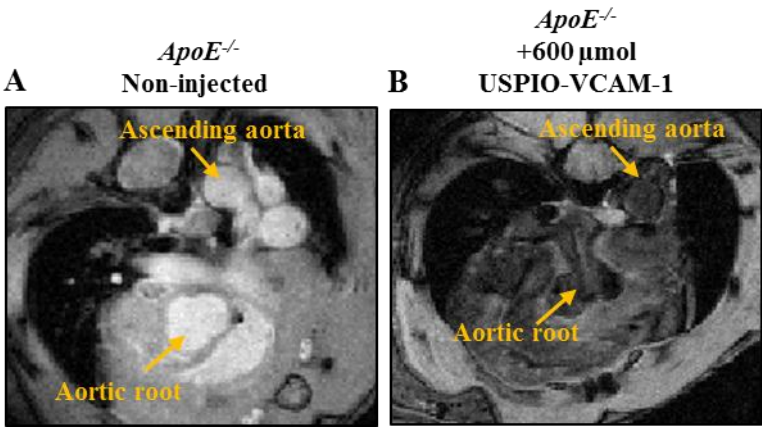

Figure 4.21. ***In vivo*** **MR T2*-weighted images of aortic root region from** ***ApoE***$^{-/-}$ **mice (n=3) obtained via FLASH sequence (A) prior to and (B) 1 hour after injection of 600 μmol/kg USPIO-VCAM-1 particles.**

Further MR acquisition of aorta and aortic root 6 hours post contrast agent application did not allow to visualize aorta without the noise (**Figure 4.22**).

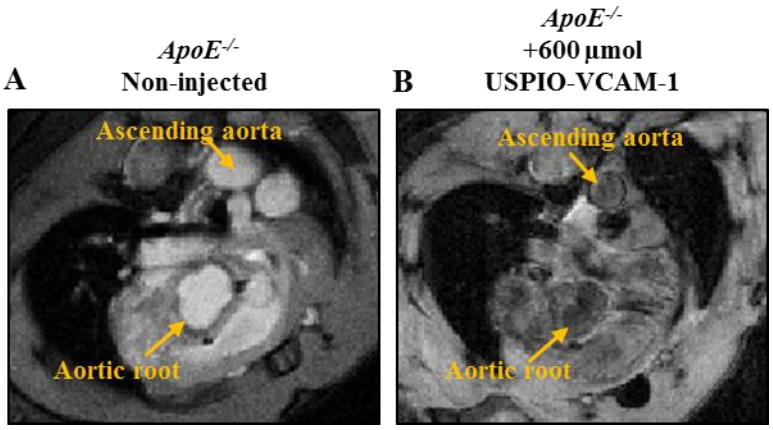

Figure 4.22. ***In vivo*** **MR T2*-weighted images of aortic root region from** ***ApoE*****$^{-/-}$ mice (n=3) obtained via FLASH sequence (A) prior to and (B) 6 hours after injection of 600 µmol/kg USPIO-VCAM-1 particles.**

These initial findings gave the evidence that the best time for imaging was 24 hours, when all particles were cleared from the blood stream as confirmed by pharmacokinetics analysis (**Figure 4.9 - 4.12**, and **Figure 4.23**).

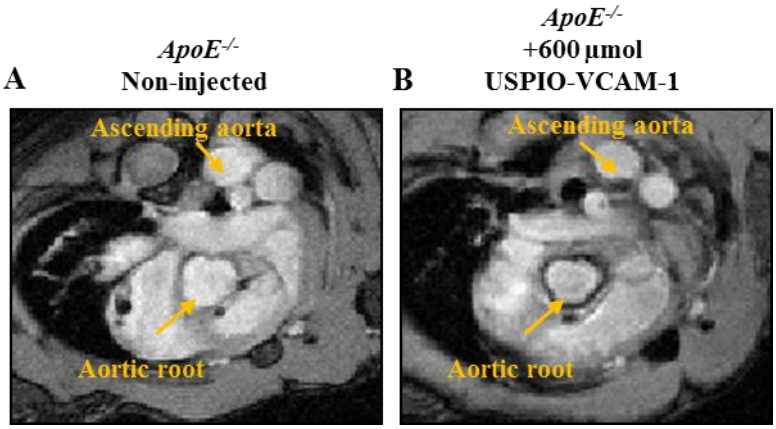

Figure 4.23. ***In vivo*** **MR T2*-weighted images of aortic root region from** ***ApoE*****$^{-/-}$ mice (n=3) obtained via FLASH sequence (A) prior to and (B) 24 hours after injection of 600 µmol/kg USPIO-VCAM-1 particles.**

After completion of the initial *in vivo* MR experiments, aorta and aortic roots pre and 24 hours post injection of 600 µmol/kg USPIO-VCAM-1 and USPIO particles were visualized within 12 and 30 week old healthy control C57Bl/6 and *ApoE*$^{-/-}$ mice. Ultra-high resolved T2*-weighted images of the aortic root areas from healthy control C57Bl/6 mice

demonstrated no signal loss within the aortic wall pre and post injection of USPIO-VCAM-1 particles (**Figure 4.24 A - B**). Signal intensity within the aortic root pre and 24 hours post USPIO-VCAM-1 application in the 12 and 30 week old control C57Bl/6 mice was analyzed by calculating the SNR and CNR values. Signal to noise ratio (SNR) was defined as the signal intensity measured within the arterial wall ($SI_{aortic\ wall}$) pre and 24 hours post contrast agent injection. In addition to SNR, the CNR value was determined. Contrast to noise ratio (CNR) value characterized the signal intensity derived from the blood (SI_{blood}) and aortic wall ($SI_{aortic\ wall}$) pre and post contrast agent injection (detailed information described in Method chapter: 3.5.4. Data Analysis). The SNR as well as the CNR values within the 12 and 30 week old control group pre and post application of USPIO-VCAM-1 particles remained unaltered (**Figure 4.29 A - B**).

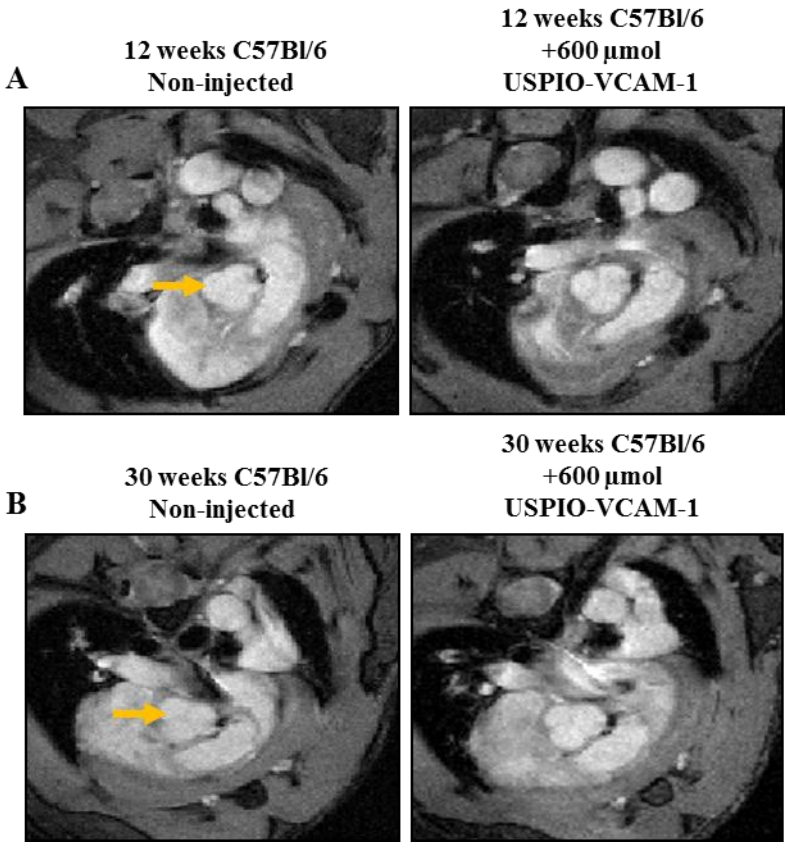

Figure 4.24. *In vivo* ultra-high field MR images of 12 and 30 week old control C57Bl/6 mice. (**A**) T2*- weighted image of young 12 week old C57Bl/6 mice pre and 24 hours post USPIO-VCAM-1 injection, (**B**) T2*-weighted image of 30 week old C57Bl/6 mice pre and 24 hours post USPIO-VCAM-1 injection. Representative images from n= 6. Yellow arrows indicate aortic root region.

The group of atherosclerotic *ApoE*$^{-/-}$ mice was analyzed as next. The intravenous injection of 600 µmol/kg dose of USPIO-VCAM-1 particles into 12 week old *ApoE*$^{-/-}$ mice with

early lesions showed the partial still significant signal loss within the aortic wall demonstrated on T2*-weighted MR images (**Figure 4.25 A**). The same significant but more intense observation was done within the group of 30 week old *ApoE*$^{-/-}$ mice with advanced plaques (**Figure 4.25 B**). This group of *ApoE*$^{-/-}$ mice treated with USPIO-VCAM-1 particles presented notable darkening within the aortic root area.

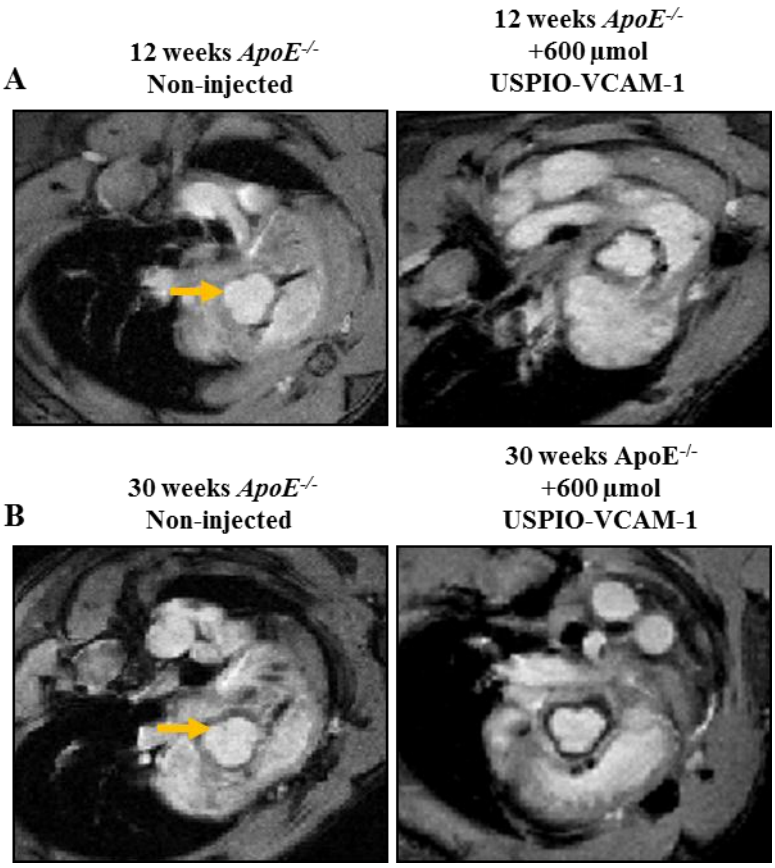

Figure 4.25. *In vivo* ultra-high field MR images of 12 and 30 week old *ApoE*$^{-/-}$ mice. (**A**) T2*-weighted image of young 12 week old *ApoE*$^{-/-}$ mice pre and 24 hours post USPIO-VCAM-1 injection noticed as partial signal loss within arterial wall. (**B**) T2*-weighted image of 30 week old *ApoE*$^{-/-}$ mice pre and 24 hours post USPIO-VCAM-1 injection detected as marked, darkening within the aortic wall. Representative images from n= 6. Yellow arrows indicate aortic root region. This figure was published in a similar format in (*Michalska, Machtoub et al. 2012*).

The quantified SNR values of 12 and 30 week old *ApoE*$^{-/-}$ mice injected with USPIO-VCAM-1 particles significantly declined when compared to the SNR values before injection (**Figure 4.29 A**). Additionally, the CNR values of 12 week old *ApoE*$^{-/-}$ mice pointed 2 fold alteration post USPIO-VCAM-1 injection and almost 3 fold increase in 30 week old *ApoE*$^{-/-}$ mice treated with targeted particles. As the signal variations increased within aortic root region 24 hours post USPIO-VCAM-1 injection, the CNR values

remained positive (**Figure 4.29 B**). The SNR and CNR semi-quantification highlighted the relevance of detected signal loss within the early and advanced lesions of 12 and 30 week old *ApoE*$^{-/-}$ mice injected with USPIO-VCAM-1 contrast agent. In addition, the analysis of *ex vivo* and *in vivo* results correlated well and revealed the same findings (**Figure 4.26**). The extent of the signal loss associated with the application of targeted USPIO-VCAM-1 particles was slight within the early lesions detected by *ex vivo* and *in vivo* MR experiments (**Figure 4.26 A**). The *in vivo* signal loss pattern post USPIO-VCAM-1 injection appeared stronger and was more excessive within the advanced lesions also confirmed by *ex vivo* MR results (**Figure 4.26 B**).

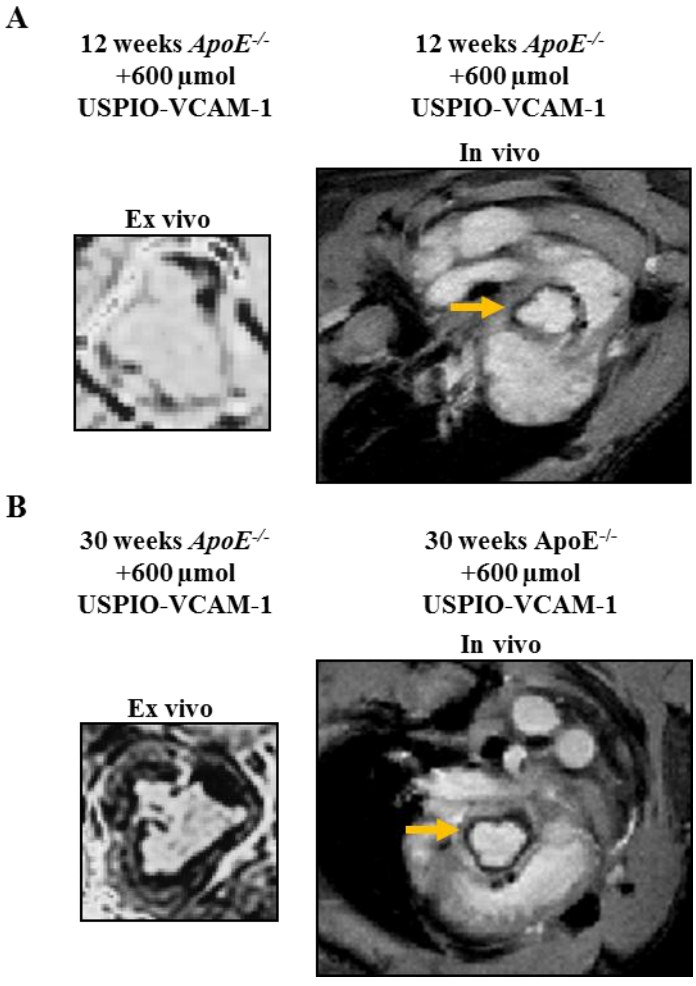

Figure 4.26. Determination of the inflammatory process within early and advanced plaques by USPIO-VCAM-1 particles. (**A**) *Ex vivo* (n=3) and *in vivo* (n=6) MR images of partial signal loss within the aortic root region of early lesions detected by application of targeted iron oxide nanoparticles. (**B**) *Ex vivo* (n=3) and *in vivo* (n=6) MR images of intensive darkening within the aortic root of advanced lesions detected by application of USPIO-VCAM-1. Yellow arrows indicate aortic root region.

The use of targeted iron oxide USPIO-VCAM-1 contrast agent revealed interesting results within the group of 12 and 30 week old *ApoE*$^{-/-}$ mice and led to assessment of the early and advanced plaques. To check the specificity of applied USPIO-VCAM-1 and to verify the significance of obtained *ex vivo* and *in vivo* results, USPIO particles were also tested and applied *in vivo*. Control 12 and 30 week old C57Bl/6 mice were analyzed pre and 24 hours post 600 µmol/kg dose of USPIO injection as first. *In vivo* application of non-targeted USPIO particles emerged no darkening within aortic root of healthy control mice (**Figure 4.27**). The calculated SNR and CNR values from young and old control C57Bl/6 mice pre- and post-USPIO administration remained unchanged (**Figure 4.29 A, B**).

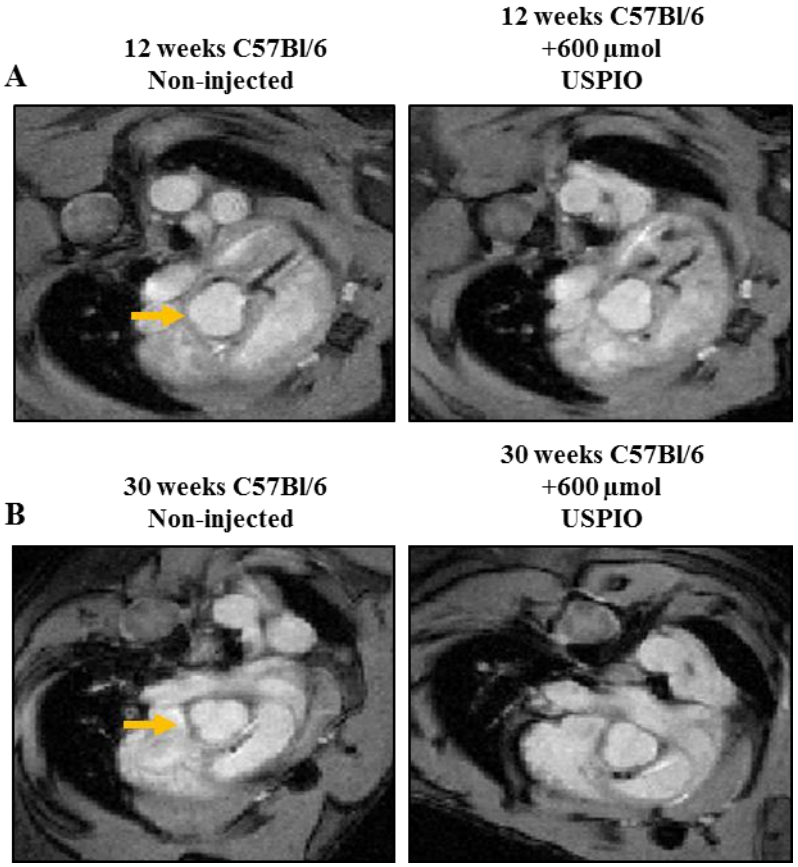

Figure 4.27. *In vivo* ultra-high field MR images of 12 and 30 week old control C57Bl/6 mice. (**A**) T2*-weighted image of young 12 week old C57Bl/6 mice pre and 24 hours post USPIO injection, (**B**) T2*-weighted image of 30 week old C57Bl/6 mice pre and 24 hours post USPIO injection. Representative images from n= 6. Yellow arrows indicate aortic root region.

Injection of 600 µmol/kg dose of non-targeted USPIO into 12 week old *ApoE*$^{-/-}$ mice showed no signal alteration within the aortic wall compared to non-injected mice and was unsuccessful to detect the early changes (**Figure 4.28 A**). In addition, application of USPIO particles into the group of 30 week old *ApoE*$^{-/-}$ mice manifested only slight and

mild signal loss within the aortic root areas (**Figure 4.28 B**). Quantified SNR and CNR values pre and post injection of USPIO particles indicated non-significant signal change within the early and advanced lesions of 12 and 30 week old *ApoE*$^{-/-}$ mice (**Figure 4.29 A, B**).

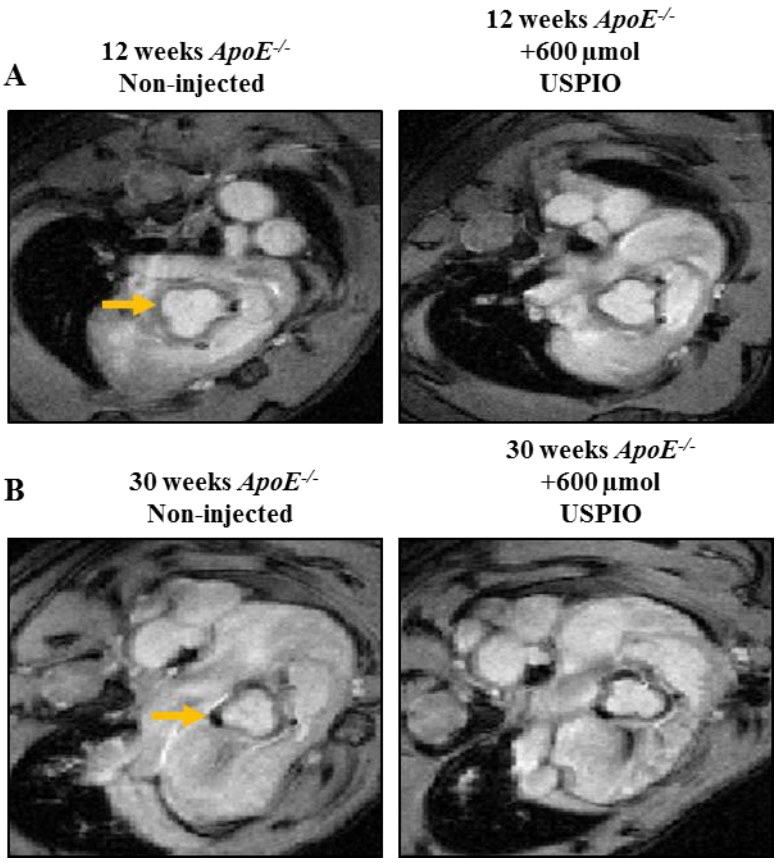

Figure 4.28. *In vivo* ultra-high field MR images of the 12 and 30 week old *ApoE*$^{-/-}$ mice. (**A**) T2*-weighted image of aortic root of 12 week old *ApoE*$^{-/-}$ mice pre and 24 hours post application of 600 µmol/kg dose of USPIO particles, (**B**) T2*-weighted image of aortic root of 30 week old *ApoE*$^{-/-}$ mice pre and 24 hours post injection of 600 µmol/kg dose of USPIO particles. Slight and non-significant darkening observed within aortic wall after injection of 600 µmol USPIO particles into 30 week old *ApoE*$^{-/-}$ mice. Representative images from n=6. Yellow arrows indicate aortic root region. This figure was published in a similar format in (*Michalska, Machtoub et al. 2012*).

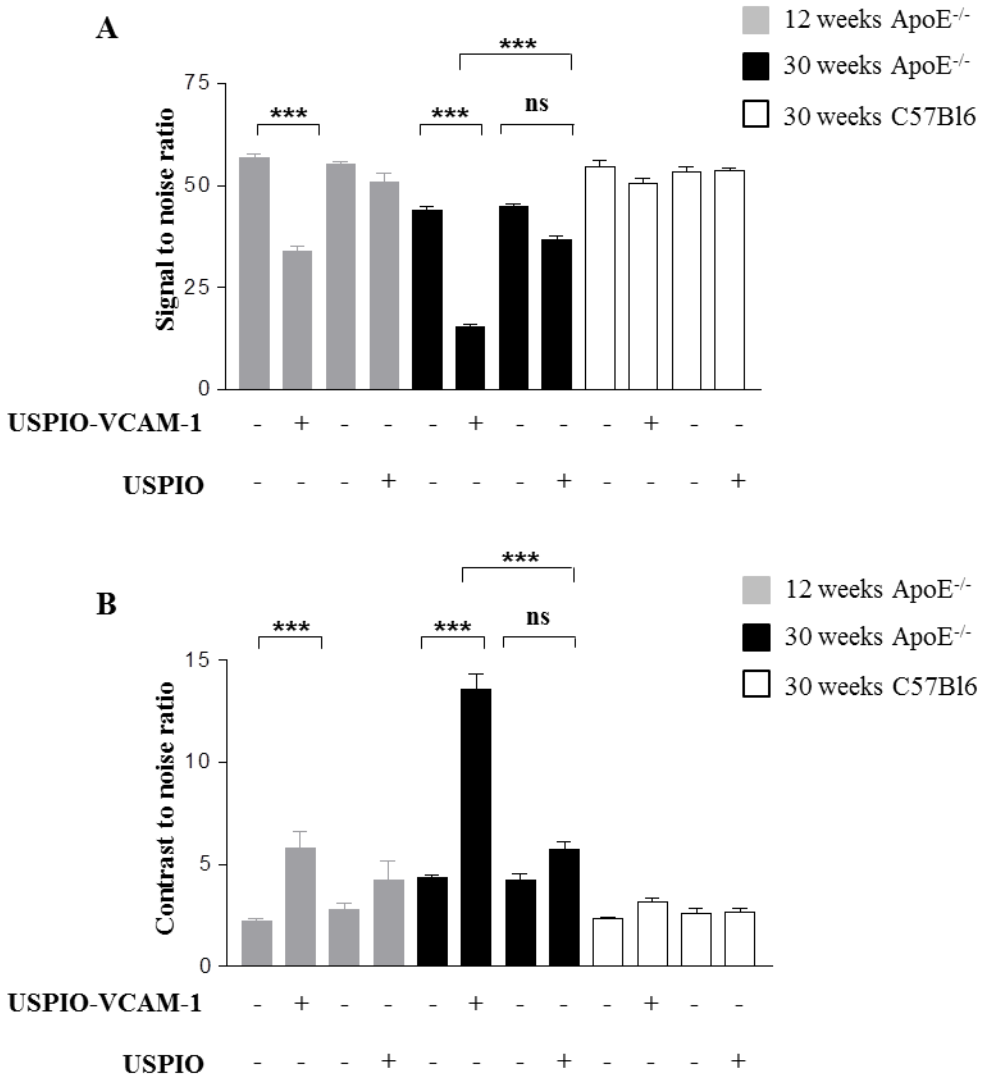

Figure 4.29. Semi-quantitative assessment of signal alteration pre and post application of USPIO-VCAM-1 and USPIO particles. Representation of (**A**) signal to noise ratio (SNR) and (**B**) contrast to noise ratio (CNR) value within aortic root region of control C57Bl/6 and *ApoE*$^{-/-}$ mice (n=6 / group) treated with USPIO-VCAM-1 or USPIO particles. Significant signal alteration within aortic wall of control and atherosclerotic mice pre and post contrast agent application presented via 1-way ANOVA test when P<0.05, ns (nonsignificant). This figure was published in a similar format in (*Michalska, Machtoub et al. 2012*).

In vivo conducted MR experiments within the 12 and 30 week old *ApoE*$^{-/-}$ mice demonstrated the feasibility of targeted iron oxide particles USPIO-VCAM-1 to detect early and advanced plaques. USPIO-VCAM-1 successfully visualized *ex vivo* and *in vivo* inflammatory changes within the aortic wall of atherosclerotic mice and further enabled monitoring the plaque progression by imaging the vascular adhesion molecules. In

contrast, USPIO particles were unable to monitor early lesions and showed *ex vivo* and *in vivo* only modest alterations within the group of 30 week old *ApoE*$^{-/-}$ mice. Thus targeted USPIO conjugated to the specific VCAM-1 peptide presented promising contrast agent for monitoring of early and advanced inflammatory process of atherosclerosis.

4.4. Cellular localization of USPIO conjugated to the VCAM-1 peptide

The last part of this study investigated the localization of iron oxide particles conjugated to the VCAM-1 peptide within the diverse immune cells involved in the early and advanced lesion formation. As the USPIO-VCAM-1 aimed to target the vascular cell adhesion molecules, its co-localization within the cells expressing VCAM-1 was further examined. The analysis of iron distribution was conducted via electron microscopy and histology using Prussian Blue and immunofluorescent staining.

4.4.1. Distribution of USPIO conjugated to the VCAM-1 peptide

Localization of iron oxide nanoparticles was examined by Prussian Blue staining. USPIO-VCAM-1 particles were found not only in the luminal region of the formed plaques but also deeper in the intimal areas of the fibrous cap and plaque shoulders of 12 and 30 week old *ApoE*$^{-/-}$ mice. Moreover iron particles were also found within the border line to the media. The adjacent sections from the Prussian Blue stained aortic root areas were further analyzed and immune-stained for VCAM-1 expression. The immune VCAM-1 staining of these sections revealed the findings that in the atherosclerotic root regions of USPIO-VCAM-1 treated *ApoE*$^{-/-}$ mice, where the iron oxide particles were detected, the strong VCAM-1 expression was present (**Figure 4.30**). The manifestation of VCAM-1 expression within the early and advanced plaques of 12 and 30 week old *ApoE*$^{-/-}$ mice was strong and extensive (**Figure 4.30**, **Figure 4.3 B**, **Figure 4.6 B**).

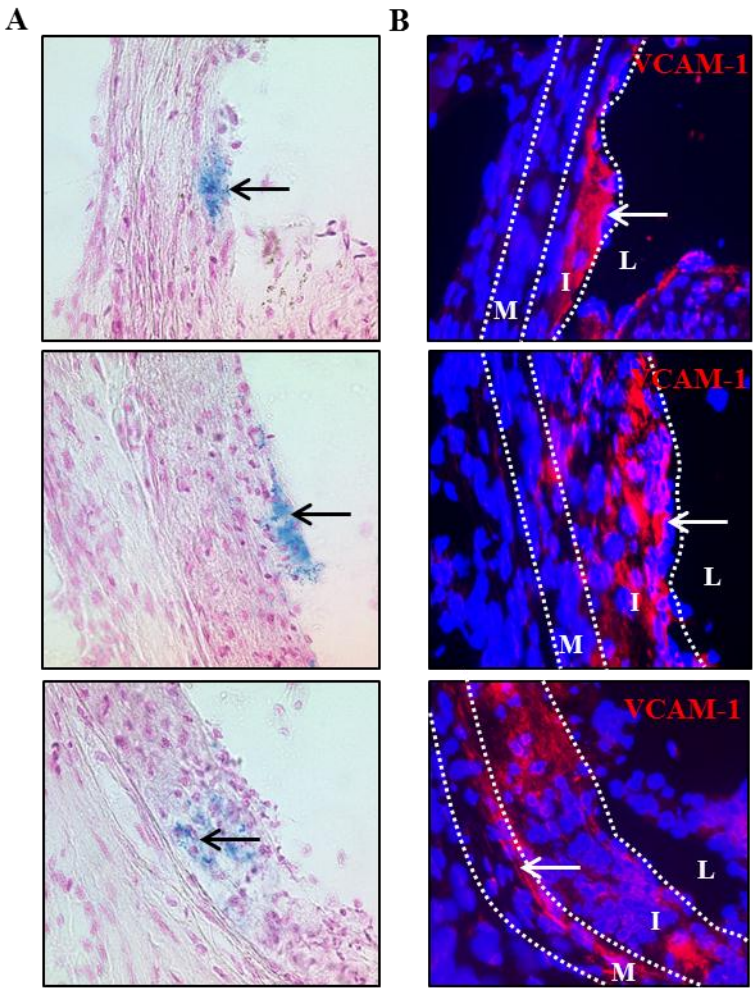

Figure 4.30. Co-localization of iron oxide particles with the VCAM-1 staining within the atherosclerotic lesions of *ApoE*$^{-/-}$ mice treated with USPIO-VCAM-1 contrast agent. (**A**) Prussian Blue stained regions of aortic root demonstrated the iron particles within the luminal areas, intima and within the border to the medial regions (pointed by arrows, magnification x40), (**B**) VCAM-1 red staining of aortic root within lumen, intima and media (pointed by arrows, magnification x40). L- lumen, I- intima, M- media. Representative images from n=6 mice. This figure was published in a similar format in (*Michalska, Machtoub et al. 2012*).

In contrast, Prussian Blue staining of 12 and 30 week old *ApoE*$^{-/-}$ mice injected with USPIO alone demonstrated no detectable iron within the arterial wall of aortic root (**Figure 4.31 A**, **B**). Additionally to the 12 and 30 week old USPIO injected *ApoE*$^{-/-}$ mice, application of either USPIO or USPIO-VCAM-1 into healthy control C57Bl/6 mice emerged no iron within the aortic root regions (**data not shown**). These histological findings evidenced that the significant signal loss observed *ex vivo* and *in vivo* within the

aortic roots of 12 and 30 week old *ApoE*$^{-/-}$ mice was only associated with application of USPIO-VCAM-1 particles.

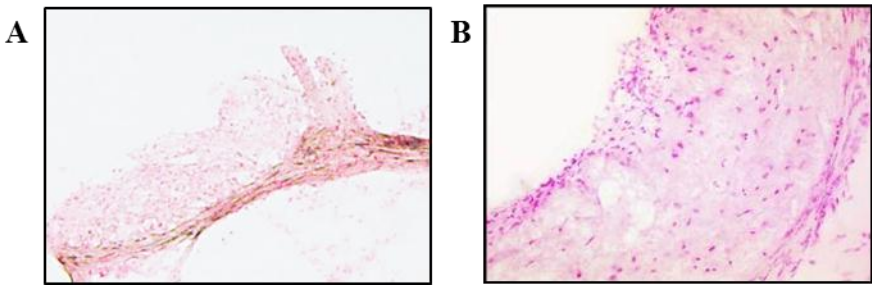

Figure 4.31. Prussian Blue staining of early and advanced plaques from (A) 12 and (B) 30 week old *ApoE*$^{-/-}$ mice injected with USPIO particles (magnification x40). Representative images from n=3 mice.

As USPIO-VCAM-1 particles were detected in the aortic root regions of 12 and 30 week old *ApoE*$^{-/-}$ mice where the endothelial cells, smooth muscle cells and macrophages were present, the double staining of these cells with VCAM-1 was planned subsequently. The immune staining was performed in the adjacent sections to the Prussian Blue stained regions to verify whether these immune cells, where the iron particles were found, express vascular cell adhesion molecules. Double staining of VCAM-1 (CD106) with endothelial cells (vWF), VCAM-1 with macrophages (CD68) and VCAM-1 with smooth muscle cells (α smooth muscle cell actin) emerged that all of these cells possessed VCAM-1 expression (**Figure 4.32** and **Figure 4.33**) as also demonstrated in earlier double immunofluorescent experiments (**Figure 4.3 B-E** and **Figure 4.6 B-E**). In addition, Prussian Blue together with double immune staining confirmed the USPIO-VCAM-1 particle specific binding to the regions owning extensive VCAM-1 expression not only within the intimal endothelial cells but also within smooth muscle cells and macrophages and further within the medial smooth muscle cells throughout the early and advanced plaques (**Figure 4.32 A-C**, **Figure 4.33 A-B**).

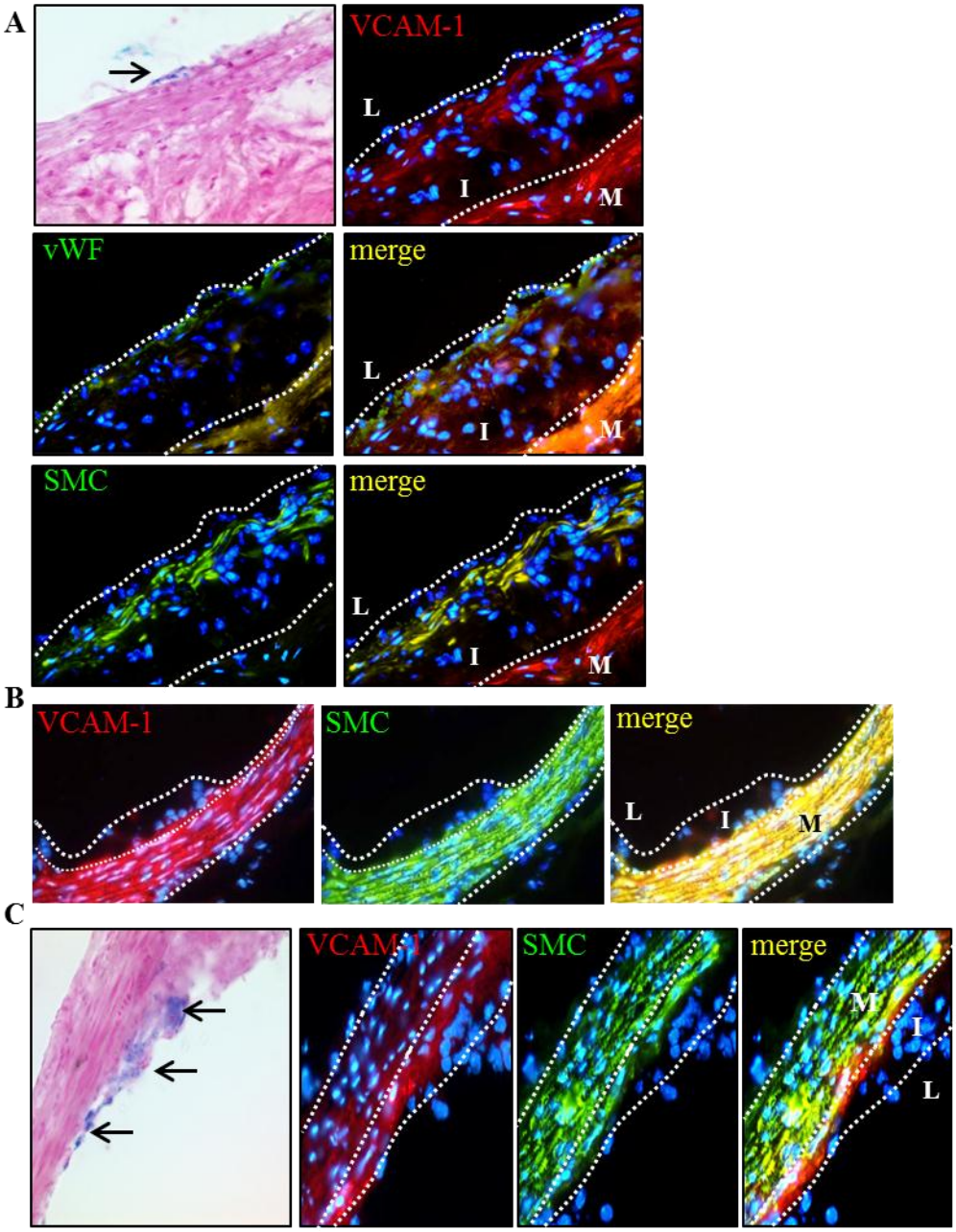

Figure 4.32. Co-localization of USPIO-VCAM-1 particles within the cells expressing vascular cell adhesion molecules in the aortic wall of *ApoE*$^{-/-}$ mice. (**A**, **C**) Distribution of iron particles within the intimal and medial immune cells (indicated by arrows, magnification of x20). (**A**, **B**, **C**) VCAM-1 molecules (red stain) appeared in the regions of plaque endothelial (vWF) (green stain) and smooth muscle (SMC) cells (green stain) where USPIO-VCAM-1 particles were found (magnification x40), L- lumen, I- intima, M- media. Yellow merge represents co-localization of VCAM-1 molecules with endothelium (vWF) and smooth muscle cells (SMC). This figure was published in a similar format in (*Michalska, Machtoub et al. 2012*).

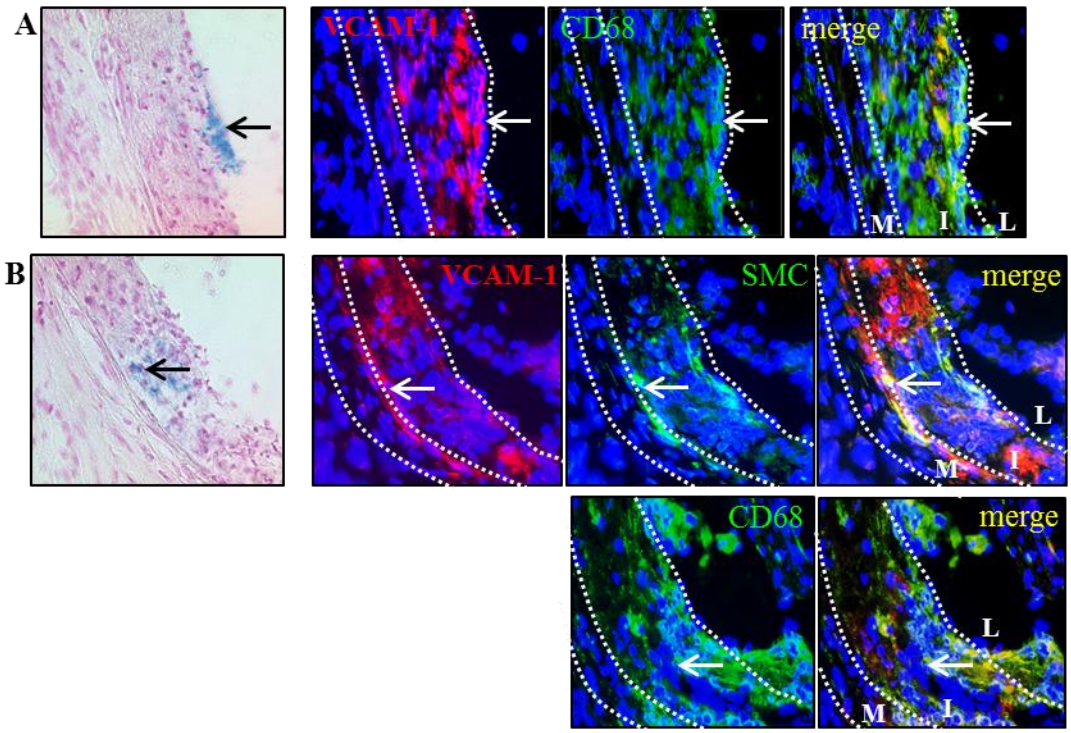

Figure 4.33. Co-localization of USPIO-VCAM-1 particles within the cells expressing vascular cell adhesion molecules in the aortic wall of *ApoE*$^{-/-}$ mice. (**A**, **B**) Distribution of iron particles within the intimal and medial immune cells (indicated by arrows, magnification of x20), (**A**) VCAM-1 expression (red stain) localized within the plaque macrophages (CD68) (green stain) where USPIO-VCAM-1 particles were found (magnification x40), (**B**) VCAM-1 molecules (red stain) appeared in the region of medial smooth muscle cells (SMC) (green stain) and in this region USPIO-VCAM-1 particles were found (magnification x40), L- lumen, I- intima, M- media. Yellow merge represents co-localization of VCAM-1 molecules with macrophages (CD68) and smooth muscle cells (SMC).

While USPIO-VCAM-1 particles were found within the VCAM-1 positive cells as intimal endothelial and smooth muscle cells, and macrophages, the Prussian Blue staining of medial plaque region revealed only modest detectable iron deposition despite very strong expression of vascular cell adhesion molecules within medial smooth muscle cells. One drawback of Prussian Blue staining is low sensitivity, therefore supplementary experiments were performed in order to investigate the exact localization of targeted iron oxide nanoparticles within intima and media. Additionally to the histological assessment of USPIO-VCAM-1 distribution, electron microscopy was conducted in the adjacent section of the Prussian Blue stained aortic root regions. Electron microscopy further examined whether the iron oxide particles conjugated to the VCAM-1 specific peptide were located extra- or intracellular. The analyses of USPIO-VCAM-1 injected 12 and 30 week old

ApoE$^{-/-}$ mice demonstrated iron particles within the intima, enclosed in the large endosomes of the endothelial cells, as well as in the extracellular matrix between the smooth muscle and endothelial compartments. Further electron microscopy localized iron oxide particles within the surface of the intimal smooth muscle cells and in the medial smooth muscle cells' regions rich in collagen filaments (**Figure 4.34**).

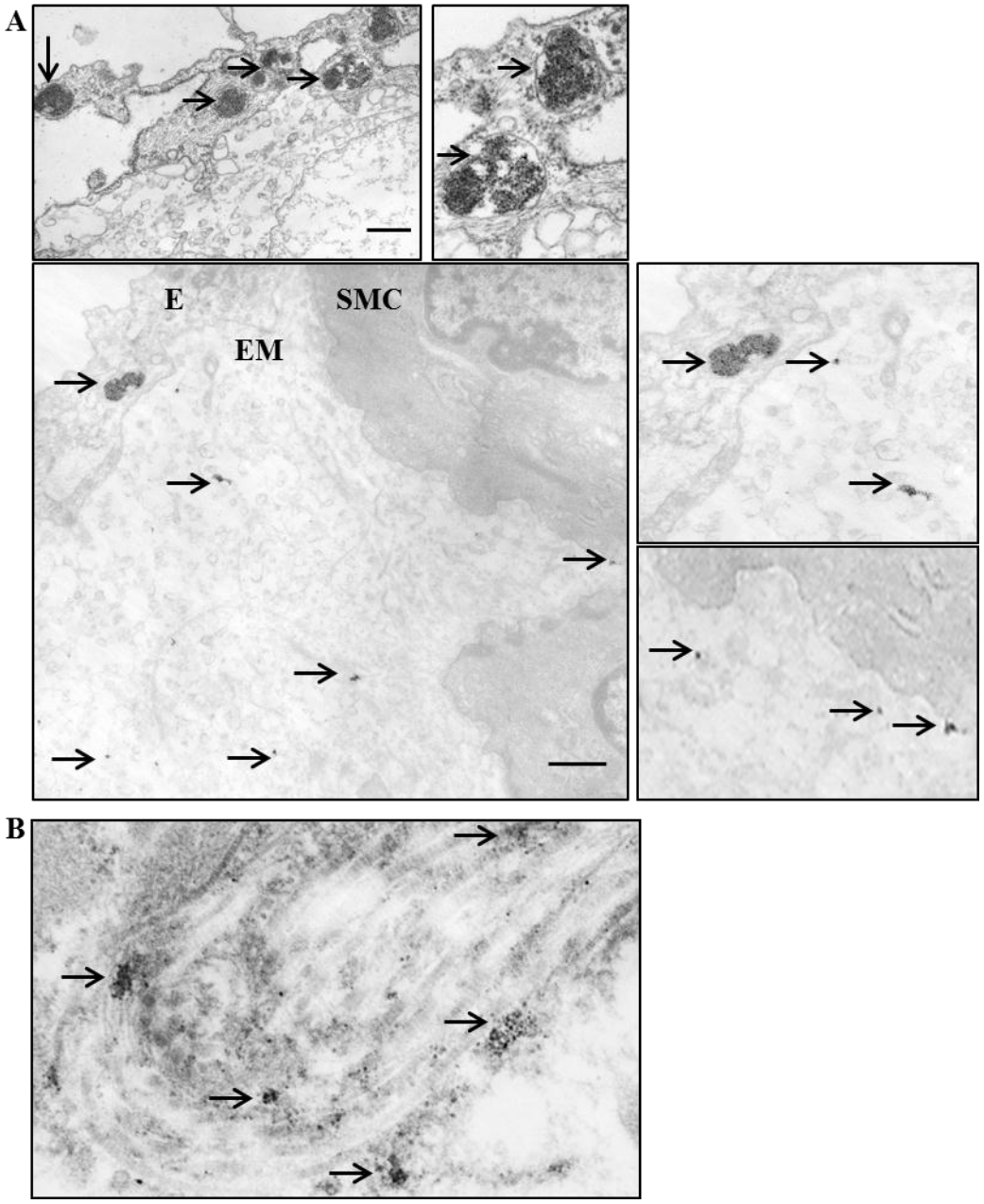

Figure 4.34. Electron microscopy image of aortic root section from USPIO-VCAM-1 injected *ApoE*$^{-/-}$ mice (n=2). (**A**) USPIO-VCAM-1 particles were detected within the intimal endothelial cells (E) as well as intimal smooth muscle cells (SMC) and in the extracellular matrix (EM). (**B**) Medial region revealed accumulation of USPIO-VCAM-1 particles within collagen filaments (iron particles pointed by arrows, scale bar 1 μm). (*Michalska, Machtoub et al. 2012*)

5. Discussion

Vascular cell adhesion molecules have an enormous function within the early and advanced atherosclerotic plaques (*Huo and Ley 2001; Ley and Huo 2001; Libby 2002; Blankenberg, Barbaux et al. 2003*). They emerge before the onset of atherosclerotic lesions and control the whole chronic inflammatory process of atherosclerosis by accelerating the leukocytes' recruitment (*Iiyama, Hajra et al. 1999; Huo and Ley 2001; Libby, Ridker et al. 2002*). They are expressed on endothelial cells only in the face of inflammation at the atheroma-prone sites initiating subsequent alterations within the arterial wall (*Nakashima, Raines et al. 1998; Cybulsky, Iiyama et al. 2001; Huo and Ley 2001; Ley and Huo 2001; Libby 2002*). Their exceptional expression pattern and significance in the origin of atherosclerosis has been shown by diminished plaque growth in the genetically modified mouse model lacking VCAM-1 gene (*Cybulsky, Iiyama et al. 2001; Libby 2002; Libby, Ridker et al. 2002*). Lesion formation in *ApoE*$^{-/-}$ mouse models represents similar morphology to those found in human plaques (*Nakashima, Plump et al. 1994; Iiyama, Hajra et al. 1999; Pendse, Arbones-Mainar et al. 2009*). As with *ApoE*$^{-/-}$ mouse models, VCAM-1 molecules appear early in the human atherosclerotic lesions, initiating leukocyte recruitment from aortic lumen and further promoting enhanced leukocyte invasion from new microvessels of the adventitia region in advanced plaques (*Davies, Gordon et al. 1993; O'Brien, Allen et al. 1993*). Hence, VCAM-1 is a compelling marker for the early as well as advanced inflammatory alterations within the affected arterial wall in both animal models and humans (*Libby 2002*). Therefore, selection and targeting of VCAM-1 molecules would allow monitoring of the inflammation, and would further help to establish early prevention of atherosclerosis (*Blankenberg, Barbaux et al. 2003*) before the origin of the thrombus formation, of which late recognition leads to myocardial infarction.

Exactly this work presented the VCAM-1 concept as a suitable approach to monitor early alterations and advanced lesions of atherosclerosis. This thesis involved *ex vivo* and *in vivo* experiments and was divided into four parts. In the first part (described in the chapter: 5.1. Vascular adhesion molecules (VCAM-1) participate in early lesion formation and promote plaque growth), this study demonstrated the early and advanced plaque alterations and localization of immune cells enrolled in the intimal and medial region of the aortic wall of 12 and 30 week old atherosclerotic *ApoE*$^{-/-}$ mice. Among investigation of plaque immune cell distribution, vascular cell adhesion (VCAM-1) expression was

examined and proven to emerge within the involved immune plaque cells. Hence it indicated the substantial role of VCAM-1 molecules not only in early but also in advanced lesions. These important findings of the first part of this thesis influenced the decision of selecting VCAM-1 as an excellent marker for monitoring the atherosclerotic lesions in the established murine atherosclerotic model. In the second and third part (described in the chapter: 5.2. USPIO conjugated to VCAM-1 cyclic peptide detects early and advanced lesions *ex vivo* and 5.3. USPIO conjugated to VCAM-1 cyclic peptide detects early and advanced lesions *in vivo* and monitors inflammation), this thesis showed the proof of principle and capability of the newly designed iron oxide contrast agent functionalized with the cyclic peptide specific for VCAM-1 recognition. The experimental validation studies including ultra-high MRI enabled further *ex vivo* and *in vivo* detection of applied USPIO-VCAM-1 (P03011) particles within the aortic root region of early and advanced atherosclerotic plaques. In the last part (described in the chapter: 5.4. USPIO conjugated to VCAM-1 cyclic peptide localizes within the plaque cells expressing VCAM-1), this thesis illuminated and proved by histology and electron microscopy that USPIO-VCAM-1 particles specifically targeted VCAM-1 molecules and accumulated within plaque cells. Concluding, the newly designed USPIO-VCAM-1 particles presented in this thesis gave evidence that this functionalized approach offers a promising method for evaluation of early changes and advanced alterations of atherosclerosis.

5.1. Vascular adhesion molecules (VCAM-1) participate in early lesion formation and promote plaque growth

This study firstly evaluated the early and advanced alterations of the aortic wall of 12 and 30 week old *ApoE* $^{-/-}$ mice. The group of 12 week old *ApoE*$^{-/-}$ mice, kept on a high fat diet for 8 weeks, already demonstrated small sized plaques with the initiated inflammatory process within endothelial cells, appearance of smooth muscle cells within intima, and mild recruitment of leukocytes within the atheroma-prone sites. The early lesions with characteristic cell infiltration presented a relentless face of activation. Plaque endothelial as well as macrophages demonstrated strong phagocytic activity and deposited fatty droplets as shown by Oil Red O Staining. These experiments supported the hypothesis that the high fat diet promotes the lipid accumulation and inflammation within the intima (*Libby 2002; Hansson and Hermansson 2011*). In response, oxidized lipids (oxLDLs) lead to activation

of endothelial cells, macrophages, and smooth muscle cells which consequently express vascular cell adhesion (VCAM-1) molecules (*Iiyama, Hajra et al. 1999; Libby 2002; Chi and Melendez 2007*). The inflammatory process together with the presence of oxidized LDLs might further enhance the phagocytic activity of intimal smooth muscle cells. It has been previously shown that smooth muscle cells possess similar scavenger receptors as macrophages, which recognize LDLs and contribute to foam cell creation (*Schrijvers, De Meyer et al. 2007; Doran, Meller et al. 2008*). The study within this thesis also found the accumulation of lipids in the intimal smooth muscle cells. Surprisingly, in the medial region fatty droplets were also detected. This could be associated with the inflammatory cascade within early lesions where the activated medial smooth muscle cells proliferate and change their phenotype from contractile to proinflammatory (*Doran, Meller et al. 2008; Boettger, Beetz et al. 2009*). The enhanced activation of smooth muscle cells and their participation in the early plaque formation of 12 week old *ApoE*$^{-/-}$ mice was further demonstrated by the presence of collagen filaments in the intimal and medial atherosclerotic regions. In contrast to the young mice, 30 week old *ApoE*$^{-/-}$ mice, kept on a high fat diet for 26 weeks, represented the massive alteration and thickening process of the arterial wall associated with the expanded advanced plaques. The advanced lesions differed from the early fatty streaks of 12 week old *ApoE*$^{-/-}$ mice and were characterized by the presence of a formed fibrous cap where, besides activated endothelium and intimal smooth muscle cells, highly prevalent macrophage content was observed. All of the mentioned cells revealed strong phagocytic activity and lipid accumulation within the fibrous cap. Moreover the advanced plaques manifested the presence of a more complex necrotic core containing apoptotic cells and spindle smooth muscle cells. The necrotic core region within advanced plaques of 30 week old *ApoE*$^{-/-}$ mice revealed also fatty droplets. These regions with mostly distributed apoptotic cells usually lack the active phagocytic activity nevertheless, positive Oil Red O staining of the necrotic core could be explained by the fact that cholesterol, derived from overwhelmed intracellular macrophage storage, freely accumulated in extracellular space (*Choudhury and Fisher 2009; Gui, Shimokado et al. 2012*). It has been also published that cell necrosis with increased quantities of extracellular lipids prompts further inflammation (*Tabas 2005; Insull 2009*). The histological assessment within this thesis demonstrated that a high fat diet, extensive immune cells' recruitment and simultaneous cell apoptosis contributed to and changed completely the morphology of the aortic wall of 30 week old *ApoE*$^{-/-}$ mice. Highlighting the enormous changes within the atherosclerotic wall of 12 and 30 week old *ApoE*$^{-/-}$ mice,

these alterations would not have appeared without the upregulation of vascular cell adhesion (VCAM-1) molecules. The vast role of VCAM-1 molecules in atherosclerosis emerges via the α4β1 integrin binding motif, promoting the adhesion and capture of immune cells as monocytes and lymphocytes (*Braun, Pietsch et al. 1999; Huo and Ley 2001; Ley and Huo 2001; Libby 2006)*. Enhanced upregulation of VCAM-1 expression participates in the luminal leukocyte recruitment as well as in migration of immune cells into the plaques from adventitia regions (*O'Brien, Allen et al. 1993; O'Brien, McDonald et al. 1996; Huo and Ley 2001*). This study showed that VCAM-1 expression could be found in the atherosclerotic plaques of early and advanced lesions in the intimal as well as in the deeper regions of the formed lesions. The thesis findings demonstrated furthermore that VCAM-1 molecules co-localized within inflamed intimal endothelial as well as intimal smooth muscle cells and macrophages of 12 and 30 week old *ApoE*$^{-/-}$ mice. In addition to these findings, the strong VCAM-1 expression pattern was detected within the media and adventitia of the aortic wall where medial smooth muscle cells resided. The results presented in this thesis gave evidence that upregulation of VCAM-1 was continuously present in the inflammatory process within 12 and 30 week old *ApoE*$^{-/-}$ mice and thus disclosing that VCAM-1 expression is as equally important in the early as in the advanced plaque growth. The immune VCAM-1 staining of atherosclerotic aortae, presented in this work, also revealed the interesting observation that VCAM-1 was strongly expressed on macrophages and smooth muscle cells within the intima and media rather than on intimal endothelium of early and advanced plaques as also observed by O'Brien et al (*O'Brien, Allen et al. 1993*). The strong presence of smooth muscle cell VCAM-1 expression, stimulated by oxidized lipids and plaque cytokines, not only supports but confirms the influence of smooth muscle cells on leukocyte migration within early and advanced lesions (*Libby and Li 1993; May, Neumann et al. 2000; Doran, Meller et al. 2008*). Thus not only endothelial cells but also smooth muscle cells are engaged in the recruitment of leukocytes via VCAM-1 molecules (*Braun, Pietsch et al. 1999*). Additionally the observations of this thesis on plaque macrophage VCAM-1 expression could be explained by the fact that macrophages express VCAM-1 in response to produced cytokines during plaque formation (*O'Brien, Allen et al. 1993; Iiyama, Hajra et al. 1999*). While leukocytes' adhesion and capture is associated with VCAM-1 expression, presented on intimal plaque cells, medial smooth muscle cells also express VCAM-1 molecules (*Braun, Pietsch et al. 1999*). The experiments of this thesis, including double staining of the smooth muscle cells and

VCAM-1, confirmed the co-localization of the medial smooth muscle cells with vascular cell adhesion molecules.

In summary, this thesis shows that VCAM-1 molecules appear to be one of the most important factors controlling the inflammatory process of atherosclerosis, and thus represent a compelling target for noninvasive visualization and its translation in clinical use. Owing to exceptional presence of VCAM-1 only upon the face of inflammation, targeting of these molecules would enable specific recognition and the evaluation of the extent of inflammation in atherosclerotic lesions. VCAM-1 molecules bear relation to involved immune cells, which leads to detrimental alterations within the arterial wall. Therefore this thesis focused firstly on the importance of biological background in order to depict the VCAM-1 expression within the early and advanced formed plaques. The evidence of presented work that VCAM-1 is extensively expressed within the intimal and medial cells of the atherosclerotic aortic wall influenced the decision of selecting VCAM-1 as an excellent marker for monitoring the atherosclerotic lesions in the established murine atherosclerotic model. Thus targeting of VCAM-1 by a specific contrast agent could contribute to early detection and monitoring of the inflammatory process of atherosclerosis.

5.2. USPIO conjugated to VCAM-1 cyclic peptide detects early and advanced lesions *ex vivo*

Secondly, this thesis examined the feasibility of newly designed ultrasmall superparamagnetic iron oxide particles. As vascular cell adhesion molecules were extensively expressed on endothelial cells, macrophages, and smooth muscle cells within the intima and media of 12 and 30 week old *ApoE*$^{-/-}$ mice, the newly developed USPIO (P03011) iron oxide contrast agent, functionalized with VCAM-1 specific binding cyclic peptide, was utilized.

During the inflammatory process of atherosclerosis, the leukocyte ligand α4β1 binds to VCAM-1 receptors, and this interaction is crucial for leukocyte recruitment into atheroma-prone sites (*Braun, Pietsch et al. 1999; May, Neumann et al. 2000; Huo and Ley 2001; Ley and Huo 2001; Ley, Miller et al. 2011*). Hence development of small peptides, based on α4β1 active sites, is promising for targeting and detection of vascular cell

adhesion molecules and could further contribute to the therapeutic strategies (*You, Maxwell et al. 2002*). The selected cyclic peptide, used in this thesis, represents similarity to the α4β1 complex and holds the potential to only bind to cells expressing VCAM-1 molecules (*Patent number WO2004/058 275, US 2004/253181, Guerbet Research, France*). As USPIO particles conjugated to specific VCAM-1 peptide were newly developed, this study firstly scrutinized the specificity and sensitivity of this targeted approach and conducted *ex vivo* experiments.

5.2.1. Targeted USPIO particles represented high affinity for VCAM-1 molecules

The USPIO particles and the VCAM-1 peptide was synthetized and validated by Guerbet Research Laboratory in France. As described in the patent number WO2004/058 275 (US 2004/253181), the cyclic peptide Cys-Asn-Asn-Ser-Lys-Ser-His-Thr-Cys (C-NNSKSHT-C), used for synthesis of the functionalized USPIO-VCAM-1 contrast agent, was selected through cloning procedure. This specific sequence C-NNSKSHT-C revealed the active sites of the α4β1 integrin complex and thus the highest affinity for VCAM-1 molecules (*Patent WO2004/058 275, US 2004/253181, Guerbet Research, France*). The occurrence of the particular amino acids in the cyclic peptide sequence such as serine (S), histidine (H), threonine (T), and lysine (K) held the potential for specific VCAM-1 binding. Within the peptide, serine (S), histidine (H), and threonine (T) are important for active binding, interaction and further coordination with the VCAM-1 receptor (*Irie, Kamata et al. 1997; You, Maxwell et al. 2002; Burtea, Laurent et al. 2009*). Moreover lysine (K) is responsible for stabilization of peptide binding within VCAM-1 (*Irie, Kamata et al. 1997; You, Maxwell et al. 2002; Burtea, Laurent et al. 2009*). In order to stabilize the complete peptide sequence, selected peptide was further modified into cyclic form (*Krumpe and Mori 2006*) and thus strengthening the specific VCAM-1 binding. The peptide sequence C-NNSKSHT-C represented the high affinity for VCAM-1 in murine as well as in the human endothelial cells (*Patent WO2004/058 275, US 2004/253181, Guerbet Research, France*) which was an essential step for further intended synthesis of targeted USPIO-VCAM-1 particles and their *in vivo* application.

The conjugation of the specific cyclic peptide to the surface of iron oxide nanoparticles needs to be implemented in a homogenous and controlled manner

(*Delehanty, Boeneman et al. 2010*). USPIO particles were conjugated to the cyclic VCAM-1 peptide via carboxylate (RCOO-) group and gem-bisphosphonate compounds $(CH(PO_3H_2)_2)_n$ that covered the USPIO particles. Such a conjugation allowed stable grafting of the VCAM-1 peptide and ensured the presence of the peptide active sites on the surface of the iron oxide nanoparticles (*Patent WO2004/058 275, US 2004/253181, Guerbet Research, France*). Electron microscopy analyses confirmed and demonstrated the homogenous distribution and sustained stability of the targeted USPIO-VCAM-1 particles.

Based on superparamagnetic characteristics of iron oxide contrast agents, the high relaxivity rate (r2) of targeted and non-targeted USPIO particles, demonstrated in *ex vivo* measurements in the 17.6 T MR system, assured significant T2 and T2* contrast related to the presence of iron oxide particles.

5.2.2. Targeted USPIO particles improved pharmacokinetics and shortened half-life time

Evaluation of pharmacokinetics and biodistribution of newly developed nanoparticles is relevant for potential *in vivo* application and visualization (*Lee, Veiseh et al. 2010*). The structure, particle size, and additional binding ligand influence the circulation time and the internalization of the contrast agent within the targeted tissue (*Corot, Robert et al. 2006; Thorek, Chen et al. 2006; Lee, Veiseh et al. 2010; Weinstein, Varallyay et al. 2010*). Therefore proper structure and target design may promote the passage of nanoparticles from the blood stream allowing nanoparticle binding and capture within targeted atherosclerotic plaques (*Corot, Robert et al. 2006; Lee, Veiseh et al. 2010*). Many of the non-targeted large size iron oxide particles lack the specificity and are promptly eliminated by the phagocytic cells localized in the spleen, bone marrow, lymph nodes, and liver, limiting *in vivo* application and further clinical use (*Corot, Robert et al. 2006; Lee, Veiseh et al. 2010*). Too short a circulation time hampers the access of large nanoparticles to attain atherosclerotic plaques. Therefore small size iron oxide particles such as USPIOs are a better approach to reach atherosclerotic plaques and have a longer half-life time (*Kooi, Cappendijk et al. 2003; Corot, Robert et al. 2006; Tang, Muller et al. 2009*).

Prior to the *ex vivo* and *in vivo* imaging procedure, the pharmacokinetic and biodistribution studies of targeted USPIO-VCAM-1 (P03011) as well as non-targeted

USPIO (P3007) particles were conducted in order to evaluate the influence of iron coating and VCAM-1 binding peptide on particle half-life time and to explore the best optimal imaging time in the murine model. The pharmacokinetic analyses of targeted USPIO-VCAM-1 particles enabled the assessment of the half-life time that ranged between 4±2.4 hours in atherosclerotic *ApoE*$^{-/-}$ mice. Compared to healthy control C57Bl/6 mice, where the calculated half-life time of non- and targeted particles was almost exactly equal to about 6 hours, USPIO-VCAM-1 particles resulted in a shorter half-life time in atherosclerotic mice. On the contrary, the calculated half-life time of non-targeted USPIO revealed an extended circulation time of 6 hours in *ApoE*$^{-/-}$ mice which could be explained by the fact that USPIO did not possess the specific peptide attachment. Additionally it could be associated with the USPIO surface modification by polyethylene glycol (PEG) which prolonged the retention of the nanoparticles in the blood stream (*Laurent, Forge et al. 2008; Lee, Veiseh et al. 2010*). However both non-targeted USPIO as well as targeted USPIO-VCAM-1 particles possessed the PEG coating and due to this the prolonged half-life time of USPIO particles could be entailed by the lack of specific peptide binding. These pharmacokinetic analyses helped to make an initial conclusion that surface modification by the conjugation process of cyclic VCAM-1 peptide to USPIO particles could bear the advantage over the non-specific USPIO binding and thus shorten the half-life time of USPIO-VCAM-1 particles. The shorter circulation time of targeted iron particles could be also related to a controlled passage of nanoparticles to the specific cells expressing VCAM-1 within atherosclerotic lesions (*Delehanty, Boeneman et al. 2010*). Owing to the knowledge of the nanoparticles' clearance and half-life time, the optimal *in vivo* imaging time was defined. The assessment of half-life time of USPIO-VCAM-1 and USPIO was mandatory to image specifically iron particles within atherosclerotic lesions, ruling out the artifacts derived from unspecific binding or still circulating particles in the blood stream.

The concentration of injected USPIO-VCAM-1 as well as USPIO nanoparticles analyzed within 24 hours reverted mostly into the basic level in the serum. These findings allowed verification of the optimal *ex vivo* and *in vivo* imaging time point which matched with the biodistribution studies pointing to the huge elimination of biocompatible small USPIO nanoparticles through the phagocytic cells in the liver and spleen during that time point. Besides the distribution of USPIO-VCAM-1 within the macrophages, recognized as Kupffer cells of the liver and within the macrophages of splenic red pulp, kidneys and

lymph nodes were positively stained for USPIO-VCAM-1 particles and due to that they appeared to participate in the iron elimination. Additionally, the presence of USPIO-VCAM-1 particles in the subcapsular sinus region of the lymph nodes and in the cortex and medulla region of the kidneys could be associated with the enhanced atherosclerotic inflammatory process and the appearance of immune cells expressing VCAM-1 within these organs.

Murine models of atherosclerosis are beneficial for experimental work and provide valuable information about the pathophysiological occurrence of this disease (*Daugherty 2002; Zaragoza, Gomez-Guerrero et al. 2011; Getz and Reardon 2012*). However it is important to remember that the laboratory conditions are not always equal to those found in humans. Pharmacokinetic analyses and half-life time of particles used in the mouse atherosclerotic model could differ completely when applied to humans. Therefore human studies including pharmacokinetics, biodistribution, and assessment of toxicity are mandatory to evaluate potential particle use for future *in vivo* clinical translation.

5.2.3. Targeted USPIO particles allowed *ex vivo* detection of early and advanced atherosclerotic lesions

An initial *ex vivo* MR dose-dependent validation studies on agar phantoms containing excised atherosclerotic aortae of USPIO-VCAM-1 and USPIO injected *ApoE*$^{-/-}$ mice, demonstrated the feasibility of targeted particles and further enabled verification of the optimal injection dose for detecting atherosclerotic plaques. The 600 μmol/kg dose of injected USPIO-VCAM-1 particles was evaluated to produce significant signal loss (blooming effect) within atherosclerotic areas and to show the best T2/T2* contrast. The 600 μmol/kg dose of injected USPIO particles also caused signal loss within atherosclerotic root regions, however the signal loss was unostentatious when confronted with applied targeted USPIO-VCAM-1 particles. These initial findings emphasized that a 600 μmol/kg dose of USPIO-VCAM-1 contrast agent successfully marked *ex vivo* atherosclerotic plaques, pointing to its potential for further *in vivo* application. On the contrary, equal doses of USPIO particles were not sufficient to create the same significant T2 effect, as it was revealed in T2-weighted images of agar phantoms from *ApoE*$^{-/-}$ mice injected with USPIO-VCAM-1. Further these *ex vivo* experiments indicated that

application of specific USPIO-VCAM-1 particles enables a reduction of the injection dose almost by half in comparison to previous studies on visualization of atherosclerosis, where the dose of 1000 µmol/kg USPIOs was utilized in murine mouse model (*Morris, Olzinski et al. 2008; Klug, Kampf et al. 2009; Sigovan, Bessaad et al. 2010*).

Applied USPIO-VCAM-1 and USPIO particles (600 µmol/kg dose) were analyzed *ex vivo* and *in vivo* pre and 24 hours post injection to follow the pharmacokinetic data. According to the pharmacokinetics, concentration of 600 µmol/kg USPIO-VCAM-1 as well as USPIO nanoparticles had mostly cleared from the blood stream within 24 hours. As a result of the initial preliminary experiments, 24 hours imaging time point was considered as optimal for subsequent *ex vivo* and *in vivo* imaging in the mouse model. Given a USPIO-VCAM-1 half-life time of 4±2.4 hours and almost complete particle clearance, *ex vivo* and *in vivo* imaging was performed 24 hours post USPIO-VCAM-1 injection, allowing the specific detection of internalized contrast agents within atherosclerotic plaques and excluding unspecific artifacts generated by circulating particles near to the vessel wall.

Ex vivo MR experiments of aortae placed in agar from 12 and 30 week old *ApoE*$^{-/-}$ mice injected with dose of 600 µmol/kg USPIO-VCAM-1 particles revealed strong signal loss within aortic root regions. These observations are in line with preliminary *ex vivo* dose-dependent studies which confirm significant detection of USPIO-VCAM-1 particles within atherosclerotic lesions in comparison to non-significant results from non-targeted USPIO injected 12 and 30 week old *ApoE*$^{-/-}$ mice. *Ex vivo* MR data of early and advanced lesions provided further information about the thickening process within the aortic wall of atherosclerotic mice which were kept on the high fat diet over time. T2-weighted MR images also indicate that the observed signal loss within the early and advanced plaques of USPIO-VCAM-1 injected *ApoE*$^{-/-}$ mice correlate with the thickening process of the aortic wall. Signal loss associated with applied USPIO-VCAM-1 particles was broadly magnified within the advanced lesions of 30 week old *ApoE*$^{-/-}$ mice and only partially within early lesions of 12 week old *ApoE*$^{-/-}$ mice. USPIO-VCAM-1 particles were identified as dark areas in the intima but also in the media of early and advanced atherosclerotic plaques. Histological staining confirmed further the VCAM-1 expression within the intimal and medial region of early and advanced atherosclerotic plaques where the signal loss areas of USPIO-VCAM-1 particles were found.

In summary, these findings of the thesis do point out that targeted USPIO-VCAM-1 particles enable a specific detection of early and advanced plaques and can be utilized to monitor the inflammatory process at discrete time points *ex vivo*.

5.3. USPIO conjugated to VCAM-1 cyclic peptide detects early and advanced lesions *in vivo* and monitors inflammation

The preliminary studies on USPIO-VCAM-1 efficiency demonstrated a homogenous particle distribution, sustained stability, biocompatibility, sufficient clearance, and good T2/T2* contrast. USPIO conjugation to the specific VCAM-1 binding peptide contributed to sensitive and specific detection of atherosclerotic lesions *ex vivo* in comparison to a low nonspecific USPIO particle uptake. These preliminary experiments are fundamental for further *in vivo* application.

Intravenous administration of targeted USPIO-VCAM-1 and non-targeted USPIO particles into control C57Bl/6 and atherosclerotic *ApoE*$^{-/-}$ mice revealed the same findings as the pharmacokinetic data and *ex vivo* MRI, pointing to the optimal imaging time appearing within 24 hours. The acquired preliminary *in vivo* MR images at 1 hour and 6 hours illustrate difficulties in obtaining clear images with high signal to noise ratios. At a calculated half-life time of 4 to 7 hours for USPIO-VCAM-1 and USPIO, the contrast agent was still in the blood and therefore produced artifacts generated by circulating particles in the vicinity of the vessel wall. As blood flow is rapid in the center of the aorta, but slow within the vessel wall, it is likely to be very challenging to clearly distinguish signal loss from the contrast agent capture in the atherosclerotic lesions from signals, which originate from iron particles circulating near to the vessel wall. This explains clearly the occurrence of *in vivo* MRI pre and 24 hours post USPIO-VCAM-1 or USPIO application in the control C57Bl/6 and *ApoE*$^{-/-}$ mice.

MR imaging of control and *ApoE*$^{-/-}$ mice was approached at 17.6 T MR System. Such a system with a high magnetic field and strong gradients contributes to and allows imaging of small aortic vessels with high spatial resolution. As the T2*-weighted imaging was proposed to be optimal for the sensitive detection of iron oxide nanoparticles (*Corot, Robert et al. 2006; Tang, Muller et al. 2009*), a FLASH sequence with a very short echo time of 1 millisecond was used for the imaging. The alterations of signal intensity within

the aortic root pre and 24 hours post USPIO-VCAM-1 or USPIO injection were presented on T2*-weighted MR images. To avoid susceptibility artifacts that might influence the T2*, a shimming protocol, a short time of acquisition and an ECG triggering was applied and contributes to the high signal to noise ratio images excluding motion artifacts. In addition, application of a very short echo time of 1 millisecond further reduced artifacts derived from the chemical shift from water-fat face. The implemented shim protocol, short echo time, fat saturation, and the triggering by ECG prevented image disturbance elucidating only an increase in signal loss in association with applied iron particles within the aortic wall. The *in vivo* findings were also corroborated by *ex vivo* 3D MSME visualization of the aortic root regions, where a magnified increase in signal loss and decay in T2 time of USPIO-VCAM-1-injected *ApoE*$^{-/-}$ mice was presented.

In the present study, the application of 600 µmol/kg USPIO-VCAM-1 particles revealed significant signal loss within the aortic root of early and advanced lesions. T2*-weighted MR images of the aortic wall of 12 week old *ApoE*$^{-/-}$ mice, kept on a high fat diet for 8 weeks, demonstrated visible partial darkening within early lesions associated with application of USPIO-VCAM-1 particles. A further USPIO-VCAM-1 injection in 30 week old *ApoE*$^{-/-}$ mice, kept on a high fat diet for 26 weeks, exhibited very strong darkening within the whole atherosclerotic aortic wall. These findings were in line with the *ex vivo* MR data and the histological staining of VCAM-1 expression. *Ex vivo* high resolved T2-weighted MR images confirmed similarly, that partial signal loss occurred within the early lesions of 12 week old *ApoE*$^{-/-}$ mice, as indicated by T2*-weighted *in vivo* MRI. Histological staining of VCAM-1 expression showed the presence of VCAM-1 molecules in the regions of the observed partial signal loss caused by USPIO-VCAM-1 particles. In contrast, administration of 600 µmol/kg USPIO particles had no influence and no effect on determination of early plaques *in vivo*. The *ex vivo* and *in vivo* MR results of USPIO-VCAM-1 treated 30 week old *ApoE*$^{-/-}$ correlated well. *Ex vivo* T2- and *in vivo* T2*-weighted MR images showed that the strong broad signal loss occurred within advanced lesions of 30 week old *ApoE*$^{-/-}$. The strong signal drop within the aortic wall of advanced plaques corresponded further to intense VCAM-1 expression. The *ex vivo* and *in vivo* MR experiments of USPIO-VCAM-1 injected mice visualized the atherosclerotic alterations of 12 and 30 week old *ApoE*$^{-/-}$ mice, thus elucidating that application of targeted USPIO-VCAM-1 particles could help to early recognize atherosclerotic changes and monitor the inflammatory process at different time points *in vivo*.

The signal loss caused by iron oxide deposits found on T2*-weighted FLASH MR images was semi-quantified and presented as a signal to noise ratio (SNR) and contrast to noise ratio (CNR) value. These data represented the signal variations within the aortic wall pre- and post-USPIO-VCAM-1, and USPIO contrast agent administration. The calculation of the SNR values relied only on the measured signal intensities (SI) within the aortic root pre and post contrast agent administration, and was demonstrated as the decreased SNR due to the signal loss associated with the iron oxide deposition within the aortic vessel. The calculated CNR values were based on signal distinction between the blood, which was defined as internal signal reference, and the aortic root, but in addition were standardized and corrected to the noise of the image (*Klug, Kampf et al. 2009; Michalska, Machtoub et al. 2012*). As the signal intensity of blood pre and post iron oxide contrast agent was proposed as internal reference, a total elimination of particles from the blood was also substantial for the calculation of the contrast to noise ratio (CNR). On the contrary, SNR values were not based on an internal signal reference and therefore the results on calculated SNR could be affected by variations in the signal intensities caused by experiments executed on different days or changing the mouse position within the coil. Thus the CNR provided valuable additional information to the SNR values and corrected for differences in the signal intensity pre and post iron oxide particles injection. Calculated SNR values of *ApoE*$^{-/-}$ fed a high fat diet for 8 and 26 week resulted in a significant signal decline post USPIO-VCAM-1 application. The same magnified findings were observed with the assessed CNR values of young and advanced atherosclerotic *ApoE*$^{-/-}$ mice treated with USPIO-VCAM-1 particles. These results of SNR and CNR of 12 and 30 week old *ApoE*$^{-/-}$ mice confirmed the significant signal intensity alterations within the aortic root associated with USPIO-VCAM-1 injection. Compared to the significance of USPIO-VCAM-1 particles in detection of early and advanced atherosclerotic plaques, USPIO injection within 12 and 30 week old atherosclerotic *ApoE*$^{-/-}$ mice had no remarkable effect on signal intensity alterations. In 12 week old *ApoE*$^{-/-}$ mice, there were no signal intensity change of the SNR and CNR values pre and post USPIO injection. In 30 week old *ApoE*$^{-/-}$ mice, the calculated SNR and CNR values showed minimal and non-significant signal intensity alteration within the aortic wall after USPIO injections. Hence the semi-quantification, reflected by SNR and CNR values, confirmed the success of USPIO-VCAM-1 *in vivo* imaging of atherosclerotic plaques.

Using an ultra-high field MRI, this work enabled USPIO-VCAM-1 visualization within early and advanced atherosclerotic plaques. It was unlikely to mark the atherosclerotic lesions with non-targeted USPIOs using the same 600 µmol/kg injection dose, preparation, equal MR sequences, and imaging time as represented with applied targeted USPIO-VCAM-1 particles. Previously published studies however have shown macrophage uptake of non-targeted USPIO contrast agent and MRI visualization of advanced atherosclerotic plaques in murine models (*Morris, Olzinski et al. 2008; Klug, Kampf et al. 2009; Sigovan, Bessaad et al. 2010*) and hyperlipidemic rabbits (*Ruehm, Corot et al. 2001; Sigovan, Boussel et al. 2009*) . USPIO particles have also been utilized in order to image human carotid lesions (*Kooi, Cappendijk et al. 2003; Trivedi, JM et al. 2004*). All of these studies have used USPIO particles that possessed a dextran coating, which might explain the deposition of USPIO contrast agent within the plaques. In contrast to previous studies on dextran USPIO plaque deposition, gem-bisphosphonate coated USPIO, used in this study, allowed only marginal detection of signal within advanced plaques, but not the early lesions. The reason for non-significant and weak signal intensity loss could be associated with gem-bisphosphonate coating of USPIOs injected 30 week old *ApoE*$^{-/-}$ mice. Further it could be explained by the fact that the dose of only 600 µmol/kg iron particles was utilized in this work, which differed from the 1000 µmol/kg doses of previous studies on dextran USPIOs. This illuminates that the cellular non-targeted USPIO approach requires a very high injection dose in order to visualize the plaques. This emphasizes the specificity and potential of the targeted USPIO-VCAM-1 particles.

There have been earlier studies that have approached VCAM-1 molecules for imaging of atherosclerosis. Former investigations have utilized antibodies as a binding ligand coupled to microbubbles and detected by ultrasound *ex vivo* (*Kaufmann, Sanders et al. 2007; Ferrante, Pickard et al. 2009*). Another work has demonstrated MR imaging of VCAM-1 molecules by antibodies and linear peptide attached to iron oxide particles (*Kelly, Nahrendorf et al. 2006; Nahrendorf, Jaffer et al. 2006; McAteer, Schneider et al. 2008*). There were also studies using perfluorocarbon for VCAM-1 detection presented by 19F magnetic resonance (*Southworth, Kaneda et al. 2009*). Nuclear imaging has also targeted VCAM-1 molecules with fluorine (*Nahrendorf, Keliher et al. 2009*) or radiolabeled with technetium (*Broisat, Hernot et al. 2012*). These studies have used the VCAM-1 approach. However, they differed from this work. For instance, Kelly et al (*Kelly, Nahrendorf et al. 2006*) and Nahrendorf et al (*Nahrendorf, Jaffer et al. 2006*),

utilized linear peptide sequence VHPKQHR (VINP 28) conjugated to CLIO iron oxide particles to facilitate *ex vivo* and *in vivo* visualization of VCAM-1 molecules within atherosclerotic plaques by MRI. Further the identical linear peptide sequence VHPKQHR functionalized with fluorine 18F was synthetized and used for VCAM-1 detection of atherosclerotic lesions by PET-CT approach (*Nahrendorf, Keliher et al. 2009*). The purpose of linear peptide VHPKQHR was expanded and another group exploited this linear peptide conjugated to perfluorocarbon in order to image renal inflammatory process in *ApoE*$^{-/-}$ mice by *ex vivo* MRI (*Southworth, Kaneda et al. 2009*). Besides elaborated linear peptide use, there have been also studies demonstrating ultrasound detection of atherosclerotic plaques by VCAM-1 antibody linked to microbubbles in *ex vivo* and *in vivo* *ApoE*$^{-/-}$ mice (*Kaufmann, Sanders et al. 2007; Ferrante, Pickard et al. 2009*). In addition to the above presented work, there were also studies on double targeted iron oxide particles particularly MPIO linked to antibodies against P-Selectins and VCAM-1. That approach enabled luminal depiction of adhesion molecules by *ex vivo* MRI of atherosclerotic aortae from *ApoE*$^{-/-}$ mice (*McAteer, Schneider et al. 2008*). Recently, another group presented concept of nanobodies radiolabeled with technetium for detection of inflamed plaques in *ApoE*$^{-/-}$ mice (*Broisat, Hernot et al. 2012*). Nevertheless, none of the aforementioned studies employed the USPIO-VCAM-1 contrast agent utilized in this thesis.

In this thesis, a USPIO particle with gem-bisphosphonate coating and the specific cyclic VCAM-1 peptide (*Patent number WO2004/058 275/ US 2004/253181, Guerbet Research France*) differed for instance from the functionalized VINP28 contrast agent utilized by Kelly et al and Nahrendorf et al (*Kelly, Nahrendorf et al. 2006; Nahrendorf, Jaffer et al. 2006*). The disparity of USPIO-VCAM-1 particles, used in this work, compared to previously developed VINP28, was based on different particle size, coating, and specific VCAM-1 peptide sequence. Due to these differences, the cyclic peptide conjugated to USPIO particles (P03011) was cleared from the blood stream within a short period of time, terminating in a half-life time of 4.0±2.4 hours after administration in *ApoE*$^{-/-}$ mice, while VINP28 circulated for 17.7 hours (*Nahrendorf, Jaffer et al. 2006*). The experiments, within this thesis, concentrated on the visualization of the aortic root region in *ApoE*$^{-/-}$ mice fed a high fat diet at various time points. Further *in vivo* high resolution MRI was conducted 24 hours post USPIO-VCAM-1 application. A half life time of USPIO-VCAM-1 of 4±2.4 hours allowed the imaging time at 24 hours after USPIO-VCAM-1 injection, when iron particles were completely eliminated from the circulation,

enabling the specific detection of the internalized USPIO-VCAM-1, withdrawing unspecific artifacts originated from circulating particles next to the vessel wall. Use of an ultra-high field MRI system allowed high resolution imaging and identification of inflammation within small sized plaques. Therefore, this work could visualize the specific cyclic USPIO-VCAM-1 particles within the early and advanced atherosclerotic lesions in *ApoE*$^{-/-}$ mice *ex vivo* and *in vivo*.

5.4. USPIO conjugated to VCAM-1 cyclic peptide localizes within the plaque cells expressing VCAM-1

Investigation of the cellular localization of the USPIO-VCAM-1 contrast agent within the aortic root region, demonstrated by Prussian Blue staining, revealed iron particles in early and advanced atherosclerotic lesions of USPIO-VCAM-1 injected *ApoE*$^{-/-}$ mice but not in control C57Bl/6 mice. The deposition of iron particles was found within intimal endothelial, smooth muscle cells, and macrophages. Modest accumulation of USPIO-VCAM-1 particles was also detected within the border to the medial areas. In addition to those observations, these plaque cells presented very strong VCAM-1 expression. Thus it indicated the specificity of USPIO-VCAM-1 binding to the cells expressing VCAM-1 molecules. Nevertheless, low sensitivity of the Prussian Blue technique was noticed and due to that only iron particles that accumulated in larger numbers could be detected. Therefore electron microscopy was also performed. Using this technique, for the first time iron particles were identified not only in the lumen of the plaque and deeper in the intima but also in the medial regions. With this modality, it was further possible to exactly define the deposition of iron particles found in the intracellular luminal endothelial cells within endosomes. Next, the iron particle deposits were observed within the extracellular matrix between the intimal smooth muscle and endothelial cells. In addition iron particles were found on the outer surface of smooth muscle cells and in the medial region where the collagen filaments and medial smooth muscle cells occurred. Compared with histology, the medial region was also positively stained for VCAM-1 demonstrating the specificity of USPIO-VCAM-1 binding not only in the intima region but also in the media where smooth muscle cells expressed VCAM-1. This corroborated the results that USPIO-VCAM-1 particles explicitly targeted cells expressing VCAM-1 molecules within early and

advanced plaques and provided further the essential information about the luminal and medial cell contribution in the plaque formation in murine models of atherosclerosis.

The nonspecific uptake of USPIO might be present within endothelial cells and macrophages (*Ruehm, Corot et al. 2001; Kooi, Cappendijk et al. 2003; Morris, Olzinski et al. 2008*). This work also detected minimal nonspecific signal loss, related to USPIO application, within the aortic root region of 30 weeks old *ApoE*$^{-/-}$ mice. Nevertheless the signal loss was irrelevant when compared to the group of *ApoE*$^{-/-}$ mice injected with USPIO-VCAM-1 particles. Including positive iron staining of atherosclerotic lesions of USPIO-VCAM-1 injected *ApoE*$^{-/-}$ mice, from these observations, high specificity of targeted iron particles beyond non-targeted USPIO uptake emerged.

Using a combination of histology and electron microscopy, this study could specifically point to distribution of functionalized USPIO-VCAM-1 particles within early and advanced atherosclerotic process. This work could further localize for the first time functionalized iron particles not only in luminal region of the plaque but also in deeper plaque areas where medial smooth muscle cells resided in early and advanced lesions.

5.5. Clinical consideration of USPIO-VCAM-1 versus USPIO application

Although there have been successful previous clinical studies on non-targeted USPIO particles termed as Ferumoxtran-10 (Sinerem, Guerbet) for imaging of macrophage uptake in advanced and prone to rupture carotid plaques of human patients, this non-targeted approach has revealed some limitations in clinical practice (*Kooi, Cappendijk et al. 2003; Tang, Muller et al. 2009*). The main problem referred to the half-life time of Ferumoxtran-10 (Sinerem), which was equated to 24 to 36 hours (*Tang, Muller et al. 2009*). This circulation time was considered too long for visualizing macrophages in human plaques. Another issue regarding the use of USPIO particles in clinics was related to MR imaging pre and post iron oxide application. However the pre and post imaging procedure is needed to distinguish the signal loss associated with applied iron particles from the blood degradation products that might appear on acquired images (*Kooi, Cappendijk et al. 2003; Tang, Muller et al. 2009*). Moreover imaging with non-targeted USPIO particles has demonstrated only advanced and prone to rupture carotid human plaques, which in terms

of clinical use, could be a limitation. USPIO particles, confined to recognition of advanced plaques, did not allow early plaque detection. Due to that the functionalized USPIO-VCAM-1 particles could be a better approach allowing specific target-oriented detection of early and advanced plaques.

5.6. Conclusion and perspectives of USPIO-VCAM-1 application

This thesis presented the potential of specific USPIO conjugated to the VCAM-1 binding peptide over unspecific USPIOs for preclinical application and evaluation of atherosclerosis. It firstly demonstrated that selection of VCAM-1 molecules offers a good and potential strategy for imaging of atherosclerosis, as these vascular cell adhesion molecules play an explicit role in the early phase of inflammation and are also continuously up-regulated within the advanced plaque in the murine models as well as in humans (*Davies, Gordon et al. 1993; O'Brien, Allen et al. 1993; Ley and Huo 2001*). Secondly, this thesis showed the capability of the newly designed USPIO contrast agent conjugated to the specific cyclic peptide for VCAM-1 recognition. The experimental studies including ultra-high field MRI, histology, and electron microscopy enabled further *ex vivo* and *in vivo* detection of applied USPIO-VCAM-1 particles within the aortic root region of early and advanced atherosclerotic plaques of 12 and 30 week old *ApoE*$^{-/-}$ mice. Hence functionalized USPIO particles targeting VCAM-1 molecules allow specific and sensitive detection of early and advanced plaques at the molecular level, giving the new possibilities for early detection of atherosclerotic plaques. Therefore the use of a functionalized contrast agent could also offer promising method for clinical evaluation of early atherosclerotic alterations. However besides advantages, these functionalized particles also have some limitations. One drawback of the USPIO-VCAM-1 contrast agent is the still long circulation time of 4±2.4 hours, which hampers the allowance of pre and post contrast MR imaging within narrow intervals without changing the position of the patients inside the coil. A relatively short half-life time of the contrast agent is mandatory for one stop acquisition MRI to rule out undesired background signals from circulating nanoparticles during the measurement and to prevent possible toxic effects. To consider this targeted approach with USPIO-VCAM-1 particles for a human application, the particle design needs to be improved further to shorten half-life time, allowing sensitive detection within atherosclerotic plaques at low administration doses.

This thesis demonstrated a semi-quantification approach to the signal loss associated with iron oxide deposits within atherosclerotic root regions. The great opportunity to visualize plaque is realized by specially designed sequences that would transform the signal loss, derived from applied iron oxide particles, allowing further quantification of the exact iron particle amount in post-processing step. Such sequences would accurately highlight the location of iron oxide particles within the plaque regions without any further confirmation by *ex vivo* histology, also enabling subtraction of the signal differences related to iron particles from artifacts that might presumably occur (*Dahnke, Liu et al. 2008*).

Bibliography

Ait-Oufella, H., S. Taleb, et al. (2009). "Cytokine network and T cell immunity in atherosclerosis." Semin Immunopathol **31**(1): 23-33.

Amirbekian, V., M. J. Lipinski, et al. (2007). "Detecting and assessing macrophages in vivo to evaluate atherosclerosis noninvasively using molecular MRI." Proc Natl Acad Sci U S A **104**(3): 961-6.

Amstad, E., S. Zurcher, et al. (2009). "Surface functionalization of single superparamagnetic iron oxide nanoparticles for targeted magnetic resonance imaging." Small **5**(11): 1334-42.

Balogh, P., Y. Aydar, et al. (2002). "Appearance and phenotype of murine follicular dendritic cells expressing VCAM-1." Anat Rec **268**(2): 160-8.

Birdsall, H. H., C. Lane, et al. (1992). "Induction of VCAM-1 and ICAM-1 on human neural cells and mechanisms of mononuclear leukocyte adherence." J Immunol **148**(9): 2717-23.

Blackwell, G. G., G. B. Cranney, et al. (1992). "MRI: Cardiovascular System." Gower Medical Publishing.

Blankenberg, S., S. Barbaux, et al. (2003). "Adhesion molecules and atherosclerosis." Atherosclerosis **170**(2): 191-203.

Boettger, T., N. Beetz, et al. (2009). "Acquisition of the contractile phenotype by murine arterial smooth muscle cells depends on the Mir143/145 gene cluster." J Clin Invest **119**(9): 2634-47.

Braun, M., P. Pietsch, et al. (1999). "Cellular adhesion molecules on vascular smooth muscle cells." Cardiovasc Res **41**(2): 395-401.

Broisat, A., S. Hernot, et al. (2012). "Nanobodies targeting mouse/human VCAM1 for the nuclear imaging of atherosclerotic lesions." Circ Res **110**(7): 927-37.

Bulte, J. W. and D. L. Kraitchman (2004). "Iron oxide MR contrast agents for molecular and cellular imaging." NMR Biomed **17**(7): 484-99.

Burtea, C., S. Laurent, et al. (2008). "Molecular imaging of alpha v beta3 integrin expression in atherosclerotic plaques with a mimetic of RGD peptide grafted to Gd-DTPA." Cardiovasc Res **78**(1): 148-57.

Burtea, C., S. Laurent, et al. (2009). "Magnetic resonance molecular imaging of vascular cell adhesion molecule-1 expression in inflammatory lesions using a peptide-vectorized paramagnetic imaging probe." J Med Chem **52**(15): 4725-42.

Carlos, T. M. and J. M. Harlan (1994). "Leukocyte-endothelial adhesion molecules." Blood **84**(7): 2068-101.

Chen, I. Y. and J. C. Wu (2011). "Cardiovascular molecular imaging: focus on clinical translation." Circulation **123**(4): 425-43.

Chen, K., J. Chen, et al. (2005). "Adhesion molecule expression in fibroblasts: alteration in fibroblast biology after transfection with LOX-1 plasmids." Hypertension **46**(3): 622-7.

Chen, W., D. P. Cormode, et al. (2010). "Nanoparticles as magnetic resonance imaging contrast agents for vascular and cardiac diseases." Wiley Interdiscip Rev Nanomed Nanobiotechnol.

Chi, Z. and A. J. Melendez (2007). "Role of cell adhesion molecules and immune-cell migration in the initiation, onset and development of atherosclerosis." Cell Adh Migr **1**(4): 171-5.

Choi, S. H., W. K. Moon, et al. (2007). "Lymph node metastasis: ultrasmall superparamagnetic iron oxide-enhanced MR imaging versus PET/CT in a rabbit model." Radiology **242**(1): 137-43.

Choudhury, R. P. and E. A. Fisher (2009). "Molecular imaging in atherosclerosis, thrombosis, and vascular inflammation." Arterioscler Thromb Vasc Biol **29**(7): 983-91.

Cormode, D. P., T. Skajaa, et al. (2008). "Nanocrystal core high-density lipoproteins: a multimodality contrast agent platform." Nano Lett **8**(11): 3715-23.

Corot, C., P. Robert, et al. (2006). "Recent advances in iron oxide nanocrystal technology for medical imaging." Adv Drug Deliv Rev **58**(14): 1471-504.

Corti, R. and V. Fuster (2011). "Imaging of atherosclerosis: magnetic resonance imaging." Eur Heart J **32**(14): 1709-19b.

Corti, R., V. Fuster, et al. (2001). "New understanding of atherosclerosis (clinically and experimentally) with evolving MRI technology in vivo." Ann N Y Acad Sci **947**: 181-95; discussion 195-8.

Cybulsky, M. I., J. W. Fries, et al. (1991). "Gene structure, chromosomal location, and basis for alternative mRNA splicing of the human VCAM1 gene." Proc Natl Acad Sci U S A **88**(17): 7859-63.

Cybulsky, M. I. and M. A. Gimbrone, Jr. (1991). "Endothelial expression of a mononuclear leukocyte adhesion molecule during atherogenesis." Science **251**(4995): 788-91.

Cybulsky, M. I., K. Iiyama, et al. (2001). "A major role for VCAM-1, but not ICAM-1, in early atherosclerosis." J Clin Invest **107**(10): 1255-62.

Dahnke, H., W. Liu, et al. (2008). "Susceptibility gradient mapping (SGM): a new postprocessing method for positive contrast generation applied to superparamagnetic iron oxide particle (SPIO)-labeled cells." Magn Reson Med **60**(3): 595-603.

Daugherty, A. (2002). "Mouse models of atherosclerosis." Am J Med Sci **323**(1): 3-10.

Davies, M. J., J. L. Gordon, et al. (1993). "The expression of the adhesion molecules ICAM-1, VCAM-1, PECAM, and E-selectin in human atherosclerosis." J Pathol **171**(3): 223-9.

Debbage, P. and W. Jaschke (2008). "Molecular imaging with nanoparticles: giant roles for dwarf actors." Histochem Cell Biol **130**(5): 845-75.

Delehanty, J. B., K. Boeneman, et al. (2010). "Peptides for specific intracellular delivery and targeting of nanoparticles: implications for developing nanoparticle-mediated drug delivery." Ther Deliv **1**(3): 411-33.

Devries-Seimon, T., Y. Li, et al. (2005). "Cholesterol-induced macrophage apoptosis requires ER stress pathways and engagement of the type A scavenger receptor." J Cell Biol **171**(1): 61-73.

Dong, Z. M., A. A. Brown, et al. (2000). "Prominent role of P-selectin in the development of advanced atherosclerosis in ApoE-deficient mice." Circulation **101**(19): 2290-5.

Doran, A. C., N. Meller, et al. (2008). "Role of smooth muscle cells in the initiation and early progression of atherosclerosis." Arterioscler Thromb Vasc Biol **28**(5): 812-9.

Feng, B., P. M. Yao, et al. (2003). "The endoplasmic reticulum is the site of cholesterol-induced cytotoxicity in macrophages." Nat Cell Biol **5**(9): 781-92.

Ferrante, E. A., J. E. Pickard, et al. (2009). "Dual targeting improves microbubble contrast agent adhesion to VCAM-1 and P-selectin under flow." J Control Release **140**(2): 100-7.

Fischer, A. H., K. A. Jacobson, et al. (2008). "Hematoxylin and eosin staining of tissue and cell sections." CSH Protoc **2008**: pdb prot4986.

Getz, G. S. and C. A. Reardon (2012). "Animal models of atherosclerosis." Arterioscler Thromb Vasc Biol **32**(5): 1104-15.

Grant, C. V., S. L. Sit, et al. (2007). "An efficient (1)H/(31)P double-resonance solid-state NMR probe that utilizes a scroll coil." J Magn Reson **188**(2): 279-84.

Grenier, N. and P. Brader (2011). "Principles and basic concepts of molecular imaging." Pediatr Radiol **41**(2): 144-60.

Gui, T., A. Shimokado, et al. (2012). "Diverse roles of macrophages in atherosclerosis: from inflammatory biology to biomarker discovery." Mediators Inflamm **2012**: 693083.

Hahn, M. A., A. K. Singh, et al. (2011). "Nanoparticles as contrast agents for in-vivo bioimaging: current status and future perspectives." Anal Bioanal Chem **399**(1): 3-27.

Hansson, G. K. (2001). "Immune mechanisms in atherosclerosis." Arterioscler Thromb Vasc Biol **21**(12): 1876-90.

Hansson, G. K. and A. Hermansson (2011). "The immune system in atherosclerosis." Nat Immunol **12**(3): 204-12.

Hansson, G. K., A. K. Robertson, et al. (2006). "Inflammation and atherosclerosis." Annu Rev Pathol **1**: 297-329.

Hartley, C. J., A. K. Reddy, et al. (2000). "Hemodynamic changes in apolipoprotein E-knockout mice." Am J Physiol Heart Circ Physiol **279**(5): H2326-34.

Hauger, O., C. Delalande, et al. (2000). "Nephrotoxic nephritis and obstructive nephropathy: evaluation with MR imaging enhanced with ultrasmall superparamagnetic iron oxide-preliminary findings in a rat model." Radiology **217**(3): 819-26.

Hayes, C. E. (1985). "An Efficient, Highly Homogeneous Radiofrequency Coil for Whole-Body NMR Imaging at 1.5 T." J. Magn. Reson.

Herold, V. (2010). " In vivo MR-Mikroskopie am kardiovaskulären System der Maus."

Herold, V., J. Wellen, et al. (2009). "In vivo comparison of atherosclerotic plaque progression with vessel wall strain and blood flow velocity in apoE(-/-) mice with MR microscopy at 17.6 T." MAGMA **22**(3): 159-66.

Hession, C., P. Moy, et al. (1992). "Cloning of murine and rat vascular cell adhesion molecule-1." Biochem Biophys Res Commun **183**(1): 163-9.

Hillaireau, H. and P. Couvreur (2009). "Nanocarriers' entry into the cell: relevance to drug delivery." Cell Mol Life Sci **66**(17): 2873-96.

Humphries, M. J., J. Sheridan, et al. (1995). "Mechanisms of VCAM-1 and fibronectin binding to integrin alpha 4 beta 1: implications for integrin function and rational drug design." Ciba Found Symp **189**: 177-91; discussion 191-9.

Huo, Y. and K. Ley (2001). "Adhesion molecules and atherogenesis." Acta Physiol Scand **173**(1): 35-43.

Hynes, R. O. (1992). "Integrins: versatility, modulation, and signaling in cell adhesion." Cell **69**(1): 11-25.

Iiyama, K., L. Hajra, et al. (1999). "Patterns of vascular cell adhesion molecule-1 and intercellular adhesion molecule-1 expression in rabbit and mouse atherosclerotic lesions and at sites predisposed to lesion formation." Circ Res **85**(2): 199-207.

Insull, W., Jr. (2009). "The pathology of atherosclerosis: plaque development and plaque responses to medical treatment." Am J Med **122**(1 Suppl): S3-S14.

Irie, A., T. Kamata, et al. (1997). "Multiple loop structures critical for ligand binding of the integrin alpha4 subunit in the upper face of the beta-propeller mode 1." Proc Natl Acad Sci U S A **94**(14): 7198-203.

Jaffer, F. A., P. Libby, et al. (2006). "Molecular and cellular imaging of atherosclerosis: emerging applications." J Am Coll Cardiol **47**(7): 1328-38.

Jaffer, F. A. and R. Weissleder (2004). "Seeing within: molecular imaging of the cardiovascular system." Circ Res **94**(4): 433-45.

Junqueira, L. C., G. Bignolas, et al. (1979). "Picrosirius staining plus polarization microscopy, a specific method for collagen detection in tissue sections." Histochem J **11**(4): 447-55.

Kaufmann, B. A., J. M. Sanders, et al. (2007). "Molecular imaging of inflammation in atherosclerosis with targeted ultrasound detection of vascular cell adhesion molecule-1." Circulation **116**(3): 276-84.

Kelly, K. A., M. Nahrendorf, et al. (2006). "In vivo phage display selection yields atherosclerotic plaque targeted peptides for imaging." Mol Imaging Biol **8**(4): 201-7.

Kietselaer, B. L., C. P. Reutelingsperger, et al. (2004). "Noninvasive detection of plaque instability with use of radiolabeled annexin A5 in patients with carotid-artery atherosclerosis." N Engl J Med **350**(14): 1472-3.

Kinkel, A. D., M. E. Fernyhough, et al. (2004). "Oil red-O stains non-adipogenic cells: a precautionary note." Cytotechnology **46**(1): 49-56.

Klug, G., T. Kampf, et al. (2010). "Intracellular and extracellular T1 and T2 relaxivities of magneto-optical nanoparticles at experimental high fields." Magn Reson Med **64**(6): 1607-15.

Klug, G., T. Kampf, et al. (2009). "Murine atherosclerotic plaque imaging with the USPIO Ferumoxtran-10." Front Biosci **14**: 2546-52.

Knowles, J. W. and N. Maeda (2000). "Genetic modifiers of atherosclerosis in mice." Arterioscler Thromb Vasc Biol **20**(11): 2336-45.

Kooi, M. E., V. C. Cappendijk, et al. (2003). "Accumulation of ultrasmall superparamagnetic particles of iron oxide in human atherosclerotic plaques can be detected by in vivo magnetic resonance imaging." Circulation **107**(19): 2453-8.

Korosoglou, G., R. G. Weiss, et al. (2008). "Noninvasive detection of macrophage-rich atherosclerotic plaque in hyperlipidemic rabbits using "positive contrast" magnetic resonance imaging." J Am Coll Cardiol **52**(6): 483-91.

Krumpe, L. R. and T. Mori (2006). "The Use of Phage-Displayed Peptide Libraries to Develop Tumor-Targeting Drugs." Int J Pept Res Ther **12**(1): 79-91.

Kuo, Y.-T. and A. H. Herlihy (2008). "Optimization of MRI Contrast for Pre-Clinical Studies at High Magnetic Field." In Webb, G. A. (ed.), Modern Magnetic Resonance, Springer, Dordrecht.

Lancelot, E., V. Amirbekian, et al. (2008). "Evaluation of matrix metalloproteinases in atherosclerosis using a novel noninvasive imaging approach." Arterioscler Thromb Vasc Biol **28**(3): 425-32.

Lanz, T., J. Ruff, et al. (2001). "Double tuned 23Na1H nuclear magnetic resonance birdcage for application on mice in vivo." Rev. Sci. Instrum. **72**(5): 2508-2510.

Laurent, S., D. Forge, et al. (2008). "Magnetic iron oxide nanoparticles: synthesis, stabilization, vectorization, physicochemical characterizations, and biological applications." Chem Rev **108**(6): 2064-110.

Lee, M. J., O. Veiseh, et al. (2010). "Rapid pharmacokinetic and biodistribution studies using cholorotoxin-conjugated iron oxide nanoparticles: a novel non-radioactive method." PLoS One **5**(3): e9536.

Lemaitre, V., T. K. O'Byrne, et al. (2001). "ApoE knockout mice expressing human matrix metalloproteinase-1 in macrophages have less advanced atherosclerosis." J Clin Invest **107**(10): 1227-34.

Leuschner, F. and M. Nahrendorf (2011). "Molecular imaging of coronary atherosclerosis and myocardial infarction: considerations for the bench and perspectives for the clinic." Circ Res **108**(5): 593-606.

Ley, K. and Y. Huo (2001). "VCAM-1 is critical in atherosclerosis." J Clin Invest **107**(10): 1209-10.

Ley, K., Y. I. Miller, et al. (2011). "Monocyte and macrophage dynamics during atherogenesis." Arterioscler Thromb Vasc Biol **31**(7): 1506-16.

Li, A. C. and C. K. Glass (2002). "The macrophage foam cell as a target for therapeutic intervention." Nat Med **8**(11): 1235-42.

Li, H., M. I. Cybulsky, et al. (1993). "Inducible expression of vascular cell adhesion molecule-1 by vascular smooth muscle cells in vitro and within rabbit atheroma." Am J Pathol **143**(6): 1551-9.

Libby, P. (2002). "Inflammation in atherosclerosis." Nature **420**(6917): 868-74.

Libby, P. (2006). "Inflammation and cardiovascular disease mechanisms." Am J Clin Nutr **83**(2): 456S-460S.

Libby, P., M. DiCarli, et al. (2010). "The vascular biology of atherosclerosis and imaging targets." J Nucl Med **51 Suppl 1**: 33S-37S.

Libby, P. and H. Li (1993). "Vascular cell adhesion molecule-1 and smooth muscle cell activation during atherogenesis." J Clin Invest **92**(2): 538-9.

Libby, P., M. Nahrendorf, et al. (2010). "Molecular imaging of atherosclerosis: a progress report." Tex Heart Inst J **37**(3): 324-7.

Libby, P., P. M. Ridker, et al. (2002). "Inflammation and atherosclerosis." Circulation **105**(9): 1135-43.

Lipinski, M. J., K. C. Briley-Saebo, et al. (2008). ""Positive contrast" inversion-recovery with ON[corrected]-resonant water suppression magnetic resonance imaging: a change for the better?" J Am Coll Cardiol **52**(6): 492-4.

Litovsky, S., M. Madjid, et al. (2003). "Superparamagnetic iron oxide-based method for quantifying recruitment of monocytes to mouse atherosclerotic lesions in vivo: enhancement by tissue necrosis factor-alpha, interleukin-1beta, and interferon-gamma." Circulation **107**(11): 1545-9.

Lykowsky, G. (2010). "Entwicklung und Charakterisierung von Messspulen für die NMR-Bildgebung bei 17,6 Tesla."

May, A. E., F. J. Neumann, et al. (2000). "VLA-4 (alpha(4)beta(1)) engagement defines a novel activation pathway for beta(2) integrin-dependent leukocyte adhesion involving the urokinase receptor." Blood **96**(2): 506-13.

McAteer, M. A., A. M. Akhtar, et al. (2010). "An approach to molecular imaging of atherosclerosis, thrombosis, and vascular inflammation using microparticles of iron oxide." Atherosclerosis **209**(1): 18-27.

McAteer, M. A., J. E. Schneider, et al. (2008). "Magnetic resonance imaging of endothelial adhesion molecules in mouse atherosclerosis using dual-targeted microparticles of iron oxide." Arterioscler Thromb Vasc Biol **28**(1): 77-83.

Meincke, M., T. Schlorf, et al. (2008). "Iron oxide-loaded liposomes for MR imaging." Front Biosci **13**: 4002-8.

Meir, K. S. and E. Leitersdorf (2004). "Atherosclerosis in the apolipoprotein-E-deficient mouse: a decade of progress." Arterioscler Thromb Vasc Biol **24**(6): 1006-14.

Michalska, M., L. Machtoub, et al. (2012). "Visualization of vascular inflammation in the atherosclerotic mouse by ultrasmall superparamagnetic iron oxide vascular cell adhesion molecule-1-specific nanoparticles." Arterioscler Thromb Vasc Biol **32**(10): 2350-7.

Modo, M., M. Hoehn, et al. (2005). "Cellular MR imaging." Mol Imaging **4**(3): 143-64.

Moon, H., H. E. Park, et al. (2012). "Noninvasive assessment of myocardial inflammation by cardiovascular magnetic resonance in a rat model of experimental autoimmune myocarditis." Circulation **125**(21): 2603-12.

Morales, M. P., S. Veintemillas-Verdaguer, et al. (1999). "Surface and Internal Spin Canting in γ-Fe2O3 Nanoparticles." *Chem. Mater.*

Moreno, P. R., K. R. Purushothaman, et al. (2006). "Neovascularization in human atherosclerosis." Curr Mol Med **6**(5): 457-77.

Morris, J. B., A. R. Olzinski, et al. (2008). "p38 MAPK inhibition reduces aortic ultrasmall superparamagnetic iron oxide uptake in a mouse model of atherosclerosis: MRI assessment." Arterioscler Thromb Vasc Biol **28**(2): 265-71.

Nahrendorf, M., F. A. Jaffer, et al. (2006). "Noninvasive vascular cell adhesion molecule-1 imaging identifies inflammatory activation of cells in atherosclerosis." Circulation **114**(14): 1504-11.

Nahrendorf, M., E. Keliher, et al. (2009). "18F-4V for PET-CT imaging of VCAM-1 expression in atherosclerosis." JACC Cardiovasc Imaging **2**(10): 1213-22.

Nahrendorf, M., D. Sosnovik, et al. (2008). "Activatable magnetic resonance imaging agent reports myeloperoxidase activity in healing infarcts and noninvasively detects the antiinflammatory effects of atorvastatin on ischemia-reperfusion injury." Circulation **117**(9): 1153-60.

Nahrendorf, M., H. Zhang, et al. (2008). "Nanoparticle PET-CT imaging of macrophages in inflammatory atherosclerosis." Circulation **117**(3): 379-87.

Nair, B. G., T. Fukuda, et al. (2012). "Intracellular trafficking of superparamagnetic iron oxide nanoparticles conjugated with TAT peptide: 3-dimensional electron tomography analysis." Biochem Biophys Res Commun **421**(4): 763-7.

Nakashima, Y., A. S. Plump, et al. (1994). "ApoE-deficient mice develop lesions of all phases of atherosclerosis throughout the arterial tree." Arterioscler Thromb **14**(1): 133-40.

Nakashima, Y., E. W. Raines, et al. (1998). "Upregulation of VCAM-1 and ICAM-1 at atherosclerosis-prone sites on the endothelium in the ApoE-deficient mouse." Arterioscler Thromb Vasc Biol **18**(5): 842-51.

O'Brien, K. D., M. D. Allen, et al. (1993). "Vascular cell adhesion molecule-1 is expressed in human coronary atherosclerotic plaques. Implications for the mode of progression of advanced coronary atherosclerosis." J Clin Invest **92**(2): 945-51.

O'Brien, K. D., T. O. McDonald, et al. (1996). "Neovascular expression of E-selectin, intercellular adhesion molecule-1, and vascular cell adhesion molecule-1 in human atherosclerosis and their relation to intimal leukocyte content." Circulation **93**(4): 672-82.

Oude Engberink, R. D., S. M. van der Pol, et al. (2007). "Comparison of SPIO and USPIO for in vitro labeling of human monocytes: MR detection and cell function." Radiology **243**(2): 467-74.

Patel, L. N., J. L. Zaro, et al. (2007). "Cell penetrating peptides: intracellular pathways and pharmaceutical perspectives." Pharm Res **24**(11): 1977-92.

Pedersen, S. F., M. Graebe, et al. (2010). "Gene expression and 18FDG uptake in atherosclerotic carotid plaques." Nucl Med Commun **31**(5): 423-9.

Pendse, A. A., J. M. Arbones-Mainar, et al. (2009). "Apolipoprotein E knock-out and knock-in mice: atherosclerosis, metabolic syndrome, and beyond." J Lipid Res **50 Suppl**: S178-82.

Phipps, R. P. (2008). "CD40: Lord of the endothelial cell." Blood **112**(9): 3531-2.

Pintaske, J., B. Muller-Bierl, et al. (2006). "Effect of spatial distribution of magnetic dipoles on Lamor frequency distribution and MR Signal decay--a numerical approach under static dephasing conditions." MAGMA **19**(1): 46-53.

Plump, A. S., J. D. Smith, et al. (1992). "Severe hypercholesterolemia and atherosclerosis in apolipoprotein E-deficient mice created by homologous recombination in ES cells." Cell **71**(2): 343-53.

Prufert, K., A. Vogel, et al. (2004). "The lamin CxxM motif promotes nuclear membrane growth." J Cell Sci **117**(Pt 25): 6105-16.

Quillard, T. and P. Libby (2012). "Molecular imaging of atherosclerosis for improving diagnostic and therapeutic development." Circ Res **111**(2): 231-44.

Reddick, R. L., S. H. Zhang, et al. (1994). "Atherosclerosis in mice lacking apo E. Evaluation of lesional development and progression." Arterioscler Thromb **14**(1): 141-7.

Reiner, C. S., A. M. Lutz, et al. (2009). "USPIO-enhanced magnetic resonance imaging of the knee in asymptomatic volunteers." Eur Radiol **19**(7): 1715-22.

Robbins, C. S., A. Chudnovskiy, et al. (2012). "Extramedullary hematopoiesis generates Ly-6C(high) monocytes that infiltrate atherosclerotic lesions." Circulation **125**(2): 364-74.

Robbins, C. S. and F. K. Swirski (2010). "The multiple roles of monocyte subsets in steady state and inflammation." Cell Mol Life Sci **67**(16): 2685-93.

Ronald, J. A., J. W. Chen, et al. (2009). "Enzyme-sensitive magnetic resonance imaging targeting myeloperoxidase identifies active inflammation in experimental rabbit atherosclerotic plaques." Circulation **120**(7): 592-9.

Ruehm, S. G., C. Corot, et al. (2001). "Magnetic resonance imaging of atherosclerotic plaque with ultrasmall superparamagnetic particles of iron oxide in hyperlipidemic rabbits." Circulation **103**(3): 415-22.

Sanz, J. and Z. A. Fayad (2008). "Imaging of atherosclerotic cardiovascular disease." Nature **451**(7181): 953-7.

Sarai, M., D. Hartung, et al. (2007). "Broad and specific caspase inhibitor-induced acute repression of apoptosis in atherosclerotic lesions evaluated by radiolabeled annexin A5 imaging." J Am Coll Cardiol **50**(24): 2305-12.

Saraste, A., S. G. Nekolla, et al. (2009). "Cardiovascular molecular imaging: an overview." Cardiovasc Res **83**(4): 643-52.

Schafers, M., B. Riemann, et al. (2004). "Scintigraphic imaging of matrix metalloproteinase activity in the arterial wall in vivo." Circulation **109**(21): 2554-9.

Schellenberger, E. A., D. Sosnovik, et al. (2004). "Magneto/optical annexin V, a multimodal protein." Bioconjug Chem **15**(5): 1062-7.

Schmitz, S. A., S. E. Coupland, et al. (2000). "Superparamagnetic iron oxide-enhanced MRI of atherosclerotic plaques in Watanabe hereditable hyperlipidemic rabbits." Invest Radiol **35**(8): 460-71.

Schnoor, M. and C. A. Parkos (2008). "Disassembly of endothelial and epithelial junctions during leukocyte transmigration." Front Biosci **13**: 6638-52.

Schonbeck, U. and P. Libby (2001). "CD40 signaling and plaque instability." Circ Res **89**(12): 1092-103.

Schrijvers, D. M., G. R. De Meyer, et al. (2007). "Phagocytosis in atherosclerosis: Molecular mechanisms and implications for plaque progression and stability." Cardiovasc Res **73**(3): 470-80.

Schroder, L. and C. Faber (2011). "In vivo NMR Imaging: Methods and Protocols." Springer.

Schroeter, M., A. Saleh, et al. (2004). "Histochemical detection of ultrasmall superparamagnetic iron oxide (USPIO) contrast medium uptake in experimental brain ischemia." Magn Reson Med **52**(2): 403-6.

Settles, M., M. Etzrodt, et al. (2011). "Different capacity of monocyte subsets to phagocytose iron-oxide nanoparticles." PLoS One **6**(10): e25197.

Shapiro, E. M., S. Skrtic, et al. (2005). "Sizing it up: cellular MRI using micron-sized iron oxide particles." Magn Reson Med **53**(2): 329-38.

Shaw, S. Y. (2009). "Molecular imaging in cardiovascular disease: targets and opportunities." Nat Rev Cardiol **6**(9): 569-79.

Sigovan, M., A. Bessaad, et al. (2010). "Assessment of age modulated vascular inflammation in ApoE-/- mice by USPIO-enhanced magnetic resonance imaging." Invest Radiol **45**(11): 702-7.

Sigovan, M., L. Boussel, et al. (2009). "Rapid-clearance iron nanoparticles for inflammation imaging of atherosclerotic plaque: initial experience in animal model." Radiology **252**(2): 401-9.

Singh, R. B., S. A. Mengi, et al. (2002). "Pathogenesis of atherosclerosis: A multifactorial process." Exp Clin Cardiol **7**(1): 40-53.

Slevin, M., J. Krupinski, et al. (2009). "Controlling the angiogenic switch in developing atherosclerotic plaques: possible targets for therapeutic intervention." J Angiogenes Res **1**: 4.

Sosnovik, D. E. and P. Caravan (2009). "Molecular MRI of Atherosclerotic Plaque With Targeted Contrast Agents." Curr Cardiovasc Imaging Rep **2**(2): 87-94.

Soufi, M., A. M. Sattler, et al. (2002). "Molecular mechanisms involved in atherosclerosis." Herz **27**(7): 637-48.

Southworth, R., M. Kaneda, et al. (2009). "Renal vascular inflammation induced by Western diet in ApoE-null mice quantified by (19)F NMR of VCAM-1 targeted nanobeacons." Nanomedicine **5**(3): 359-67.

Strauss-Ayali, D., S. M. Conrad, et al. (2007). "Monocyte subpopulations and their differentiation patterns during infection." J Leukoc Biol **82**(2): 244-52.

Tabas, I. (2005). "Consequences and therapeutic implications of macrophage apoptosis in atherosclerosis: the importance of lesion stage and phagocytic efficiency." Arterioscler Thromb Vasc Biol **25**(11): 2255-64.

Tang, T. Y., K. H. Muller, et al. (2009). "Iron oxide particles for atheroma imaging." Arterioscler Thromb Vasc Biol **29**(7): 1001-8.

Tardif, J. C., F. Lesage, et al. (2011). "Imaging biomarkers in atherosclerosis trials." Circ Cardiovasc Imaging **4**(3): 319-33.

Temma, T. and H. Saji (2012). "Radiolabelled probes for imaging of atherosclerotic plaques." Am J Nucl Med Mol Imaging **2**(4): 432-47.

Thorek, D. L., A. K. Chen, et al. (2006). "Superparamagnetic iron oxide nanoparticle probes for molecular imaging." Ann Biomed Eng **34**(1): 23-38.

Toussaint, J. F., G. M. LaMuraglia, et al. (1996). "Magnetic resonance images lipid, fibrous, calcified, hemorrhagic, and thrombotic components of human atherosclerosis in vivo." Circulation **94**(5): 932-8.

Trivedi, R. A., U. K.-I. JM, et al. (2004). "In vivo detection of macrophages in human carotid atheroma: temporal dependence of ultrasmall superparamagnetic particles of iron oxide-enhanced MRI." Stroke **35**(7): 1631-5.

Tropp, J. (1989). "The theory of the bird-cage resonator." *J. Magn. Reson.* **82**(1): 51–62.

Tsimikas, S. and P. X. Shaw (2002). "Non-invasive imaging of vulnerable plaques by molecular targeting of oxidized LDL with tagged oxidation-specific antibodies." J Cell Biochem Suppl **39**: 138-46.

Tsimikas, S., B. P. Shortal, et al. (2000). "In vivo uptake of radiolabeled MDA2, an oxidation-specific monoclonal antibody, provides an accurate measure of atherosclerotic lesions rich in oxidized LDL and is highly sensitive to their regression." Arterioscler Thromb Vasc Biol **20**(3): 689-97.

van der Wal, A. C., A. E. Becker, et al. (1994). "Site of intimal rupture or erosion of thrombosed coronary atherosclerotic plaques is characterized by an inflammatory process irrespective of the dominant plaque morphology." Circulation **89**(1): 36-44.

van Oosten, M., E. van de Bilt, et al. (1995). "Vascular adhesion molecule-1 and intercellular adhesion molecule-1 expression on rat liver cells after lipopolysaccharide administration in vivo." Hepatology **22**(5): 1538-46.

Vilahur, G., T. Padro, et al. (2011). "Atherosclerosis and thrombosis: insights from large animal models." J Biomed Biotechnol **2011**: 907575.

Virmani, R., F. D. Kolodgie, et al. (2000). "Lessons from sudden coronary death: a comprehensive morphological classification scheme for atherosclerotic lesions." Arterioscler Thromb Vasc Biol **20**(5): 1262-75.

von zur Muhlen, C., D. von Elverfeldt, et al. (2008). "Magnetic resonance imaging contrast agent targeted toward activated platelets allows in vivo detection of thrombosis and monitoring of thrombolysis." Circulation **118**(3): 258-67.

Weber, C., A. Zernecke, et al. (2008). "The multifaceted contributions of leukocyte subsets to atherosclerosis: lessons from mouse models." Nat Rev Immunol **8**(10): 802-15.

Weinstein, J. S., C. G. Varallyay, et al. (2010). "Superparamagnetic iron oxide nanoparticles: diagnostic magnetic resonance imaging and potential therapeutic applications in neurooncology and central nervous system inflammatory pathologies, a review." J Cereb Blood Flow Metab **30**(1): 15-35.

Weishaupt, D., V. D. Kochli, et al. (2006). "How Does MRI Work." Springer.

Weissleder, R., G. Elizondo, et al. (1990). "Ultrasmall superparamagnetic iron oxide: characterization of a new class of contrast agents for MR imaging." Radiology **175**(2): 489-93.

Weissleder, R. and U. Mahmood (2001). "Molecular imaging." Radiology **219**(2): 316-33.

Winter, P. M., A. M. Morawski, et al. (2003). "Molecular imaging of angiogenesis in early-stage atherosclerosis with alpha(v)beta3-integrin-targeted nanoparticles." Circulation **108**(18): 2270-4.

Yin, J., X. Chaufour, et al. (2000). "Apoptosis of vascular smooth muscle cells induced by cholesterol and its oxides in vitro and in vivo." Atherosclerosis **148**(2): 365-74.

You, T. J., D. S. Maxwell, et al. (2002). "A 3D structure model of integrin alpha 4 beta 1 complex: I. Construction of a homology model of beta 1 and ligand binding analysis." Biophys J **82**(1 Pt 1): 447-57.

Yuan, C., K. W. Beach, et al. (1998). "Measurement of atherosclerotic carotid plaque size in vivo using high resolution magnetic resonance imaging." Circulation **98**(24): 2666-71.

Zaragoza, C., C. Gomez-Guerrero, et al. (2011). "Animal models of cardiovascular diseases." J Biomed Biotechnol **2011**: 497841.

List of Abbreviations

ApoE $^{-/-}$	Apolipoprotein E deficient animal model
B_0	Applied magnetic field
BLI	Bioluminescence imaging
BW	Bandwidth
C57Bl/6	Inbred background animal model
CD68	Cluster of Differentiation 68, glycoprotein expressed on macrophages
CD106	Cluster of Differentiation 106, vascular adhesion molecule
CNR	Contrast to noise ratio
CT	Computed tomography
DAPI	4',6-diamidino-2-phenylindole
EC	Endothelial Cells
ECG	Electrocardiography
EM	Electron Microscopy
FI	Fluorescence imaging
FID	Free induction decay
FITC	Fluorescein isothiocyanate
FLASH	Fast Low-Angle Shot
FT	Fourier transformation
Gd-DTPA	Gadolinium diethylene-triamine-pentaacetic acid
H	Hydrogen proton
H&E	Haematoxylin Eosin Stain

HCl	Hydrochloric acid
HDL	High-density lipoproteins
HNO_3	Nitric acid
HUVEC	Human umbilical vein endothelial cells
ICAM-1	Intercellular adhesion molecule-1
ICP-ES	Inductively coupled plasma emission spectroscopy
IL-1	Interleukin-1
IVUS	Intravascular ultrasound
LDL	Low-density lipoprotein
LIBS	Ligand-induced binding sites
LOX-1	Lectin-type oxidized LDL receptor 1
MCP-1	Macrophage chemoattractant protein
MMP	Matrix metalloproteinases
MRI	Magnetic Resonance Imaging
MSME	Multi Spin Multi Echo
NA	Number of averages
NaCl	Sodium chloride
NFkB	Nuclear factor-kB
NMR	Nuclear Magnetic Resonance
ORO	Oil Red O Staining
OsO_4	Osmium tetroxide
oxLDL	Oxidized low-density lipoproteins
PB	Prussian Blue Staining

PBS	Phosphate Buffered Saline
PDGF	Platelet-derived growth factor
PEG	Polyethylene glycol
PET	Positron emission tomography
PK	Pharmacokinetics
PSGL-1	P-selectin glycoprotein ligand-1
P03011	USPIO-VCAM-1 contrast agent
P3007	USPIO contrast agent
RF	Radio-frequency
ROIs	Regions of interests
ROS	Reactive Oxygen Species
R2	Relaxivity value of T2 time
αSMA	α smooth muscle actin
SMC	Smooth Muscle Cells
SNR	Signal to noise ratio
SPECT	Single-photon emission computed tomography
SR-AI, SRAII	Scavenger receptors class A
SR-PSOX/CXCL16.13	Scavenger receptors that binds phosphatidylserine and oxidised lipoprotein
TE	Echo Time
TNF-α	Tumor necrosis factor
TR	Repetition time
T1	Longitudinal (spin-latice) relaxation time

T2	Transverse (spin-spin) relaxation time
$T_{1/2}$	Half-life time
USPIO	Ultrasmall Superparamagnetic Iron Oxide Particles
VCAM-1	Vascular Cell Adhesion Molecules
vWF	Von-Willebrand-Factor
$\alpha_4\beta_1$	Subfamily of integrins (Very late antigen 4)

Units

g	Gram
mg	Milligram
mm	Millimeter
mmol/L	Millimol/Liter
mmol/kg	Millimol/kilogram
µmol/kg	Mikromol/kg
MHz	Megaherz
T	Tesla
T/m	Tesla/meter

Acknowledgement

I would like to cordially thank Professor Wolfgang Rudolf Bauer for giving me the opportunity to begin a PhD project and work within his group. I am very thankful for his excellent supervision, help, and sustained encouragement during the whole period of my doctoral studies.

I would like to express my gratitude to Dr. Alma Zernecke for brilliant guidance during my laboratory work, writing a publication and advice throughout my doctoral thesis. In addition, I would like to thank Dr. Zernecke for motivating me and for her exceptional care. Special thanks also go to Dr. Helga Manthey for helpful discussions, scientific feedback, and great assistance during preparation of a manuscript.

Next, I would like to sincerely thank Professor Peter Jakob for warm welcome in the Department of Experimental Physics and for magnificent supervision I have received.

I also thank Professor Roland Jahns for care and support as my thesis committee.

I have been fortunate to have such wonderful supervisors who have always found time for me.

I would like to acknowledge Professor Georg Krohne from Theodor-Boveri-Institute (Würzburg) for pleasant cooperation and help with electron microscopy experiments. I also thank Professor Georg Nagel and Elfriede Reisberg for providing me the possibility to perform the inductively coupled plasma emission spectrometry measurements in the Department of Botany I (Würzburg). My thanks also go to Guerbet Research Laboratory (France) for sharing the newly developed contrast agent, on which this thesis was based.

My enormous thanks go to my wonderful colleagues Carmen Bundschuh, Sabine Voll, and Elisabeth Bauer for providing me with splendid help regarding all histological staining, for introducing me into the laboratory work, and for lasting help also outside the lab.

I would like to also express my acknowledgements to Dr. Markus Hildenbrand, Thomas Kampf, Dr. Volker Behr, Dr. Volker Herold, Dr. Karl-Heinz Hiller, Dr. Marco Parczyk, Paola Ponce Garcia, Dr. Gerd Melkus, and Dr. Xavier Helluy for sustained help and expertise in the field of magnetic resonance imaging. Many thanks go to Yuxiang Ye for continuous advice and meaningful scientific conversations. Additionally, I would like to

thank once again Dr. Markus Hildenbrand, Thomas Kampf, Dr. Volker Behr, Elisabeth Bauer and Sabine Voll for thesis proofreading.

My sincere thanks go to "750-er" group and the whole Institute of Experimental Physics for great and friendly working atmosphere.

I would like to also acknowledge Graduate School of Life Sciences for continuous support and the Deutsche Forschungsgemeinschaft SFB 688 for funding opportunity which enabled me to start this PhD project.

Finally, I would like to especially thank my wonderful family and Patrick for being always with me in good and hart times. Thank you for your endless love and care.

Curriculum vitae

Affidavit

I hereby confirm that my thesis entitled “Molecular Imaging of Atherosclerosis” is the result of my own work. I did not receive any help or support from commercial consultants. All sources and / or materials applied are listed and specified in the thesis.

Furthermore, I confirm that this thesis has not yet been submitted as part of another examination process neither in identical nor in similar form.

Würzburg, March 25, 2013